Evaluation and Validation of Equivalent Circuit Photovoltaic Solar Cell Performance Models

by

MATTHEW T. BOYD

A thesis submitted in partial fulfillment of
the requirements for the degree of

MASTER OF SCIENCE
(MECHANICAL ENGINEERING)

at the

UNIVERSITY OF WISCONSIN – MADISON

2010

Approved by

Professor Sanford A. Klein

Professor Douglas T. Reindl

January 13th, 2010

Abstract

The "five-parameter model" is an electrical performance model for photovoltaic solar cells that predicts the voltage and current output by representing the cells as an equivalent electrical circuit with radiation and temperature dependent components. This research evaluated the five-parameter model and modifications based on alternative equivalent circuits intended to enhance performance but requiring only input data provided by module manufacturers on their published datasheets. The performance of the five-parameter model and its variants is assessed using approximately thirty days of field-measured meteorological and module data (Dougherty, 2005) from a wide range of cell technologies including: monocrystalline, polycrystalline, and amorphous silicon and copper indium selenide (CIS).

The five-parameter model accurately predicts the performance of a monocrystalline and a polycrystalline silicon module but is not as accurate for a thin-film CIS and an amorphous silicon array. The difference between model-predicted and measured maximum power values on clear days for the amorphous technology is 20% RMS compared to 6% for the second worst modeled CIS array. These large errors for the amorphous technology are reduced to 5% RMS by using input data obtained after the module underwent an initial degradation in output due to aging, which is a characteristic behavior of amorphous silicon. Accurate model predictions were also obtained for every investigated module and array using model parameters calculated from operating data; these modeling errors are within 2% RMS of those calculated using data measured at standard rating conditions. The short-circuit temperature coefficient, a necessary datum for parameter calculation, was not accurately

calculated in this research; however, a sensitivity analysis of the five-parameter model shows that a single representative value can be used for every technology. All other inputs that are difficult to determine and not provided by manufacturer datasheets such as glazing material properties, the semiconductor band gap energy , and the ground reflectance, may also be generalized.

Modifications to the five-parameter model that were tested during this research did not appreciably improve overall model performance. The temperature and radiation dependence of the model parameters well approximate the data behavior and additional dependence introduced by a seven-parameter model had less than a 1% RMS effect on maximum power predictions for the amorphous technology but increased the modeling errors for this array 4% RMS at open-circuit conditions. Adding a current sink to the equivalent circuit to better model recombination currents was found to have little effect on model behavior.

Acknowledgments

This thesis is dedicated to my girlfriend Kellie for her patience, encouragement, and hard work taking care of me these past two years.

I would first like to thank my advisors, Professors Sandy Klein and Doug Reindl for giving their time and effort offering comments and suggestions, which guided me through my research and vastly improved my thesis. I wish to acknowledge NREL for providing the funding to complete this project and Nate Blair and other researchers at NREL for their feedback and oversight.

I am also grateful to Professor William Beckman for lending his experience and helping me overcome the technical obstacles present in this research. I offer thanks to Brian Dougherty and Bill Healy at NIST for providing me with invaluable data and for being good hosts during my stay at NIST this past summer. I would also like to thank Professor Franklin Miller for serving on my Master's committee.

I would like to thank Ty Neises for the valuable work he completed during his time as my undergraduate assistant. I'm glad all the monotonous simulations and plotting I had you do didn't turn you away from graduate school and the SEL.

I want to thank all the members of the Solar Energy Laboratory who made the lab a fun and comfortable place to work, especially my officemates Michael, Lukas, Will, Ty, Mandy, Rote, Mike, and Pete. Special thanks goes to Lukas, the rock star of our office, for showing us that it is okay to have fun as a graduate student, by sleeping in, watching hours of soccer in the office, partying late, and then finishing the work the night before.

Lastly, I owe special thanks to my good friend Tim Miller for helping me see the bigger picture as I move forward to new challenges in my life.

Table of Contents

List of Figures

List of Tables

Nomenclature

A_i	anisotropy index (-) (HDKR model)
a	ideality factor (V)
C	band gap temperature coefficient (%/K)
d_i	thickness of intrinsic layer (m)
E_e	effective irradiance (W/m^2)
E_g	band gap energy (eV)
f	modulating factor (-) (HDKR model)
G	total radiation on a horizontal surface (W/m^2)
G_b	beam radiation (W/m^2)
$G_{b,n}$	beam radiation normal to a plane (W/m^2)
G_d	diffuse radiation (W/m^2)
G_{on}	extraterrestrial radiation normal to a plane (W/m^2)
G_T	incident radiation on a tilted surface (W/m^2)
I	current (A)
I_D	diode current (A)
I_L	light current (A)
I_{mp}	maximum power current (A)
I_o	diode reverse saturation current (A)
I_{rec}	recombination current (A)
I_{sc}	short-circuit current (A)

I_{sh}	shunt current (A)
K	extinction coefficient (m^{-1})
L	thickness of module glazing (m)
m	diode reverse saturation current radiation dependence (-)
n	refractive index (-)
N_j	number of cell junctions (-)
N_s	number of cells in series (-)
P_{mp}	maximum power (W)
R_b	ratio of beam radiation on a tilted surface to beam radiation on a horizontal surface (-)
R_s	series resistance (Ω)
R_{sh}	shunt resistance (Ω)
S	absorbed radiation (W/m^2)
T	temperature (°C)
V	voltage (V)
V_{bi}	built-in cell voltage (V)
V_c	built-in single junction cell voltage (V)
V_{mp}	maximum power voltage (V)
V_{oc}	open-circuit voltage (V)

Greek Letters

α_{Imp}	maximum power current temperature coefficient (A/°C)

α_{Isc}	short-circuit current temperature coefficient (A/°C)
β	slope of module (°)
β_{Vmp}	maximum power voltage temperature coefficient (V/°C)
β_{Voc}	open-circuit voltage temperature coefficient (V/°C)
χ	current-sink parameter (V)
δ	declination (°) (radiation model)
	non-linear series resistance temperature dependence (%/°C) (seven-parameter model)
γ	maximum power temperature coefficient (%/K)
ω	hour angle (°)
ρ_g	ground reflectance (-)
φ	latitude (°)
$(\tau\alpha)$	transmittance-absorptance product
θ	incidence angle (°)
θ_r	angle of refraction (°)
θ_z	zenith angle (°)

Subscripts

b	beam radiation component
c	cell
d	diffuse radiation component
g	ground-reflected radiation component

mp	maximum power
oc	open-circuit
ref	reference condition
sc	short-circuit

Acronyms

2-a-Si	Tandem-Junction Amorphous Silicon
CIS	Copper Indium Selenide
EST	Eastern Standard Time
I-V	Current versus Voltage
MAE	Mean Absolute Error
MBE	Mean Bias Error
Mono-Si	Monocrystalline Silicon
NIST	National Institute of Standards and Technology
NREL	National Renewable Energy Laboratory
POA	Plane-Of-Array
Poly-Si	Polycrystalline Silicon
PV	Photovoltaic
RMSE	Root Mean Square Error
SNL	Sandia National Laboratories
SRC	Standard Rating Conditions
TST	True Solar Time

Chapter 1

Introduction

1.1 Project Purpose

The ability to predict the instantaneous and annual power output of photovoltaic (PV) solar panels is an integral part of system sizing, economic analyses, and electric power grid management. Several models already exist for predicting maximum power and current-voltage relationships, but improvements may be possible by utilizing additional data recently provided by manufacturers. The purpose of this project is to evaluate alternative formulations of PV performance models using this additional manufacturer's data.

1.2 Photovoltaic Technologies

1.2.1 Cell Composition

A PV solar cell directly converts solar radiation to electricity, using no moving parts or heat power. A PV cell is the building block of a PV module, and a module is in turn a building block of an array. Photovoltaic cells are composed of layered semiconductors in contact with metal electrodes and covered by a protective transparent glazing. When the semiconductor material absorbs photons with an energy level greater than its band gap energy, electrons are freed and carried away by metal electrodes. Power is produced by connecting the electrodes to an external load. The semiconductor material used in cells is predominantly silicon because the band gap energy of silicon results in a theoretical efficiency very near to the maximum for solar radiation (Luque, 2003). The maximum efficiency of a PV cell can be increased further if multiple semiconductor layers, or junctions, are stacked. In this case, the

band gap of each layer is optimized for a different range of photon energies, thereby taking advantage of a greater range of the solar spectrum and improving the overall cell efficiency.

1.2.2 Production of Cell Technologies

Monocrystalline silicon (Mono-Si) is grown as a single crystal into cylindrical ingots and cut into thin wafers. These Mono-Si wafers are often cut into squares or squares with rounded corners to maximize the power area density; the cells made from these wafers are therefore quite distinguishable, as shown in Figure 1.1.

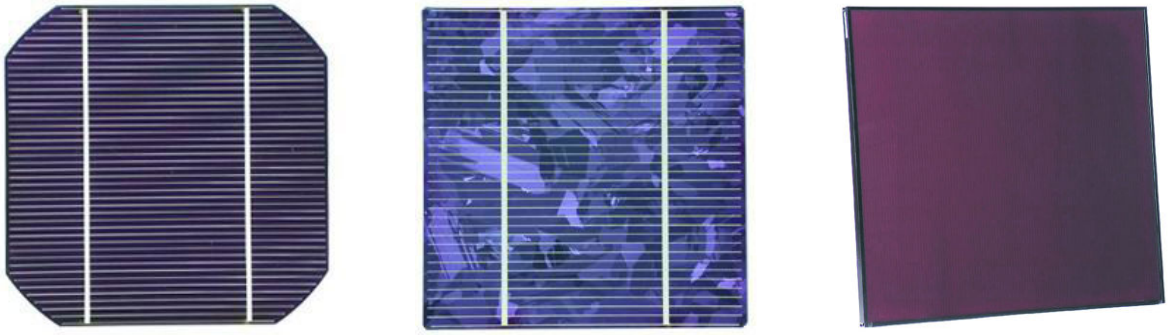

Figure 1.1: A monocrystalline silicon cell (left) (Xinchang, 2009), a polycrystalline silicon cell (middle) (Xinchang, 2009), and a thin-film amorphous silicon module (right) (not to scale) (Kaneka, 2009)

Polycrystalline silicon (Poly-Si) is produced by melting and crystallization, block-casting, or drawing into ribbons, where multiple crystals grow from numerous nucleation sites (Luque, 2003). These processes are typically more economical than that used for Mono-Si, but the resulting cells have lower efficiencies, as shown in Figure 1.2 (Nozik, 2005). Amorphous silicon (a-Si) and other thin-film technologies are produced by substrate deposition processes and result in noncrystalline materials (Luque, 2003). These deposition processes are also

used to produce multiple junction cells. Thin-film cells have some of the lowest production costs, and efficiencies vary, as shown in Figure 1.2.

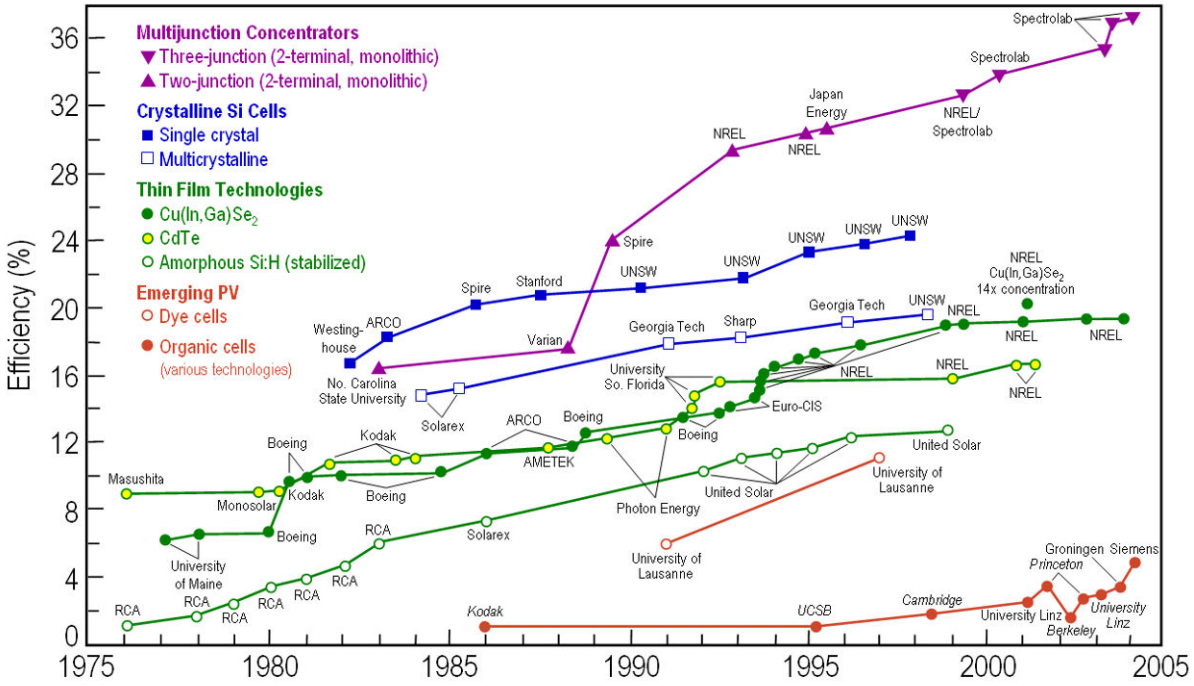

Figure 1.2: Research cell efficiencies of various technologies and their progression over the previous thirty years (Nozik, 2005)

1.2.3 Cell Market Share

Ninety-five percent of the total PV cell market share is silicon based: 42% percent is Mono-Si, 47% is Poly-Si (including string ribbon), and 5% is a-Si (Hirshman, 2008). Non-silicon technologies account for only five percent of the PV cell market share, and consist almost entirely of cadmium telluride (CdTe), copper indium selenide (CIS), and copper indium gallium selenide (CIGS) thin-film technologies. The lowest module price per peak watt

($/$W_p$) in December 2009 of the three main cell technologies is \$2.70/W_p for Mono-Si, \$1.98/W_p for Poly-Si, and \$1.76/W_p for thin film (Solarbuzz, 2009).

1.2.4 Cell Behavior

The performance of PV solar cells is dependent on the voltage of the load, the amount of radiation absorbed by cell, and the cell temperature. Photovoltaic cells operate like a direct-current source that rapidly decreases above a certain operating voltage, with the voltage dictated by the load. The *maximum power* (P_{mp}) output of a cell, at a given radiation level and temperature, occurs near the bend in the current-voltage (I-V) curve, as shown in Figure 1.3. The current at zero voltage is termed the *short-circuit current* (I_{sc}) and the voltage point at zero current is termed the *open-circuit voltage* (V_{oc}). The current and voltage of a PV cell are both dependent on radiation and temperature; however, the current is primarily dependent on the radiation in a near-linear relationship at short-circuit conditions and the voltage is primarily dependent on the temperature in a near-linear relationship at open-circuit conditions.

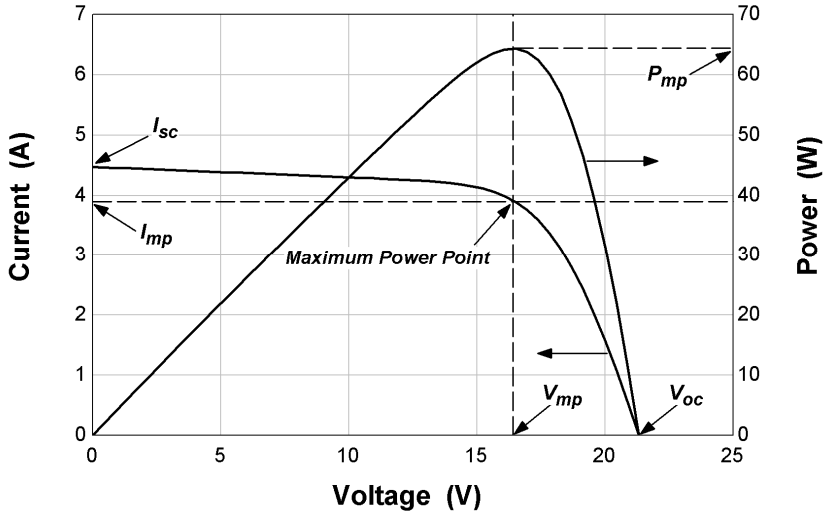

Figure 1.3: Representative I-V and P-V curves for a photovoltaic module at a given absorbed radiation and cell temperature (reproduced from Duffie and Beckman, 2006)

The individual cells can be wired in a module to increase the total current and voltage output; series wiring of the cells adds the cell voltages and parallel wiring adds the cell currents. Photovoltaic devices can be connected to a maximum power point tracker (MPPT) that regulates the cell voltage in order to keep the cells operating at maximum power. The MPPT produces a direct-current voltage suitable for supplying to an external load, which may be an inverter to convert the direct-current (DC) electricity to alternating-current (AC), which is the type supplied by electric utilities.

1.3 Description of PV Performance Models

There are many existing models that predict the output of photovoltaic devices. Most of these models need inputs of absorbed radiation and cell temperature. The absorbed radiation can be modeled by a number of radiation and cover models (Duffie and Beckman, 2006),

while the cell temperature is either assumed equal to the backside panel temperature which is measured, or approximated using empirical (King, 2004), semi-empirical (Skoplaki, (2008), Del Cueto, (2000)), or theoretical (Davis, (2000), Fuentes (1987)) 1-D heat transfer models.

Most PV performance models use one of four methodologies:

1. temperature and radiation scaling of reference measurements
2. interpolation of I-V curves
3. empirical derivation of correlations
4. electrical circuit modeling

1.3.1 Temperature and Radiation Scaling of Reference Measurements

A relatively simple and popular PV performance model is *PVFORM*, which is the performance model used in the *PVWatts* online calculation tool (Marion, 2001). *PVFORM* predicts the maximum power by scaling a reference power value based on radiation and temperature. At high irradiances the power is a linear function of radiation and temperature, and at very low irradiances, a quadratic function replaces the linear function of irradiance as given by Equations (1.1) and (1.2) (Marion, 2008).

$$P_{mp} = \frac{S}{S_{ref}} P_{mp,ref} \left(1 + \gamma \left(T - T_{ref}\right)\right) \qquad S > 125 \text{ W/m}^2 \qquad (1.1)$$

$$P_{mp} = \frac{0.008 \text{ [W/m}^2\text{]}^{-1} S^2}{S_{ref}} P_{mp,ref} \left(1 + \gamma \left(T - T_{ref}\right)\right) \qquad S \leq 125 \text{ W/m}^2 \qquad (1.2)$$

Parameters for this model are the maximum power ($P_{mp,ref}$) at the reference irradiance (S_{ref}) and temperature (T_{ref}) and the temperature coefficient of power (γ). These parameters are provided on PV manufacturer datasheets, with an example datasheet shown in Figure 1.4. The necessary inputs for this model are the absorbed radiation (S) and cell temperature (T).

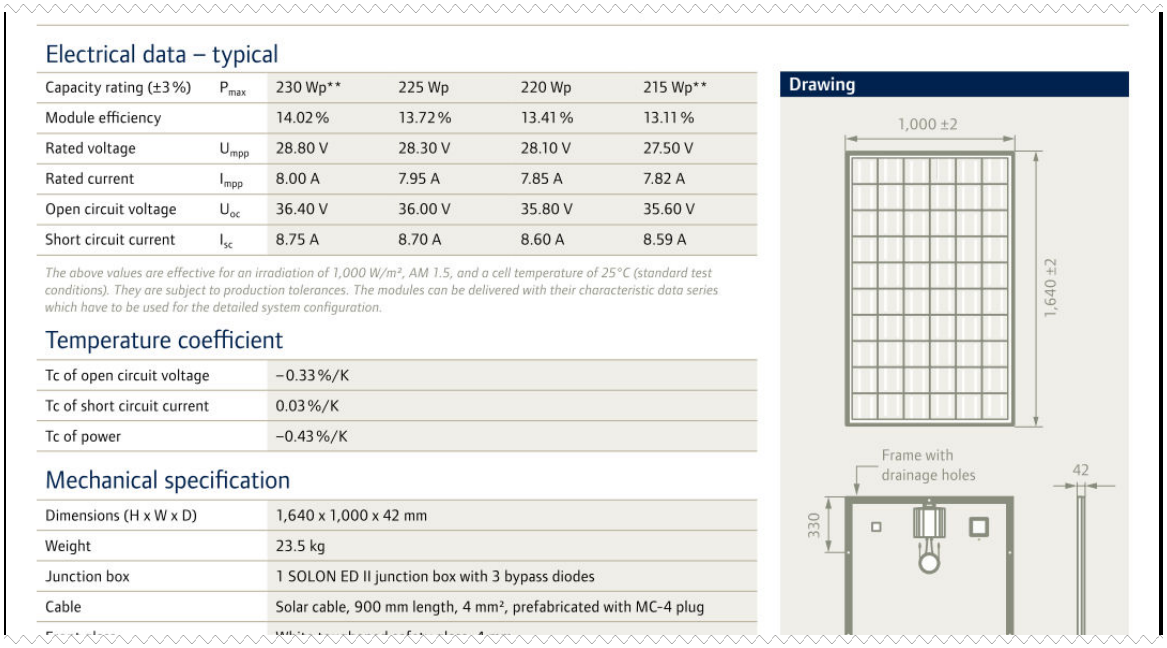

Electrical data – typical

Capacity rating (±3%)	P_{max}	230 Wp**	225 Wp	220 Wp	215 Wp**
Module efficiency		14.02%	13.72%	13.41%	13.11%
Rated voltage	U_{mpp}	28.80 V	28.30 V	28.10 V	27.50 V
Rated current	I_{mpp}	8.00 A	7.95 A	7.85 A	7.82 A
Open circuit voltage	U_{oc}	36.40 V	36.00 V	35.80 V	35.60 V
Short circuit current	I_{sc}	8.75 A	8.70 A	8.60 A	8.59 A

The above values are effective for an irradiation of 1,000 W/m², AM 1.5, and a cell temperature of 25°C (standard test conditions). They are subject to production tolerances. The modules can be delivered with their characteristic data series which have to be used for the detailed system configuration.

Temperature coefficient

Tc of open circuit voltage	−0.33%/K
Tc of short circuit current	0.03%/K
Tc of power	−0.43%/K

Mechanical specification

Dimensions (H x W x D)	1,640 x 1,000 x 42 mm
Weight	23.5 kg
Junction box	1 SOLON ED II junction box with 3 bypass diodes
Cable	Solar cable, 900 mm length, 4 mm², prefabricated with MC-4 plug

Figure 1.4: Section of a typical manufacturer datasheet for a photovoltaic module (Solon, 2009)

1.3.2 Interpolation of I-V Curves

The most developed I-V curve interpolation model is the *bilinear interpolation model*. This model predicts the electrical output at all points along an I-V curve by interpolation using four measured I-V curves (Marion, 2004). These four I-V curves are measured at combinations of two different irradiances and two different cell temperatures near the

operating limits of the cell. A visual representation of the interpolation is shown in Figure 1.5.

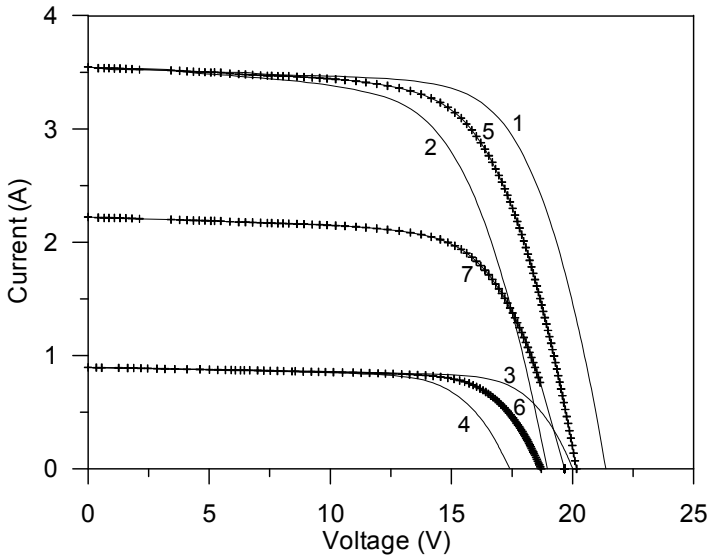

Figure 1.5: Visual representation of interpolations between four measured I-V curves at combinations of two different irradiances and temperatures as used in the *bilinear interpolation model* (Marion, 2004)

I-V curves 1 and 2 are measured at the same irradiance but different temperatures, curve 1 is at a lower temperature and curve 2 is at a higher temperature. These two curves are interpolated with respect to open-circuit voltage to get I-V curve 5. I-V curve 6 is generated the same way using the measured I-V curves 3 and 4. I-V curve 7, the I-V curve at the desired absorbed irradiance and cell temperature, is interpolated from curves 5 and 6 with respect to short-circuit current. Extrapolation, instead of interpolation, is necessary to predict I-V curves at irradiances and temperatures outside the range of the measured I-V curves.

1.3.3 Empirical Derivation of Correlations

A widely used empirical model is the *Photovoltaic Array Performance Model* created at Sandia National Labs (King, 2004). This model predicts the electrical output at short-circuit, maximum power, open-circuit, midway between short-circuit and maximum power, and midway between maximum power and open circuit, as illustrated by the points in Figure 1.6.

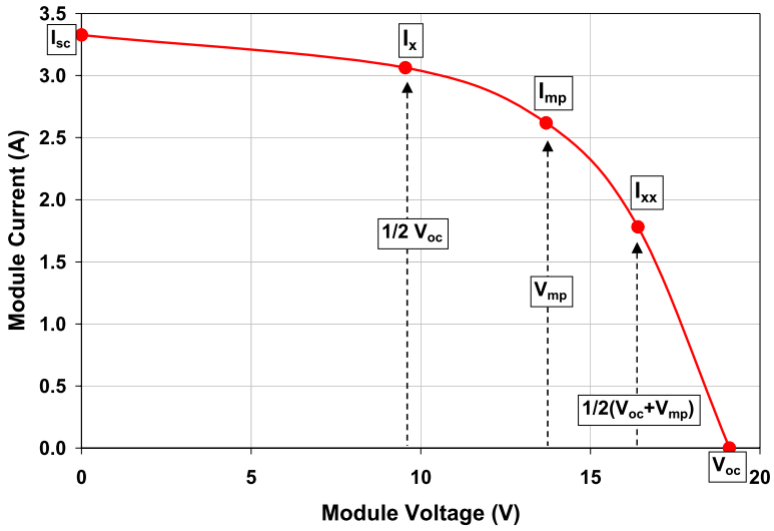

Figure 1.6: A sample I-V curve illustrating the five operating points provided by the Sandia performance model (King, 2004)

Thirty model parameters are needed for the Sandia performance model, and they include:

- 18 empirical coefficients determined from outdoor testing
- 6 reference electrical measurements
- 4 temperature coefficients
- 2 module characteristic values

These parameters include those needed for a cell temperature model and empirical polynomial relationships for the effect of spectral variations due to changes in air mass and the effect of radiation incidence angles on the module. The necessary inputs for the model are the beam and diffuse radiation, wind speed, and ambient temperature.

1.3.4 Electrical Circuit Modeling

The electrical circuit models seek to represent solar cells as an equivalent electrical circuit with radiation and temperature dependent components, like the circuit shown in Figure 1.7.

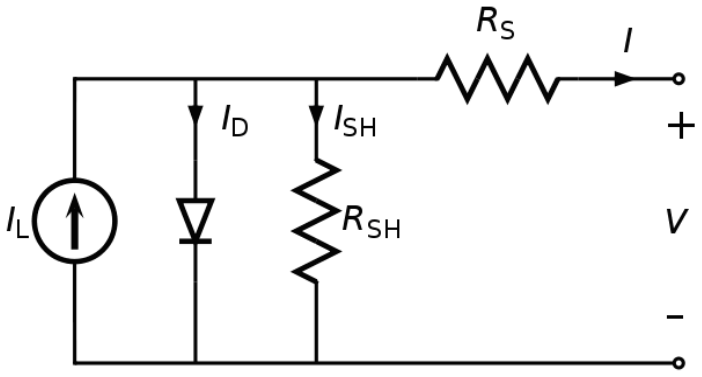

Figure 1.7: An equivalent electrical circuit used to model a PV cell

The most simple of these equivalent circuits include only a radiation-dependent current source and a temperature-dependent diode, while more complex circuits include multiple diodes as well as series and parallel resistances. These equivalent circuit models are capable of predicting the electrical output at all points along the I-V curve. Model parameters vary with the number of circuit components and their respective dependencies. The circuit shown in Figure 1.7 is used by the *Five-Parameter* model which has five model parameters that are

solvable using only data available on PV manufacturer datasheets, like the one shown in Figure 1.4 (De Soto, 2006). Parameters in more complex models that have more circuit components can be solved using nonlinear regression analysis (Müllejans, (2004), King, (1996), Eikelboom, (1997)) or successive approximation (Ken-ichi, 2005) of multiple measured I-V curves. The necessary inputs for electrical circuit models are the absorbed radiation and cell temperature.

1.4 Accuracy of PV Performance Models

The accuracy of modeled values using the previous stated models relative to approximately one year of measured data has been determined by analyses performed at Sandia National Labs (SNL) (Cameron, 2008), the National Renewable Energy Laboratory (NREL) (Marion, 2008), and the National Institute of Standards and Technology (NIST) (Fanney, 2002). Differences between modeled and measured values were calculated at SNL for three different Mono-Si and Poly-Si arrays, at NREL for eight different Mono-Si, Poly-Si, a-Si, and CdTe arrays, and at NIST for eight different Mono-Si, Poly-Si, and a-Si arrays. The results of each analysis are summarized in Table 1.1.

Table 1.1: Accuracy of modeled values using four PV performance models relative to measured data as determined by analyses performed at SNL, NREL, and NIST

	SNL	**NREL**	**NIST**
	Diff. (%)	*RMSE (%)*	*Diff. (%)*
PVFORM	9.6 – 10.2	1.9 – 4.9	–
Bilinear Interpolation	–	1 – 4.4	–
Sandia Performance	2.4 – 5.4	–	-5.4 – 6.2
Five-Parameter	6.5 – 9.1	–	-22.2 – 4.6

It is shown in Table 1.1 that all models are within 10% of the measured values except for the five-parameter model, as determined by NIST; however, the value of -22.2% was calculated for an amorphous silicon array, with the next largest difference being -9.9% for a Mono-Si array. This result coincides with those by SNL, which also found much larger differences for noncrystalline than crystalline arrays for all three of the tested models.

1.5 Project Analysis

The model under analysis in this research is the five-parameter model by De Soto (2006). This current-voltage model uses only information provided on manufacturer's data sheets so no prior testing or empirical data fitting are necessary. A current-voltage model also has the advantage over a maximum power model in that it is capable of predicting the electrical output at all points along the I-V curve and therefore is independent of maximum power point tracking performance. The five-parameter model provides accurate predictions for Mono-Si and Poly-Si cell technologies but its ability to predict multi-junction and amorphous cell performance has not been established. Better agreement with these thin-film technologies is the central goal of this investigation. Additionally this model is to support the Solar Advisory Model (SAM) under development at the National Renewable Energy Laboratory (NREL). SAM is a software tool for use by researchers and industry for examining the costs, financing, and performances of various solar system technologies including photovoltaic, concentrating, and heat.

Chapter 2

PV Solar Calculations

2.1 Module Characterizations

2.1.1 Area

The surface area of a cell, module, or array is used to calculate its efficiency or estimate its power using the known efficiency and irradiance. *Area* has a number of definitions with regard to photovoltaics, with each including different amounts of inactive area, or area that does not contribute to electrical power generation. The *coverage area* will be used in this research because it is commonly used for efficiency comparisons between modules (Dougherty, 2005). The *coverage area* is defined as the total module area minus any inactive module border (Dougherty, 2005). Area measurements are given on the manufacturer datasheets, most often the total cell area and the total module area; however, the area provided is sometimes ambiguous and care must be taken in its use.

2.1.2 Glazing

The cell or module glazing is a transparent outer layer covering the semiconductor on the side exposed to the sun. The glazing commonly is comprised of an outer protective layer (such as glass), an inner protective layer, or encapsulant, (such as ethylene-vinyl-acetate, EVA), and an inner-most anti-reflective coating (such as titanium dioxide, TiO_2) (Luque, 2003). These layers are bonded to the semiconductor surface and have been shown to be well represented by a single air-glazing interface (Duffie and Beckman, 2006). The optical effects of this interface are characterized by the transmittance-absorptance ($\tau\alpha$) product,

which represents the fraction of the incident radiation transmitted through the glazing and absorbed by the semiconductor. The (τα) for a photovoltaic cell glazing is given in Equation (2.1), with Snell's law (Equation (2.2)) used to calculate the angle of refraction.

$$\tau\alpha(\theta) = e^{-(KL/\cos\theta_r)}\left[1-\frac{1}{2}\left(\frac{\sin^2(\theta_r-\theta)}{\sin^2(\theta_r+\theta)}+\frac{\tan^2(\theta_r-\theta)}{\tan^2(\theta_r+\theta)}\right)\right] \tag{2.1}$$

$$n_{air}\sin\theta = n_{glaz}\sin\theta_r \tag{2.2}$$

The (τα) product is a function of the incidence angle (θ), the refractive index of the air (n_{air}) and the glazing thickness (L), extinction coefficient (K), and refractive index (n_{glaz}). The module glazings present in this research and their respective material property values are given in Table 2.1.

Table 2.1: Module glazing materials

Glazing Material	$L \cdot 10^3$ **(m)**	K [1] **(m^{-1})**	n_{glaz} **(-)**
Glass	3 – 6	4	1.526
ethylene tetrafluoroethylene (ETFE)	0.05 - 1	4	1.4
polyvinylidene fluoride (PVDF)	0.05	4	1.42

[1] Values are estimates

The extinction coefficient, K, quantifies the absorption losses of the glazing. Glass has an extinction coefficient ranging from 4 m^{-1} for 'water white' glass to 32 m^{-1} for high iron oxide glass (Duffie and Beckman, 2006). It is assumed that the glass glazings are 'water white' and that the extinction coefficient for the polymer (ETFE and PVDF) glazings are in between

the values for 'water white' and high iron oxide glass. In this range of extinction coefficients, using the manufacturer provided glazing thickness of 50 μm and refractive index of approximately 1.4 (Brandrup, 1999 and DuPont, 2006), (τα) changes by only -0.23%, (see Figure 2.1). Therefore, an extinction coefficient of 4 will be used for both the polymer glazings as the measured values could not be found.

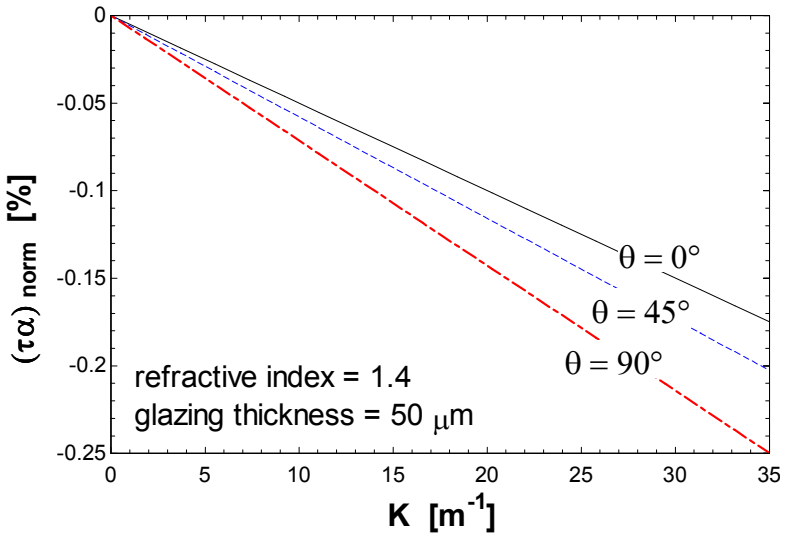

Figure 2.1: Transmittance-absorptance product (τα) verse extinction coefficient (K) for a range of K that includes values for 'water white' and high iron oxide glass

2.1.3 Performance at SRC

The standard rating condition (SRC) for module performance is 1000 W/m^2 incident normal radiation, 25°C cell temperature, and a spectral distribution characteristic of a 1.5 air mass (AM). PV manufacturers report cell and module performance data at SRC and oftentimes at other operating conditions on their datasheets. A list of the data on most manufacturer datasheets is given in Table 2.2.

Table 2.2 Information on most manufacturer datasheets

Datum	Unit	Description
I_{sc}	A	current at short-circuit
V_{oc}	V	voltage at open-circuit
I_{mp}	A	current at maximum power
V_{mp}	V	voltage at maximum power
P_{mp}	W	maximum power
α_{Isc}	A/°C	temperature coefficient of short-circuit current
β_{Voc}	V/°C	temperature coefficient of open-circuit voltage
γ_{Pmp}	W/°C	temperature coefficient of maximum power
NOCT	°C	nominal operating cell temperature at 800 W/m^2, 20°C ambient temperature, and 1 m/s wind speed
A	m^2	Area
η	%	Efficiency

The National Institute of Standards and Technology (NIST) independently measured the insulated and un-insulated nominal operating cell temperature (NOCT), current and voltage temperature coefficients at maximum power, and all module characterization data listed in Table 2.2 for all their tested modules. These values and those provided by the manufacturer are listed in Appendix A. The intention of this effort was to remove any measurement bias from manufacturer-provided data. The module characterization data measured by NIST, instead of by manufacturers, is used for all subsequent analyses, research, and model validations in this project.

2.2 Long-term Test Data

2.2.1 Test Bed

Module, solar, and environmental data were measured by NIST in Gaithersburg, Maryland at a latitude of 39.17° N and longitude of 77.17° W. Various modules were tested at three

different slopes with multiple backside configurations. Many modules were wired in either series or parallel arrays. A summary of these module test beds are given in Table 2.3.

Table 2.3: Summary of Module Test Beds

Cell Technology	Label	Glazing	Roof / Description	Slope[1] [°]
Mono-Si	A	glass	Polystyrene Insulation on Backside	90
Poly-Si	B			
	C	ETFE		
	D	PVDF		
2-a-Si	E	glass	Quiescent Room Temp. Air at Backside	
	F		Polystyrene Insulation on Backside	
CIS	G		Quiescent Room Temp. Air at Backside	
	H		Polystyrene Insulation on Backside	
Mono-Si	D		Concrete Tile Blend Roof	18
	E		PV Slate Roof	
	B		Concrete Tile Blend Roof / Back Contact	
Poly-Si	A		Concrete Tile Blend Roof	
	C			
3-a-Si	F	ETFE	Shingle Roof / Thin film	
Mono-Si	I		1-ply membrane, Back Contact	0
Mono-Si + a-Si	H	glass	Insulated Base with Standoff	
3-a-Si	G	ETFE	Thin Film	

[1] All modules oriented to true south

The modules monitored by NIST were installed in the following orientations:

- a vertical (90°) curtain wall faced due south
- a nominal 4/12 (18°) residential roof faced due south
- on a horizontal (0°) commercial roof

An aerial view of the module installations is shown in Figure 2.2.

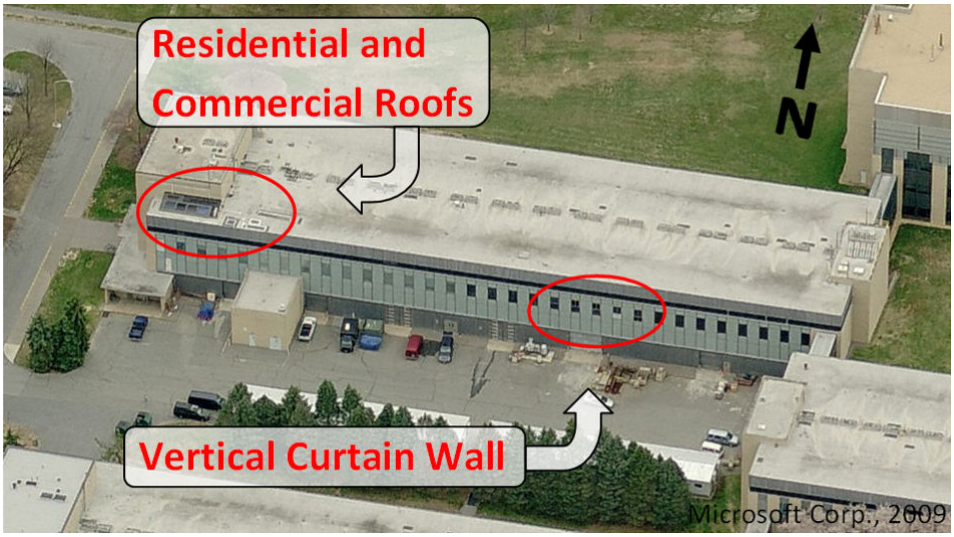

Figure 2.2: Location of vertical curtain wall, and the residential and commercial roofs

The modules in the *vertical curtain wall* were installed flush with the exterior building envelope in second floor high bay modified window frames, as shown in Figure 2.3. The backsides of the curtain wall modules were either insulated with 100 mm of extruded polystyrene (Dougherty, 2005) or were exposed to the interior high bay at approximately room temperature. All module junction boxes were installed on the interior wall next to the module instead of on the module backside panel. This alternative placement was intended to reduce temperature gradients and allow for uniform insulation installation.

Figure 2.3: Vertical Curtain Wall Test Bed
(Note: Modules shown are from a different round of tests than those used in this research)

The modules in the area identified as the "*residential roof*" were installed flush with the surrounding roof, which was composed of three separate roofing materials: asphalt shingle, slate, and concrete tile. These six residential roof arrays are shown in the center-right of Figure 2.4. The 2-a-Si array (*F*) was installed directly on top of 5/8 inch CDX plywood roof sheathing while the other arrays were installed on 1 inch high wood or metal battens with overlap from adjacent modules. Junction boxes were not removed from the module backsides as they were in the vertical curtain wall test bed.

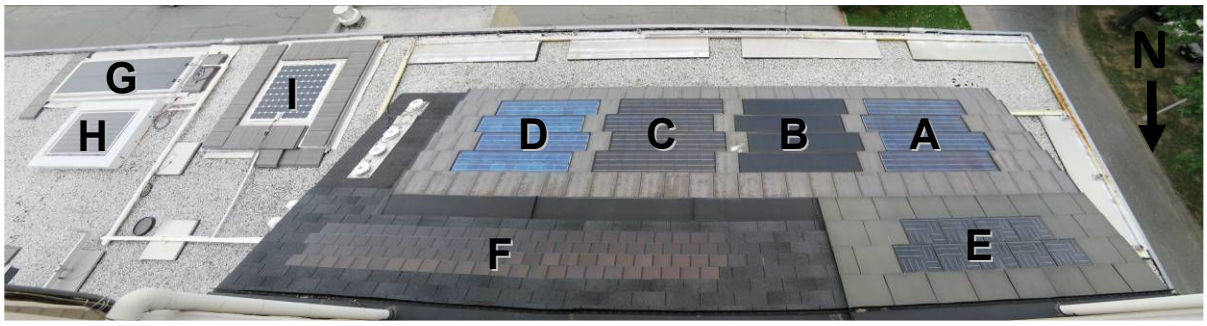

Figure 2.4: Residential and Commercial Roof Test Bed

The modules on the *commercial roof* were installed on top of a horizontal gravel and tar roof separated by an insulating material. These two modules and one array are shown in the left of Figure 2.4. Module *G* and *I* rested on 3" extruded polystyrene while module *H* rested on an integrated proprietary tile blend having an R-20 insulation value. Junction boxes were not removed from the module backsides.

2.2.2 Measurements

2.2.2.1 Module Measurements

All modules had one or more thermocouples centrally installed on the backside panel, with redundant thermocouples connected to different data acquisition systems; no spatial temperature measurements on the backside panel were available. A few modules were custom made and had embedded thermocouples to more accurately measure the *cell temperature*. This cell temperature data was used only to show that the externally measured backside panel temperature was within ±1°C of the cell temperature, except for 3% of the un-insulated panel data which occurred on the sunniest days and was within ±4°C (Dougherty, 2005). Heat flux transducers were also centrally installed on the backside panel of each residential and commercial roof array except for array *F* and module *I*, although data from these sensors were not used in this research.

Module power leads were connected to a multi-tracer that regulated the voltage and kept the modules operating at maximum power. The multi-tracer sampled module current, voltage, power, and temperature at five-second intervals and recorded the averages every five-minutes. Current-voltage (I-V) curves were traced every five minutes that measured the

module current from short-circuit (V=0) to open-circuit (I=0). Module temperature, ambient temperature, and plane-of-array (POA) irradiance data measured by a precision spectral pyranometer (PSP), were recorded immediately before and after each I-V trace.

2.2.2.2 Meteorological Measurements

Various meteorological measurements were recorded both from horizontal and POA platforms. The horizontal platform was on the highest rooftop of the building where the test beds were located and the POA platforms were located immediately adjacent to each test bed. A summary of the meteorological measurements used in this research and their corresponding instruments are given in Table 2.4. All meteorological measurements were instantaneous and taken at five-minute intervals, the same interval used for every other measurement.

Table 2.4: Meteorological measurements and corresponding instruments used in this research

Measurement	Instrument	Platform
Beam Normal Radiation (G_{bn})	Eppley Pyrheliometer	Rooftop Tracking
Diffuse Horizontal Radiation (G_d)	Shaded Disk Eppley Pyranometer[1]	
Global Horizontal Radiation (G)	Eppley Precision Spectral Pyranometer	Rooftop Fixed
Plane of Array Global Radiation (G_T)		Plane of Array

[1] either an Eppley Precision Spectral Pyranometer (PSP) or Eppley Black and White 8-48

2.2.3 PSP Calibrations

Photovoltaic current-voltage models are very sensitive to absorbed radiation and therefore it is important that uncertainty in the incident irradiance measurement be minimized. Uncertainty in pyranometer measurements can exceed ± 5% (Reda, 1999), and measurements from both a shaded and unshaded pyranometer are used to calculate incident radiation in current modeling efforts.

In an effort to minimize pyranometer measurement uncertainty, eight different calibrations from the manufacturer (Eppley), NREL, and NIST were compared, with a description of the calibrations given in Table 2.5.

Table 2.5: Description of available pyranometer calibrations from Eppley, NREL, and NIST

Calibration	Description
Eppley	Constant responsivity
NREL 45°	Constant responsivity
NREL 45-55°	Constant responsivity
NIST (Eppley)	Polynomial function of incidence angle and the Eppley calibration
NIST (NREL 45°)	Polynomial function of incidence angle and the NREL 45° calibration
NIST (NREL 45-55°)	Polynomial function of incidence angle and the NREL 45-55° calibration
NREL 9° bins (combined AM/PM)	Responsivities for 9° incidence angle bins
NREL regression	Trigonometric regression function of incidence angle and solar azimuth

The Eppley and NREL calibrations are specific to the pyranometer while the NIST calibration is a function of a constant responsivity specific to the pyranometer and the beam

incidence angle. Two of the analyzed NREL calibrations are also functions of the beam incidence angle. Figure 2.5 shows the relative differences in calibrations for one example PSP.

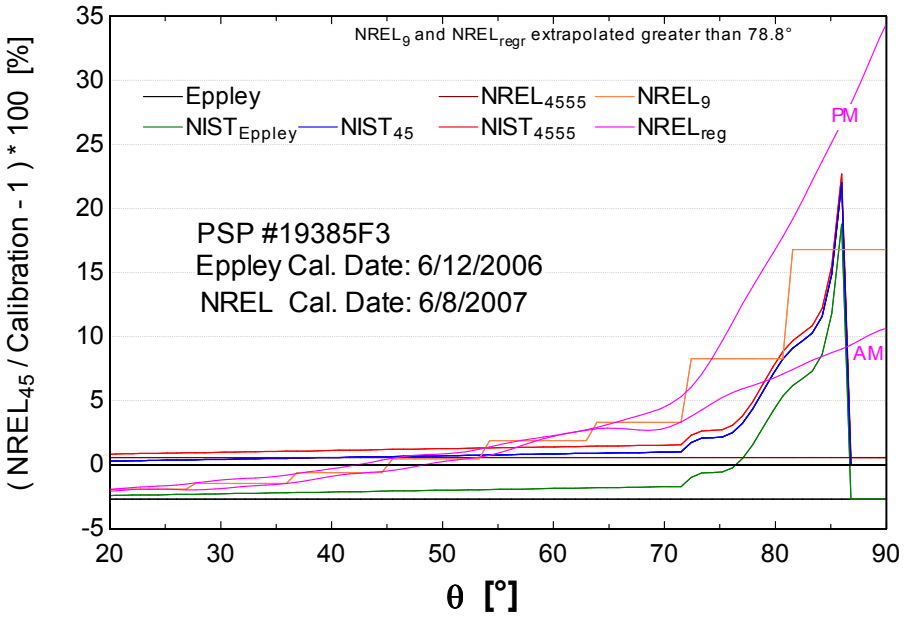

Figure 2.5: Calibrations relative to the NREL 45° calibration for one example PSP

Global horizontal irradiances measured at NIST with four Eppley PSPs using the eight different calibrations in Figure 2.5 were compared to the global irradiance calculated from the sum of pyrheliometer (beam normal) and shaded pyranometer (diffuse) measurements. Statistical differences between these two irradiance measurements were calculated for an approximately four month analysis period from sunrise to sunset with data at five minute intervals. It was found that both the diffuse and global irradiance measuring PSPs were sensitive to the calibration used and therefore it was unclear which calibration was more accurate because both the tested PSP and reference irradiance were affected by the

calibration. It was determined, however, that the different NREL calibrations all resulted in errors within 1% RMSE of another. The NIST calibration correction made no significant improvement to the original calibration, instead increasing the RMSE by less than 1%. The Eppley calibration resulted in the lowest errors, with one of the four PSPs under 5% RMSE and two under 10% RMSE. The NREL 45° resulted in the second lowest errors, 2-3% RMSE higher than the Eppley. The Eppley or NREL 45° calibration, whichever was more recent relative to the data, is applied to the respective NIST pyranometer data.

2.2.4 Compiled Data Sets

Two datasets were compiled from the *Vertical Curtain Wall* data for use validating PV performance models. One dataset, named '***Clear Days 9:30-4 EST***', contains data from 36 of the clearest days dispersed throughout the year-long data acquisition period, with the number of days from each month shown in Figure 2.6. No days were selected from April because no diffuse data was measured. Clear, irradiance stable days were chosen to minimize any transient effects in the modules and measurement instruments. These clear day data are from 09:30 - 16:00 EST to avoid times of shading, with daily unshaded durations shown in Figure 2.7.

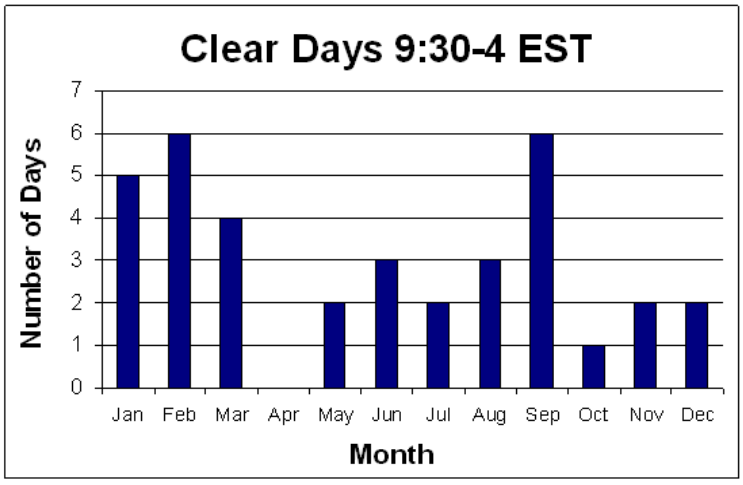

Figure 2.6: Distribution of days of data selected for the 'Clear Days 9:30-4 EST' dataset

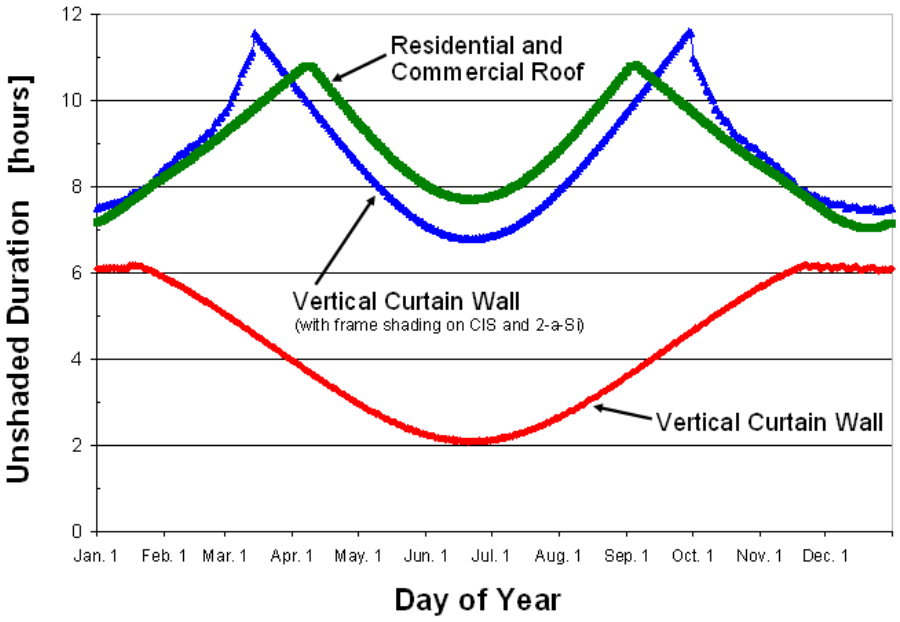

Figure 2.7: Time durations of minimal and no module shading throughout the year

Early morning and late afternoon shading occurred on select arrays and instruments, caused by neighboring buildings, walls, and module framings. The unshaded time interval is very

short in the summer on the vertical curtain wall; a second interval is shown that includes minimal shading on the CIS and 2-a-Si modules caused by their respective frames.

The second compiled dataset, named '***January – Unshaded Periods***', contains data from one month measured in January at times of no module shading (lowest curve in Figure 2.7). This data results in lower uncertainty in the calculation of absorbed radiation because there are lower incidence angles on a vertical surface in January. This dataset also contains much more diffuse and low irradiance data, as shown by the histograms of incident POA radiation in Figure 2.8.

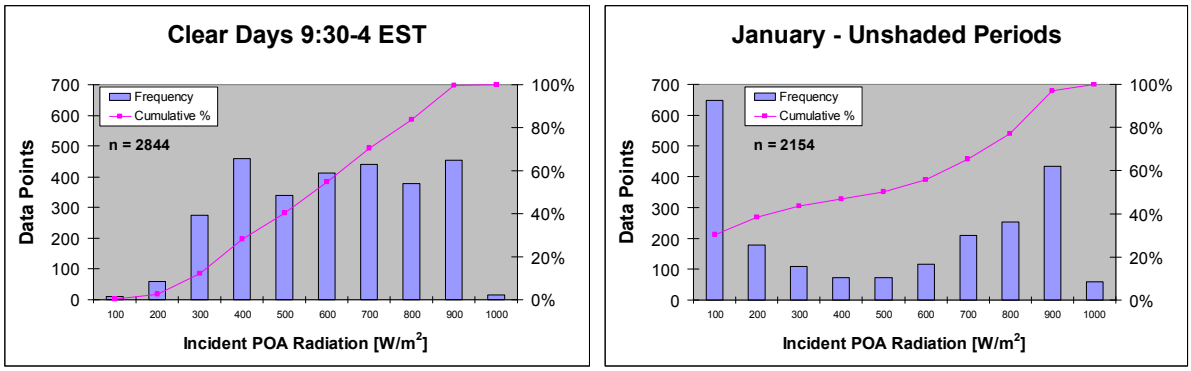

a. **b.**

Figure 2.8: Histograms of the datasets used for model validation

2.3 Radiation Modeling

Radiation modeling used for PV performance models attempts to calculate the radiation absorbed by a solar module as a function of irradiance, module geometry, and the glazing optics (Duffie and Beckman, 1991).

2.3.1 Irradiance

Solar irradiance consists of three generally distinct components: beam, diffuse, and ground-reflected radiation. Beam radiation is the component that comes directly from the sun and has not been scattered by the atmosphere. Beam radiation normal to the sun (i.e. beam normal radiation) was measured with a tracking pyrheliometer, as specified in Table 2.4. Diffuse radiation has been scattered by the atmosphere and subsequently has changed direction. Diffuse radiation incident on a horizontal surface (i.e. horizontal diffuse radiation) was measured with a horizontal pyranometer and a tracking disk to provide beam radiation shading, also specified in Table 2.4. Ground-reflected radiation originates from the sun but has been reflected or absorbed and re-emitted by the surroundings. Ground reflectance was calculated according to the radiation model used as a function of the ground reflectivity, radiation component values, and relative geometries. Much of the surrounding ground was asphalt so a reflectivity of 0.15 is assumed (ACPA, 2002).

2.3.2 Module Geometry

The module geometry relative to the irradiance determines the incidence angles of the three radiation components, and in turn their fluxes and optical behavior in the glazing. The incidence angle of beam radiation, usually just termed the incidence angle, is the angle between the sun and the normal of the module surface, with the equations necessary for calculation provided by Duffie and Beckman (2006). The diffuse and ground-reflected radiation are incident over a range of angles, but an effective incidence angle comparable to the beam incidence angle can be calculated by the integration of the beam transmittance over suitable incidence angles (Duffie and Beckman, 2006). The effective incidence angle for

diffuse radiation is approximately 60° for both a horizontal and vertical surface, while for ground-reflected radiation it is approximately 90° for a horizontal surface and 60° for a vertical surface.

2.3.3 Glazing Optics

The optics of the module glazing, along with the incidence angles of the three radiation components, determine how the irradiance is absorbed. As described in Section 2.1.2, the transmittance-absorptance product ($\tau\alpha$) and accompanying Snell's Law provide the fraction of a given radiation component transmitted through the glazing and absorbed by the semiconductor. The beam, diffuse, and ground-reflected radiation components are all incident at different angles and therefore each have a corresponding ($\tau\alpha$), which the components are then multiplied by and summed according to the radiation model.

2.3.4 Radiation Models

Various radiation models attempt to calculate absorbed radiation using some or all of these radiation components, associated incidence angles, and glazing optical properties. The most simple radiation model is the product of the total radiation measured on the plane-of-array (POA) and an average ($\tau\alpha$); however, a single ($\tau\alpha$) product does not account for the individual effects of the different radiation components. More accurate radiation models that do account for these effects include the Liu and Jordan isotropic sky, HDKR, and Perez. A study of these radiation models by Cameron, et al. (2008) comparing modeled to measured *incident* radiation showed that the Perez model is the most accurate with the HDKR model following by about 1% RMSE and 0.3% MBE. The HDKR model, however, was used for

this research instead of the Perez because it has a much simpler implementation, especially for calculating absorbed radiation; this benefit seemed to outweigh the modestly lower accuracy. The HDKR model for absorbed radiation is shown in Equations (2.3) - (2.8), where the subscripts 'b', 'd', and 'g' stand for beam, diffuse, and ground-reflected, respectively. The rest of the variables are defined in the Nomenclature.

$$S_{T,HDKR} = \left(G_b + G_d A_i\right) R_b \left(\tau\alpha\right)_b + G_d \left(1 - A_i\right)\left(\tau\alpha\right)_d \left(\frac{1+\cos\beta}{2}\right)\left[1 + f\sin^3\left(\frac{\beta}{2}\right)\right] + G\rho_g \left(\tau\alpha\right)_g \left(\frac{1-\cos\beta}{2}\right) \tag{2.3}$$

$$A_i = \frac{G_{b,n}}{G_{on}} \tag{2.4}$$

$$f = \sqrt{\frac{G_b}{G}} \tag{2.5}$$

$$G_b = G_{b,n}\cos\theta_b \tag{2.6}$$

$$G = G_b + G_d \tag{2.7}$$

$$R_b = \frac{\cos\left(\phi-\beta\right)\cos\delta\cos\omega + \sin\left(\phi-\beta\right)\sin\delta}{\cos\phi\cos\delta\cos\omega + \sin\phi\sin\delta} \tag{2.8}$$

2.3.5 POA Correction Factor

The POA data are not used in the HDKR radiation model because the three radiation components are not separable from the single value. The POA data is instead used to correct

the radiation model because the POA radiation measurement must be equal to the radiation model when transmittance and absorptance effects are omitted. The correction factor used is the ratio of the measured POA irradiance to the modeled POA irradiance. The modeled POA irradiance is given by Equation (2.3) with the (τα)'s equal to one; the correction factor and its proposed usage are given by Equations (2.9) and (2.10), where the 'T' subscript indicates a tilted surface. The effect of this correction factor on the PV performance model is quantified and presented in Section 3.2.2.

$$R = \frac{G_T}{G_{T,HDKR}} \tag{2.9}$$

$$S_{HDKR,c} = S_{HDKR} \cdot R \tag{2.10}$$

Chapter 3

Five-Parameter Model

3.1 Description

3.1.1 Equivalent Circuit

The five-parameter model is derived from the equivalent circuit of a solar cell, which consists of a current source, a diode, and two resistors, as shown in the schematic in Figure 3.1.

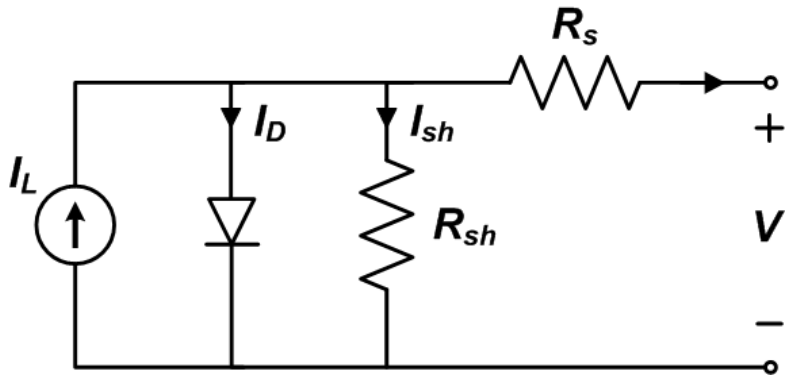

Figure 3.1: Equivalent circuit of a photovoltaic solar cell

The current source (I_L) represents charge carrier generation in the semiconductor caused by incident radiation. The shunt diode represents recombination of these charge carriers at a high forward-bias voltage ($V+I \cdot R_s$). The shunt resistor (R_{sh}) signifies high-current paths through the semiconductor along mechanical defects and material dislocations (Stutenbaeumer, 1999). The series resistor (R_s) embodies series resistance in the outer semiconductor regions, primarily at the interface of the semiconductor and the metal contacts (Stutenbaeumer, 1999).

Calculating a current balance at a point left of R_s as shown in Figure 3.1 results in Equation (3.1). Substituting in Ohm's law and the Shockley diode equation for the currents through the resistors and diode, respectively, yields the model characteristic equation, given by Equation (3.2). The variable I_o is the reverse-bias saturation current and a is the modified ideality factor, defined by Equation (3.3), where N_s is the number of solar cells in series, n is the diode ideality factor, k is Boltzmann's constant, T is the cell temperature, and q is the charge of an electron.

$$I = I_L - I_D - I_{sh} \tag{3.1}$$

$$I(V) = I_L - I_o\left(e^{\frac{V+IR_s}{a}} - 1\right) - \frac{V+IR_s}{R_{sh}} \tag{3.2}$$

$$a \equiv \frac{N_s nkT}{q} \tag{3.3}$$

3.1.2 Model Parameter Calculation

The characteristic equation of the equivalent circuit contains five independent parameters, hence the name *Five-Parameter Model*. These parameters can be determined analytically using only measurements at SRC that are available on manufacturer datasheets: current at maximum power (I_{mp}), voltage at maximum power (V_{mp}), short-circuit current (I_{sc}), open-circuit voltage (V_{oc}), and temperature coefficients of short-circuit current (α_{Isc}) and open-circuit voltage (β_{Voc}). The methodology to determine the model parameters involves first

constraining the characteristic equation at short-circuit, open-circuit, and maximum power conditions, as shown in Equations (3.4), (3.5), and (3.6), respectively. This results in three equations and five unknowns.

$$I_{sc}\big|_{ref} = \left[I_L - I_o \left(e^{\frac{I_{sc}R_s}{a}} - 1 \right) - \frac{I_{sc}R_s}{R_{sh}} \right]_{ref} \tag{3.4}$$

$$0 = \left[I_L - I_o \left[e^{\frac{V_{oc}}{a}} - 1 \right] - \frac{V_{oc}}{R_{sh}} \right]_{ref} \tag{3.5}$$

$$I_{mp}\big|_{ref} = \left[I_L - I_o \left(e^{\frac{V_{mp}+I_{mp}R_s}{a}} - 1 \right) - \frac{V_{mp}+I_{mp}R_s}{R_{sh}} \right]_{ref} \tag{3.6}$$

The second step in the parameter solving methodology is to constrain the derivative of the product of the characteristic equation for current and the voltage (which is the power) to zero at maximum power, as shown in Equation (3.7). This equation along with the previous three result in four equations and five unknowns.

$$0 = \left[I_{mp} + V_{mp} \left(\frac{\frac{-I_o}{a} e^{\frac{V_{mp}+I_{mp}R_s}{a}} - \frac{1}{R_{sh}}}{1 + \frac{I_o R_s}{a} e^{\frac{V_{mp}+I_{mp}R_s}{a}} + \frac{R_s}{R_{sh}}} \right) \right]_{ref} \tag{3.7}$$

One more equation would be needed to have an equal number of equations and unknowns, and therefore a solution to the parameters; instead, however, the next step in the methodology

is to use the known value and definition of β_{Voc} assuming linearity (Equation (3.8)) and solve for the characteristic equation evaluated at the open-circuit condition at a non-reference temperature, as shown in Equation (3.9). The temperature at which this equation is evaluated has little observed effect on the parameter solution, with a ΔT of 10 K used in this research. To solve this additional equation, the temperature dependence of each of the parameters must be known. The dependencies determined by De Soto (2004), given by Equations (3.10) – (3.14), were used in this research. A linear temperature dependence was assumed for the material band gap energy (E_g) (Van Zeghbroeck, 2007), and was calculated using the reference value and temperature coefficient for silicon. A value of unity was used for the air mass modifier (M/M_{ref}), a reasonable assumption given the results by De Soto (2004), and the equations were solved at the reference irradiance ($S = S_{ref}$). Equations (3.8) – (3.14) result in seven equations and six additional unknowns, or a total of 11 equations and 11 unknowns, and therefore provide a solution to the parameters.

$$\beta_{Voc} = \frac{V_{oc} - V_{oc,ref}}{T - T_{ref}} \tag{3.8}$$

$$0 = \left[I_L - I_o \left(e^{\frac{V_{oc}}{a}} - 1 \right) - \frac{V_{oc}}{R_{sh}} \right]_{T = T_{ref} + \Delta T} \tag{3.9}$$

$$a = a_{ref} \frac{T}{T_{ref}} \tag{3.10}$$

$$I_L = \frac{S}{S_{ref}} \frac{M}{M_{ref}} \left[I_{L,ref} + \alpha_{Isc} \left(T - T_{ref} \right) \right] \tag{3.11}$$

$$I_o = I_{o,ref}\left(\frac{T}{T_{ref}}\right)^3 \exp\left[\frac{1}{k}\left(\frac{E_g}{T}\bigg|_{T_{ref}} - \frac{E_g}{T}\right)\right] \tag{3.12}$$

$$R_{sh} = \frac{S_{ref}}{S} R_{sh,ref} \tag{3.13}$$

$$R_s = R_{s,ref} \tag{3.14}$$

Unfortunately, there is no analytical solution to these highly non-linear, coupled equations, so they must be solved numerically. In the present study, the Engineering Equation Solver (EES) software (Klein, 2009) is used, with program code and solution procedure given in Appendix B. A list of the parameters for the modules in this research is provided in Appendix C.

3.1.3 Effect of Parameters on I-V Curve Shape

The effect of each of the five parameters on the behavior of the I-V curve is shown in Figure 3.2. The model is calculated for a 2-a-Si module at an absorbed radiation and cell temperature near to the average of the corresponding yearly operating conditions, although the effect of each parameter on the I-V curve is similar for all modules and operating conditions. The bold I-V curve in each of the following plots is the result of using parameters calculated from SRC data while the other two are the result of adjusting one specified parameter above and below the original value. The following figures show that both $\underline{a}$ and I_o adjust the predicted voltage at all points on the I-V curve and I_L adjusts the

predicted current. R_s and R_{sh} have a more localized influence around the maximum power point; R_s adjusts the maximum power voltage and R_{sh} adjusts the maximum power current.

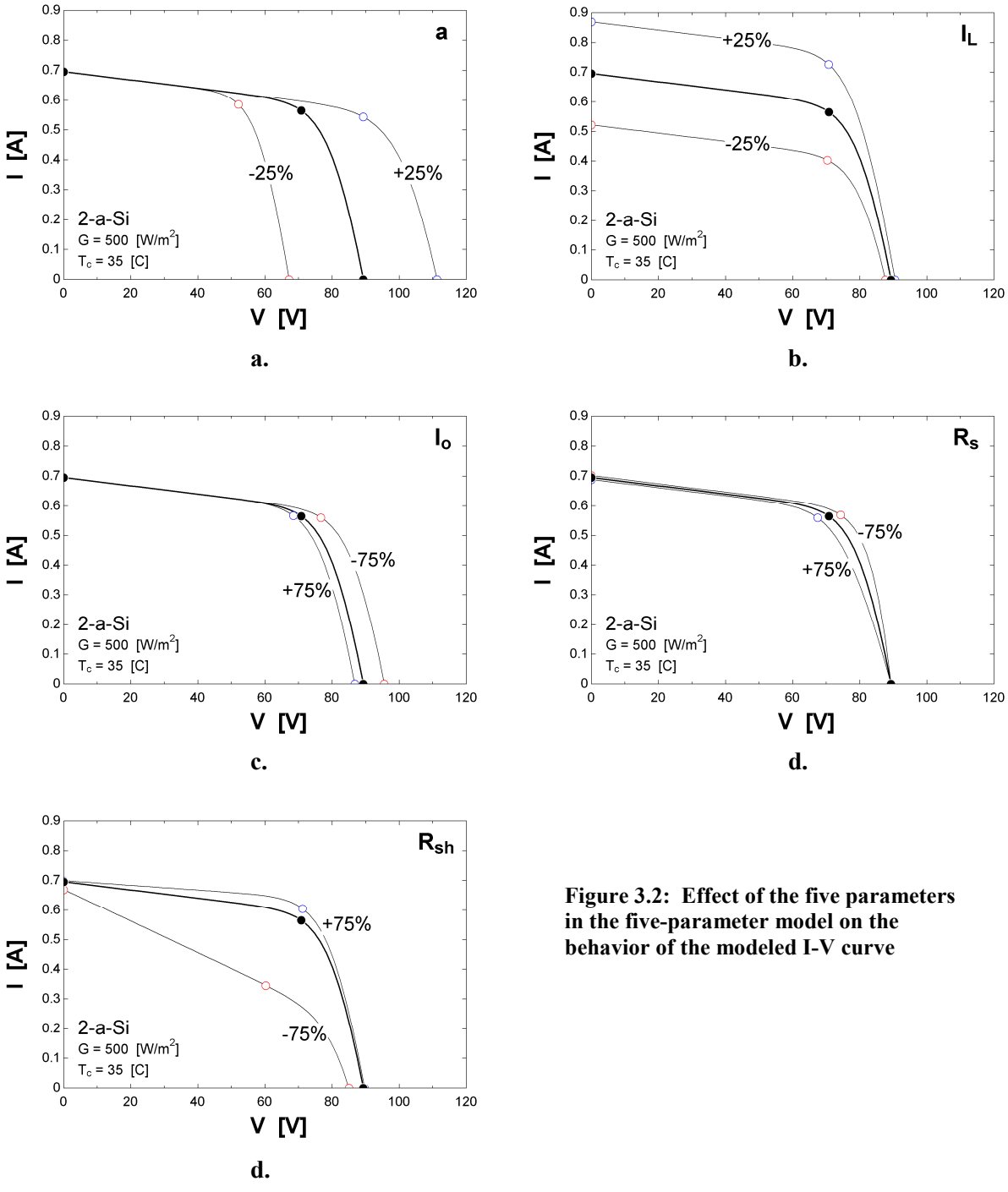

Figure 3.2: Effect of the five parameters in the five-parameter model on the behavior of the modeled I-V curve

3.2 Model Validation

3.2.1 Error Statistics

The data measured at NIST, described in Section 2.2, are used to validate the five-parameter model and its variations. Although the dataset includes entire I-V curves for comparison with the model, only the operating points at short-circuit (I_{sc}), open-circuit (V_{oc}), and maximum power (I_{mp}, V_{mp}, P_{mp}) were compared to simplify the data processing and results. Statistics employed to quantify the model's agreement to the measured data at these five operating points are the root-mean-squared error (RMSE), mean-bias-error (MBE), and mean-absolute-error (MAE), as shown in Equations (3.15) – (3.17) where y is the modeled value, x is the measured value, and n is the number of measured values.

$$RMSE = \left[\frac{1}{n}\sum_{i=1}^{n}\left(y_i - x_i\right)^2\right]^{1/2} \div \left[\frac{1}{n}\sum_{i=1}^{n} x_i\right] \times 100\% \tag{3.15}$$

$$MBE = \left[\frac{1}{n}\sum_{i=1}^{n}\left(y_i - x_i\right)\right] \div \left[\frac{1}{n}\sum_{i=1}^{n} x_i\right] \times 100\% \tag{3.16}$$

$$MAE = \left[\frac{1}{n}\sum_{i=1}^{n}\left|y_i - x_i\right|\right] \div \left[\frac{1}{n}\sum_{i=1}^{n} x_i\right] \times 100\% \tag{3.17}$$

3.2.2 Effect of POA Correction Factor

The plane of array (POA) correction factor R, as defined in Section 2.3.5, uses the measured POA radiation to correct the modeled absorbed radiation. The effects of R on the five-parameter modeling errors for the Mono-Si module installed on the *vertical curtain wall* test bed are shown in Figure 3.3 for the 'Clear Days 9:30-4 EST' and 'January – Unshaded

Periods' datasets as described in Section 2.2.4. The POA correction factor is shown to reduce the modeling errors for the Mono-Si module, as well as for the other modules in the test bed (modeling errors not shown). The POA correction factor is therefore used for all further validation work.

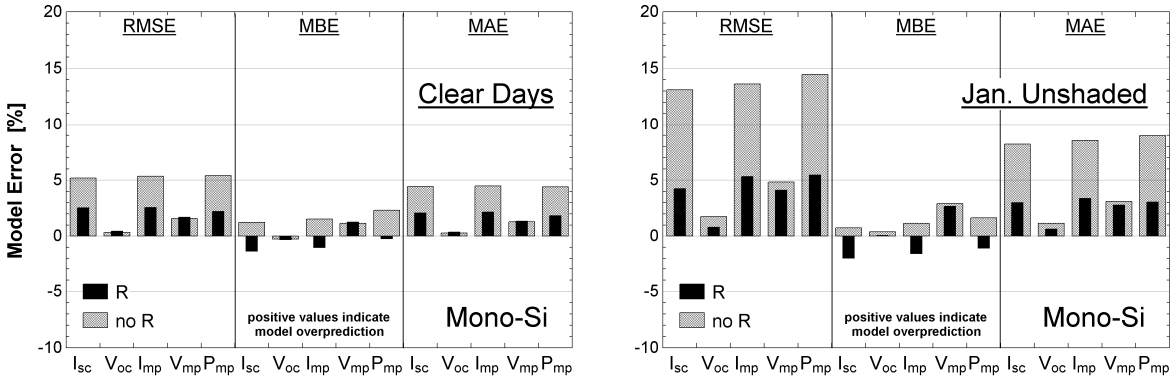

Figure 3.3: Effect of the POA correction factor *R* on the five-parameter modeling errors for the Mono-Si module for two different datasets

3.2.3 Validation Using Model Parameters Calculated from SRC Data

Modeling errors are calculated for each array in the *vertical curtain wall*, described in Section 2.2.1, with parameters derived from SRC data and using *R* to correct the absorbed radiation calculation. Statistical modeling errors are shown in Figure 3.4 with modeled versus measured values given in Appendix D. The results in Figure 3.4a-d show that the Mono-Si and Poly-Si module data are well represented by the model, but there are significantly larger errors for the 2-a-Si and CIS arrays. The model exhibits large voltage bias errors for the 2-a-Si array at both open-circuit and maximum power, which results in large corresponding RMS errors. The large voltage RMS errors for the CIS array have a comparatively lower corresponding bias error but have more scatter.

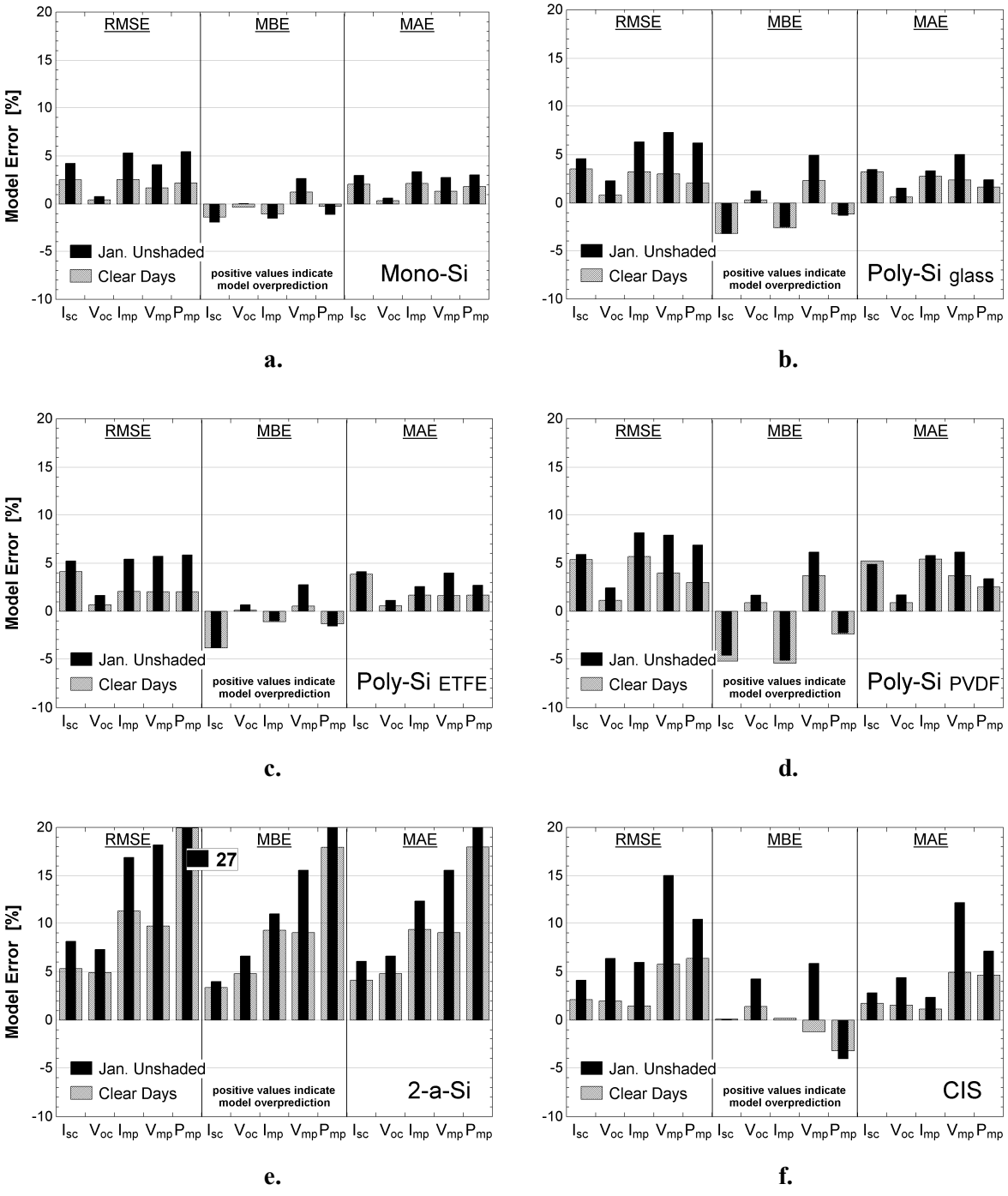

Figure 3.4: **Statistical modeling errors of the five-parameter model for the six backside insulated arrays on the *vertical curtain wall* test bed using two different datasets [a. Mono-Si, b. Poly-Si (glass cover), c. Poly-Si (ETFE cover), d. Poly-Si (PVDF cover), e. 2-A-Si, and f. CIS]**

3.2.4 Validation Using Model Parameters Calculated from Operating Data

Model parameters were calculated from operating data to determine if the larger errors shown in Figure 3.4 for the 2-a-Si and CIS arrays were caused by SRC data being uncharacteristic of the true module performance. Model parameters are calculated from a ***single*** operating point similar to how they are calculated from SRC data; however, the calculated absorbed radiation and measured temperature and module electrical output substitute for the respective SRC data. Temperature coefficients can not be calculated from a single operating point, but may be calculated from multiple points, with a partially successful attempt described in the next section.

3.2.4.1 Calculation of Temperature Coefficients from Operating Data

The following procedure was used to calculate the temperature coefficients of short-circuit current (α_{Isc}) and open-circuit voltage (β_{Voc}) from operating data. These coefficients will be used along with I_{sc}, V_{oc}, V_{mp}, I_{mp}, T (module temperature), and S (absorbed radiation) to calculate model parameters and will also be employed in model calculations. The coefficients are calculated for the back-insulated Mono-Si, Poly-Si with glass glazing, 2-a-Si, and CIS modules from the same set of operating data that contained the short-circuit, open-circuit, and maximum power reference data. The procedure, similar to that used by Fanney (2006), is described in the following sections.

3.2.4.1.1 Data Selection

Short-circuit current, open-circuit voltage, and backside panel temperature data were selected from nine clear days in the 'Clear Days…' dataset between 11:00 and 13:00 solar time. These days were selected so that the average in-plane wind speed between these times was less than 1.34 m/s (3 mph) to minimize temperature gradients in the modules (which were also backside insulated to reduce temperature gradients). This time window was chosen to minimize the irradiance range, with the peak irradiance occurring at solar noon on a clear day. The backside panel temperature was measured using a single thermocouple mounted on the rear of the panel (not spatially averaged) and time-averaged over a five-minute interval. The nine days with wind conditions fitting the above constraints were chosen so there would be three sets of three similar days distributed throughout the year. The three days of each set have similar peak irradiance values, and the average peak irradiance of each set is equally distributed in the yearly range of peak irradiances, as seen in Figure 3.5. This distribution was chosen to verify that the temperature coefficient of open-circuit voltage is independent of irradiance, as determined by King (1997).

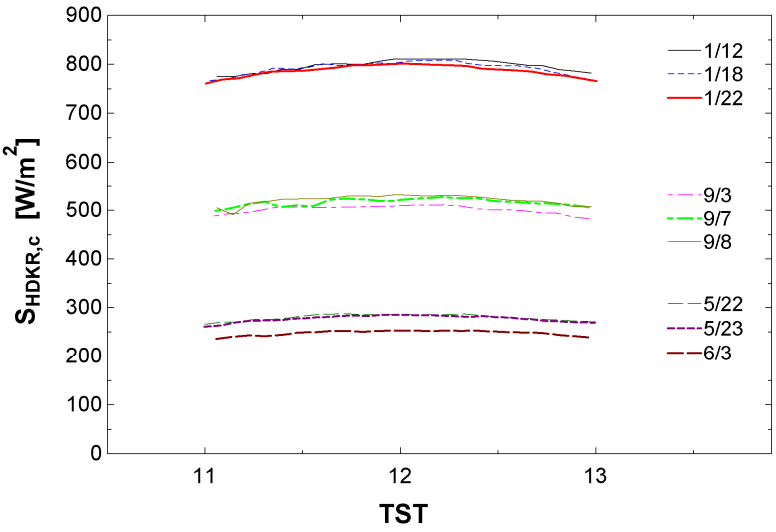

Figure 3.5: POA corrected absorbed solar radiation calculated using the HDKR radiation model verse solar time for nine clear days throughout the year

3.2.4.1.2 Translation to Reference Condition

For these nine selected days and times, the short-circuit current at reference conditions was calculated by multiplying the measured short-circuit current by the ratio of the absorbed reference irradiance to the absorbed radiation, as given in Equation (3.18). The absorbed radiation was calculated with the HDKR radiation model using beam and diffuse inputs, with model equations given in Section 2.3.4. This procedure deviates from the procedure used by Fanney (2006) where the measured short-circuit current was multiplied by the ratio of the reference irradiance to the normal irradiance, with the orientation of the modules determined with two-axis tracking. Since these data were gathered from stationary modules, the absorbed radiation was used instead of the incident normal because it compensates for cosine and reflection losses. No correction was applied to the open-circuit voltage as it is assumed the corresponding temperature coefficient has no irradiance dependence.

$$I_{sc,ref,calc} = I_{sc,meas} \cdot \frac{1000\ \left[W/m^2\right] \cdot (\tau\alpha)_n}{S_{HDKR}} \tag{3.18}$$

3.2.4.1.3 Regressions of Translated Data

A least-squares linear regression was performed for each day and for each set of three days for the short-circuit current and open-circuit voltage versus the module backside temperature. The slope of the regressions are the temperature coefficients of short-circuit current and open-circuit voltage, respectively, with the means and other statistical measures given in Table 3.1 and Table 3.2.

Table 3.1: Short-circuit current temperature coefficient and associated statistics calculated from nine days for four different cell technologies

	α_{Isc} [A/°C]			
n = 9	**Mono-Si**	**Poly-Si**	**2-a-Si**	**CIS**
mean	0.001093	0.005848	0.003390	0.016748
% error*	-37.5	52.3	465	>1000
std. dev.	0.007598	0.01116	0.003867	0.027166
max.	0.013005	0.027822	0.011703	0.078124
min.	-0.01186	-0.00995	-0.00044	-0.00558

*percent error difference of mean relative to value determined by NIST

Table 3.2: Open-circuit voltage temperature coefficients and associated statistics calculated from nine days for four different cell technologies

	β_{Voc} [V/°C]			
n = 9	**Mono-Si**	**Poly-Si**	**2-a-Si**	**CIS**
mean	-0.1500	-0.1309	-0.3871	-0.0908
% error*	1.56	-4.76	-6.04	-0.90
std. dev.	0.008689	0.006733	0.102086	0.012123
max.	-0.13866	-0.12139	-0.2339	-0.07514
min.	-0.16785	-0.14127	-0.61265	-0.11071

*percent error difference of mean relative to value determined by NIST

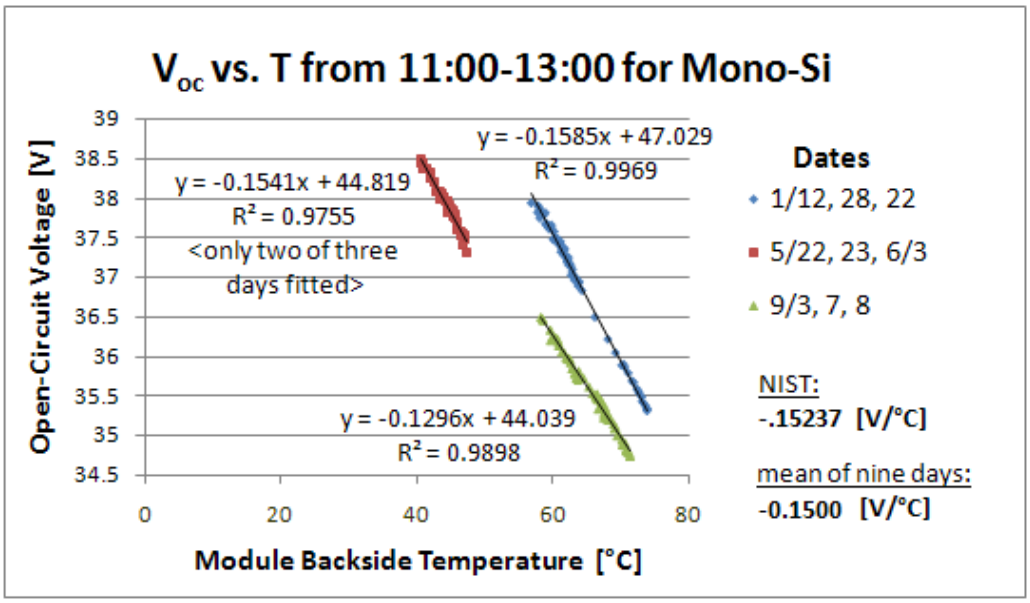

Figure 3.6: **Least-squares linear regression analysis of select operating data for open-circuit voltage verse module temperature to determine the open-circuit voltage temperature coefficient for the Mono-Si module**

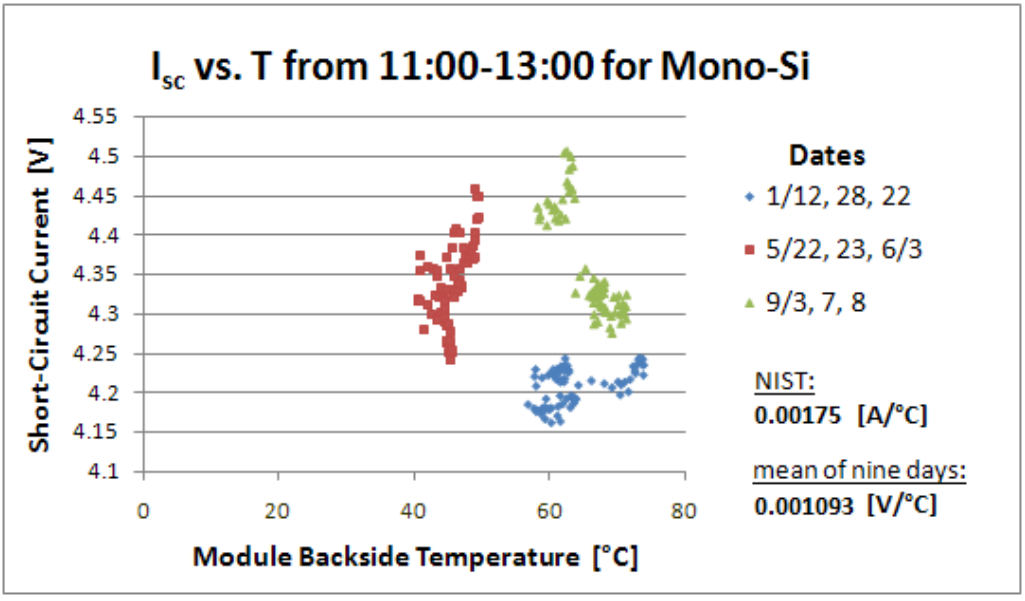

Figure 3.7: **Least-squares linear regression analysis of select operating data for short-circuit current verse module temperature to determine the short-circuit current temperature coefficient for the Mono-Si module**

It is shown in Figure 3.6 for the Mono-Si module (and in Appendix E for the other three modules) that the open-circuit voltage is not strictly a function of temperature and therefore may depend on irradiance; this dependence is similar to that displayed by the five-parameter model. In Figure 3.7 it appears that there is no direct relationship between module temperature and short-circuit current adjusted to SRC conditions according to the above procedure. The significance of these uncertainties in the two temperature coefficients is assessed by a sensitivity analysis of the five-parameter model in Section 3.4. For all model validation work, unless otherwise noted, the NIST-derived temperature coefficients will be used to calculate both the SRC and operating data derived model parameters and will be employed in model calculations. This decision is due to the close agreement of β_{Voc} calculated from operating data and the value derived by NIST and that α_{Isc} was not accurately calculated from operating data.

3.2.4.2 Variability of Operating Data Derived Parameters

A detailed study was performed to evaluate the variation in modeling errors when the model parameters are determined from operating data points at different conditions within the data analysis period (the temperature coefficients are constant and were measured by NIST). Model parameters were calculated from a subset of 11 clear days in the 'Clear Days…' dataset, with each of the days near the middle of each month of the year, except April because there were no diffuse radiation measurements during that month. Three sets of parameters were calculated from each of these days at the hours of 10:00, 12:00, and 14:00 (TST), resulting in a total of 33 different sets of model parameters.

Maximum power modeling errors for the back-insulated Mono-Si, Poly-Si with glass glazing, 2-a-Si, and CIS arrays are shown in Figure 3.8, with modeling errors at the other operating points given in Appendix F. Each point in the figures is the statistical error for the entire 'Clear Days…' dataset using the model parameters calculated at the indicated time and from the day in the middle of the indicated month. The horizontal line in the plots represents only one value and is the modeling error for the entire dataset when the model parameters were calculated using SRC data.

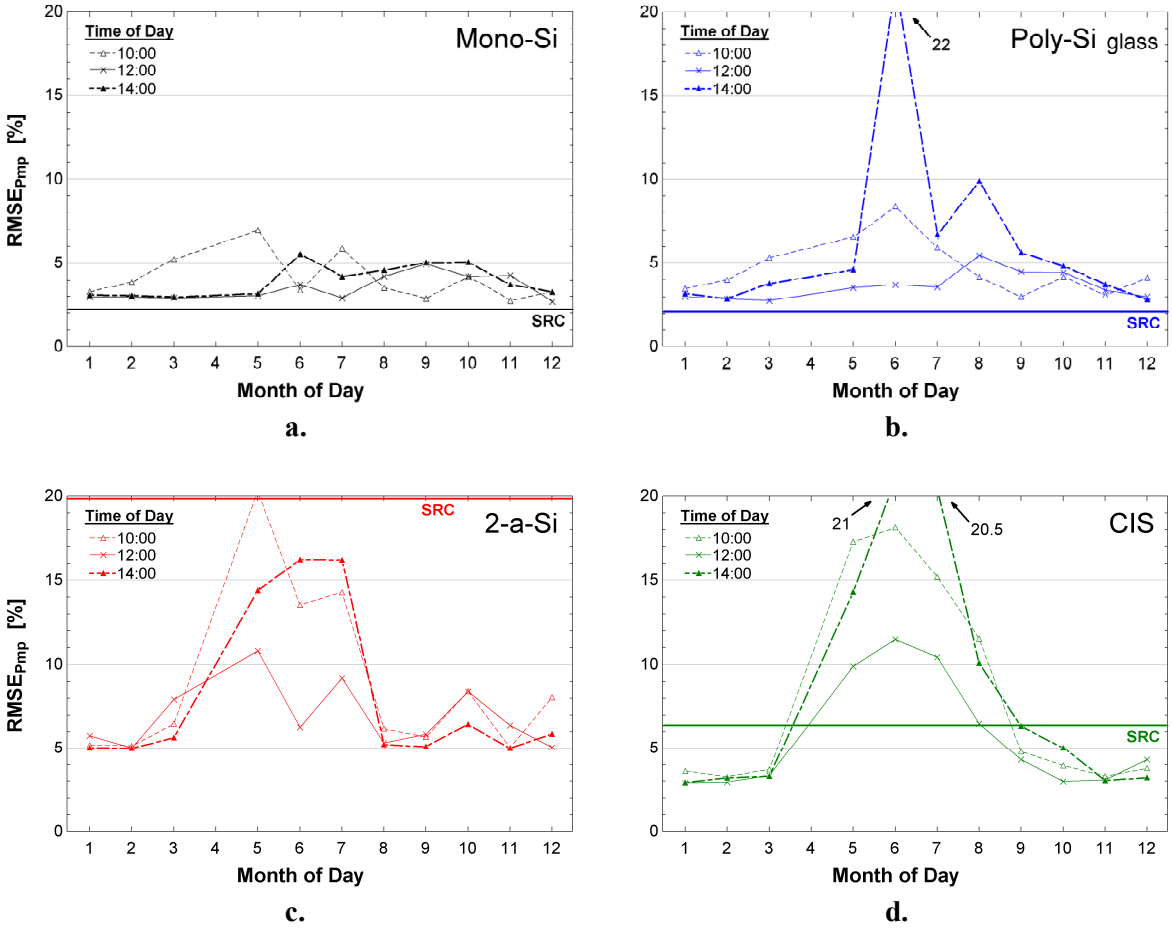

Figure 3.8: Statistical modeling errors of the five-parameter model for four backside insulated arrays on the *vertical curtain wall* test bed using the 'Clear Days…' dataset. Model parameters are calculated from operating data at the specified time from a day near the middle of the specified month.

The above figures show that the model is more accurate for 2-a-Si and CIS (i.e., the model agrees more closely with the measured data) when parameters are calculated from some select operating points than when parameters are calculated from SRC. The figures also show that there is a high variability in these modeling errors between different parameter sets. These errors range from -17% to 19% relative to errors from SRC derived parameters. Model errors using parameters calculated from SRC are generally low compared to those calculated from the operating data, except for the 2-a-Si array. The analysis was repeated for a second identical 2-a-Si array with the only difference being that it had no backside insulation. Analysis results for P_{mp} RMSE are compared to the original results in Figure 3.9, which shows that the five-parameter model predicts similar performances for both 2-a-Si arrays. The measurements for the 2-a-Si arrays therefore are considered precise, and faulty modules may not be the cause of the discrepancies with the other modules of different cell technologies. Parameters derived from SRC data will be used for all future modeling work because of the relatively low errors and that they provide a less subjective standard for comparison.

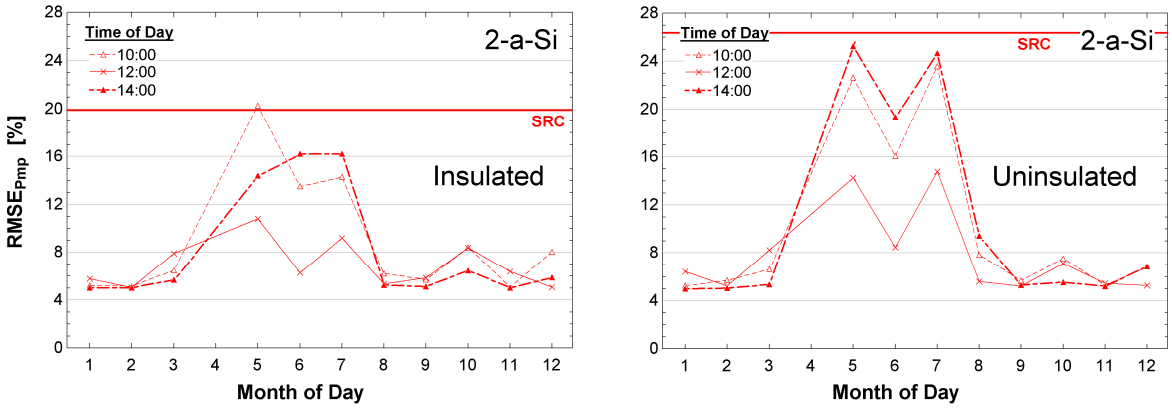

Figure 3.9: **Statistical modeling errors of the five-parameter model for two different 2-a-Si arrays on the *vertical curtain wall* test bed using the 'Clear Days…' dataset; one of the arrays is backside insulated and the other is not. Model parameters are calculated from operating data at the specified time from a day near the middle of the specified month.**

The high 2-a-Si modeling errors using SRC parameters, as shown in Figure 3.9, may be due to aging because the module was characterized at SRC before the yearly data were collected. There is no clear yearly trend in this model error data to support this hypothesis; however, this hypothesis is supported by a later analysis described in Section 4.1 that uses SRC data measured when the modules had progressively larger amounts of solar exposure.

Errors for all modules tend to be higher when parameters are calculated from summer month data. The increased errors are likely due to the uncertainty in the absorbed radiation calculation that is used for the model reference radiation. This uncertainty is introduced by the large incidence angles present during the summer, as these modules are mounted on a vertical south wall. These error plots show that if data at SRC is not available, the model will still be reasonably accurate when model parameters are derived from operating data if the

absorbed radiation can be accurately calculated, which for these test conditions with vertical module orientations is in the winter months at low incidence angles.

The modeling error plots in Figure 3.8 and Appendix F also show that there are areas for improvement in the five-parameter model. The model errors when using SRC parameters and operating data parameters derived at low incidence angles for the Mono-Si and Poly-Si are less than 4% for all characteristic performance values (I_{sc}, V_{oc}, I_{mp}, etc.). The 4% figure includes the effects of uncertainty in the measured solar radiation; perhaps the model cannot be further improved because of this inherent uncertainty in the measurements. However, the observed errors of 5-6% RMSE for the 2-a-Si I_{mp}, V_{mp}, and P_{mp} and CIS V_{mp} indicate that the five parameter model can possibly be improved for these technologies. The results show large P_{mp} and V_{mp} modeling errors for the CIS and 2-a-Si modules in summer compared to the winter, which do not correspond to large summer I_{mp} errors. These errors are likely not due to errors in the absorbed radiation calculation since they are not observed for the Mono-Si and Poly-Si modules.

3.3 Statistical Analysis of Temperature Coefficients

Due to the uncertainty in the temperature coefficients shown both in Table 3.1 and various manufacturer datasheets, a survey and statistical analysis were performed to determine if coefficients are significantly different between manufacturers and between technologies. If the differences are not significant, a representative value can be used in performance models, like the five-parameter model, as a default for when temperature coefficients are not available, thereby simplifying the input.

3.3.1 Data Collection

All cell and module datasheets that could be found on the internet, excluding BIPV and PV glass products due to their generally sparse datasheets, were collected from manufacturers who had a 2007 cell production greater than 0.1% (>4.28 MW) of the total (Hirshman, 2008), including production by subsidiaries. This amounts to 64 of approximately 170 manufacturers worldwide. Table 3.3 shows the number of cell and module models produced for each cell technology by the 64 manufacturers.

Table 3.3: The number of models of each cell technology by manufacturers who produced more than 0.1% of the total 2007 cell production

Technology	Number of Models
Monocrystalline Silicon	919
Polycrystalline Silicon	995
Amorphous Silicon	140
Copper-Indium Selenide (CIS)	8
Cadmium Telluride (CdTe)	16

It can be seen that relatively few manufacturers produce copper indium selenide (CIS), amorphous, or cadmium telluride (CdTe) cells/films. Table 3.4 shows the number of manufacturers, out of the 64, that provide the different temperature coefficients. $\partial I_{sc}/\partial T$ (α) is the temperature coefficient for short-circuit current, $\partial V_{oc}/\partial T$ (β) is for open-circuit voltage, $\partial P_{mp}/\partial T$ (γ) is for maximum power, $\partial I_{mp}/\partial T$ (α_{mp}) is for current at maximum power, and $\partial V_{mp}/\partial T$ (β_{mp}) is for voltage at maximum power.

Table 3.4: The number of manufacturers, out of the number that produced more than 0.1% of the total 2007 cell market production, who provide the five different temperature coefficients

Temperature Coefficient	Number of Manufacturers
$\partial I_{sc}/\partial T$ (α)	52
$\partial V_{oc}/\partial T$ (β)	52
$\partial P_{mp}/\partial T$ (γ)	47
$\partial I_{mp}/\partial T$ (α_{mp})	3
$\partial V_{mp}/\partial T$ (β_{mp})	3

Manufacturers provide temperature coefficients either as absolute (i.e., A/°C) or relative to SRC (i.e., 1/°C or %/°C). Relative coefficients (%/°C) will be used as the basis for comparison in this study because they are independent of cell output. Coefficients provided as absolute are converted to relative using measured SRC conditions also provided in the datasheets. Two example transformations are given by Equations (3.19) and (3.20) for the short-circuit current temperature coefficient. These transformations are similar for open-circuit voltage and maximum power.

$$\alpha\left[\%/^{\circ}C\right] = \frac{\alpha\left[A/^{\circ}C\right]}{I_{sc}\big|_{SRC}\left[A\right]} \times 100\left[\%\right] \tag{3.19}$$

$$\alpha\left[\%/^{\circ}C\right] = \alpha\left[1/^{\circ}C\right] \times 100\left[\%\right] \tag{3.20}$$

3.3.2 Assumptions

The temperature coefficients are assumed to be measured for each cell and module model. However, this may not be the case because manufacturers typically give the same coefficient

for a number of models. Usually these coefficients are relative and thus scale with output, but for a couple manufacturers they are absolute and correspond to models of different outputs. A few manufacturers even provide the same coefficients for models of different cell technologies, with the two witnessed cases being for monocrystalline and polycrystalline products.

3.3.3 Procedure

Manufacturers chosen to be included in the study are those that produced at least four models of monocrystalline and four models of polycrystalline silicon cells. An equal number of models of each technology are needed to minimize bias in the statistical analysis. The number of models was chosen arbitrarily after surveying the number of models of each technology produced by each manufacturer, see Appendix G. Eight models represent the best balance between including a high number of manufacturers and a high number of models; however, due to time and resource constraints, half that number was used. Technologies included in the analysis were restricted to mono- and polycrystalline silicon because relatively few manufacturers produce cells of the other technologies.

Of the 64 manufacturers that produced more than 0.1% of the total 2007 production, 17 met the above criterion and were included in the analysis. Four models of each technology were randomly selected from each manufacturer and the temperature coefficients of short-circuit current and open-circuit voltage were gathered from the respective manufacturer datasheets. The temperature coefficients of voltage and current at maximum power were excluded from the analysis because none of the 17 manufacturers provided them.

3.3.4 Data Summary and Analysis

An overview of the data is shown as the box-whisker plots in Figure 3.10. The dark line in the box is the median, the upper and lower edges of the box are the medians of the upper and lower half of the data, respectively, and the end reaching brackets are minimum and maximum values minus any statistical outliers. Statistics for the data set are given in Table 3.5. Data from one manufacturer were removed from the analysis because it was a distant outlier and it appeared that they were mislabeled as absolute instead of relative.

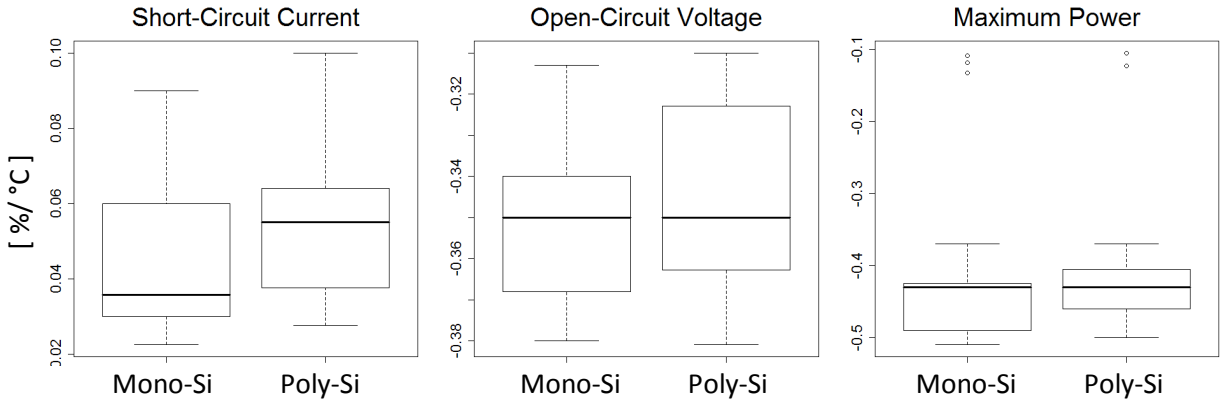

Figure 3.10: Box-whisker plots of short-circuit current, open-circuit voltage, and maximum power temperature coefficients of the four models for each of the 16 companies used in this statistical analysis, after one manufacturer's suspect data was removed

Table 3.5: Temperature coefficient statistics for two cell technologies from 36 different cell and module manufacturers

Values in [%/°C]		$\partial I_{sc}/\partial T$ (α)	$\partial V_{oc}/\partial T$ (β)	$\partial P_{mp}/\partial T$ (γ)
Mono-Si	**Mean**	0.0453	-0.3506	-0.4263
	Standard Deviation	0.0188	0.0184	0.0892
	Maximum	0.0900	-0.3130	-0.1090
	Minimum	0.0224	-0.3800	-0.5100
Poly-Si	**Mean**	0.0522	-0.3467	-0.4202
	Standard Deviation	0.0164	0.0207	0.0852
	Maximum	0.1000	-0.3100	-0.1050
	Minimum	0.0275	-0.3810	-0.5000

Three statistical two-way layouts were performed for each of the temperature coefficients, but an analysis of variance (ANOVA) showed that no temperature coefficient is statistically the same for every manufacturer. A statistical Tukey multiple comparison analysis (Wu, 2000) was performed to compare every manufacturer pair combination for each temperature coefficient, but it was found that no manufacturer has all unique coefficients. Residual plots of the statistical linear model of the two-way layouts were created and the data outliers were reexamined, but the values were still not deemed outliers. It can be seen in Table 3.5 that the mean coefficients for each cell technology are within one standard deviation of the respective means for the other technology.

3.3.5 Conclusion

The results of the statistical two-way ANOVA were that there is significant difference between manufacturer's reported temperature coefficients of short-circuit current, open-circuit voltage, and maximum power for both the Mono-Si and Poly-Si technologies. This observation is a reason against setting characteristic temperature coefficients for each

technology; however, a sensitivity analysis of the model, as described in Section 3.4, shows that the model is rather insensitive to the short-circuit current temperature coefficient (α_{Isc}) if it is set to the mean value of the Mono-Si and Poly-Si coefficients (0.049 %/°C) for all four technologies. The model *is* shown to be sensitive to the value for the open-circuit voltage temperature coefficient (β_{Voc}), but this value can be accurately calculated from operating data if it is not readily available, as shown in Section 3.2.4.1.

3.4 Sensitivity Analysis

3.4.1 Description

A sensitivity analysis was performed on the present five-parameter model (De Soto, 2006) to determine acceptable tolerances for the model inputs and to determine which inputs most significantly affect model predictions. Fifteen constant model inputs that were suspected to have significant uncertainty and a strong effect on the model performance were included in this analysis; a table of all the model inputs is given in Appendix H. The analysis was performed by adjusting one variable at a time around the actual value and calculating the root-mean-squared (RMSE) and mean-bias errors (MBE) between the model predictions and measured values for the 'Clear Days…' dataset. The analysis used data from the Mono-Si module, but a limited analysis was also performed using the 2-a-Si data with an aim to bracket the results between the best and worst modeled technologies.

3.4.2 Summary of Results

A summary of the sensitivity analysis using Mono-Si data is given in Table 3.6. This table gives the variable ranges that would result in less than 1% change in RMSE and the MBE of

the maximum power (P_{mp}) modeling error. Plots of the modeling error versus model input for each variable when using Mono-Si data are provided in Appendix I. A discussion on how to interpret the results in Table 3.5 follows.

Table 3.6: Parameter sensitivity in ascending order for the five-parameter model using Mono-Si data and the 'Clear Days…' dataset showing the variable ranges that result in less than 1% change in P_{mp} modeling error

Variable	≤ 1% |ΔRMSE P_{mp}|	≤ 1% |ΔMBE P_{mp}|
ρ_g (w/ POA)	< -100%, > 600%	< -100%, > 600%
	< 0, > 0.7	< 0, > 0.7
K	< -100%, 650%]	< -100%, 275%]
L	< -100%, 650%]	< -100%, 270%]
	< 0 m, 0.045 m]	< 0 m, 0.022 m]
ΔT_{mod}	< 1 K, > 20 K	< 1 K, > 20 K
C	[-270%, 480%]	[-130%, 160%]
α_{Isc}	[-250%, 150%]	[-94%, 92%]
	[-0.0026 A/C, 0.0044 A/C]	[0.00011 A/C, 0.0034 A/C]
	[-0.059 %/K, 0.10 %/K]	[0.0025 %/K, 0.078 %/K]
n_{glaz}	[-27%, 110%]	[-15%, 64%]
	[1.11, 3.19]	[1.29, 2.51]
ρ_g (w/o POA)	[-80%, 40%]	[-20%, 20%]
	[0.02, 0.14]	[0.08, 0.12]
$E_{g,ref}$	[-21%, 36%]	[-11%, 12%]
	[0.88 eV, 1.52 eV]	[1 eV, 1.25 eV]
$I_{sc,ref}$	< -5%, 11.8%]	< -5%, 6%]
β_{Voc}	[-8.6%, 13%]	[-4.6%, 5.0%]
$V_{oc,ref}$	[-4.4%, 5.4%]	[-2.2%, 2.1%]
$V_{mp,ref}$	[-3.8%, 2.3%]	[1.4%, 1.5%]
$I_{mp,ref}$	[-3.2%, 2.7%]	[-1.3%, 1.2%]
S_{ref}	[-2.2%, 2.8%]	[-1%, 1%]
ΔT_{ref}	[-5.4 K, 4.1 K]	[-2 K, 2 K]

3.4.3 Comparison to 2-a-Si Data

The minimum RMSE errors occur at the baseline and SRC values for all model inputs when using the Mono-Si data, but this is not the case when using the 2-a-Si data, with two comparisons given in Figure 3.11 and Figure 3.12; baseline errors are given in Table 3.7. This lack of inflection for the 2-a-Si RMSE suggests that the module characterization or absorbed radiation data for the 2-a-Si array may be inaccurate. This seemingly poor characterization of the 2-a-Si array is supported by the comparison in Section 3.2.4.2 between modeling errors using model parameters derived from SRC data and those derived from operating data; results using the two different parameter sets were similar for all modules except the 2-a-Si, which had significantly higher modeling errors when using the SRC derived parameters. This apparently poor characterization of the 2-a-Si modules does appear to be caused by module aging, which is examined in Section 4.1.

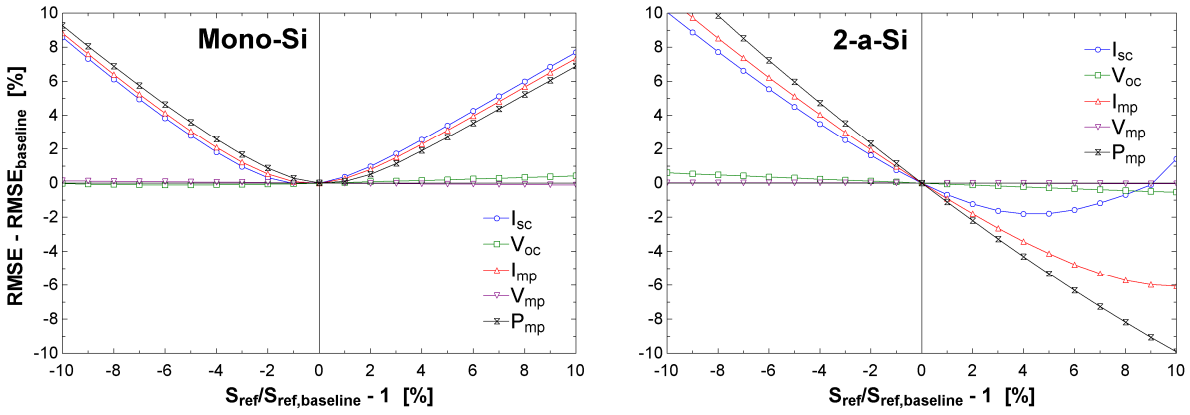

Figure 3.11: Sensitivity of five-parameter model to the standard reference irradiance using (a.) Mono-Si and (b.) 2-a-Si data

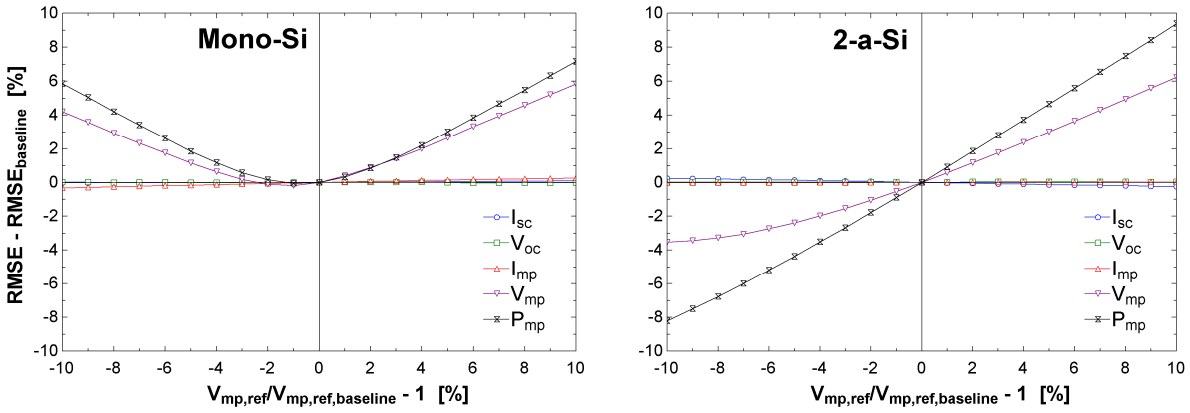

Figure 3.12: Sensitivity of five-parameter model to the maximum power voltage at SRC using (a.) Mono-Si and (b.) 2-a-Si data

Table 3.7: Baseline RMS errors between model predictions and measured values for the Mono-Si and 2-a-Si modules for the 'Clear Days…' dataset

Operating Point	Mono-Si (RMSE %)	2-a-Si (RMSE %)
I_{sc}	2.5	5.3
V_{oc}	0.43	4.9
I_{mp}	2.6	11
V_{mp}	1.7	9.7
P_{mp}	2.2	20

3.4.4 Analysis and Simplification of Model Inputs

3.4.4.1 Ground Reflectance

Ground reflectance (ρg) did not have a significant affect on model performance if the value was between 0 and 0.7, which represents conditions for no reflectance and bright snow, respectively (Duffie and Beckman, 2006), and if the absorbed radiation was corrected using the measured POA radiation. The POA radiation already contains the ground reflected radiation, so when it is used to correct the absorbed radiation it removes the model's dependence on ρg. If the absorbed radiation was not corrected with the POA radiation, than the value used for ρg would need to be accurately determined. The range for ρg without a

POA radiation correction that results in less than a 1% change in Pmp RMSE was found to be [0.02, 0.14], where 0.1 is the average value for asphalt (ACPA, 2002).

3.4.4.2 Product of Glazing Extinction Coefficient and Glazing Thickness

The glazing extinction coefficient (K) and the glazing thickness (L), which only occur as the product $K \cdot L$ in the transmittance-absorptance $(\tau\alpha)$ equation, do not have a significant effect on the model performance. These model inputs therefore do not need to be determined to a high accuracy; setting $K \cdot L$ to **0** would result in less than a 0.4% change in P_{mp} RMSE.

3.4.4.3 Short-Circuit Current Temperature Dependence

The short-circuit current temperature dependence (α_{Isc}), although given by the manufacturers, could be set to a value characteristic of the module technology. The survey of manufacturer datasheets in Section 3.3 showed that for a random sampling of 4 modules each from 17 manufacturers, the range of α_{Isc} for the Mono-Si technologies was [0.0224, 0.0900] %/°C with an average of 0.0453 %/°C. This range, along with the range found for the Poly-Si modules, is within the range determined by the sensitivity analysis using the Mono-Si data that results in less than a 1% change in P_{mp} RMSE. As a result, if the surveyed range of α_{Isc} is representative of all Mono-Si and Poly-Si modules and if the results of the sensitivity analysis do not depend on the module data used, then the average of the surveyed Mono-Si and Poly-Si coefficients (**0.049 %/K**) would be a good characteristic value for both module technologies. This value could then be used without affecting model performance and it would allow the model parameters to be found without having any manufacturer data. It was

shown in Section 3.2.4.1 that the model parameters and the temperature coefficient of open-circuit voltage (β_{Voc}) could be accurately calculated from operating data.

3.4.4.4 Glazing Refractive Index

The range of the glazing refractive index (n_{glaz}) that results in less than a 1% change in P_{mp} RMSE includes values characteristic of multiple glazing materials. The range for n_{glaz}, [1.11, 3.19] includes the values for the glazing materials of this study's modules and many others: glass (1.53) (Duffie and Beckman, 2006), ETFE (1.4) (DuPont, 2006), PVDF (1.42) (Brandrup, 2006), transparent zinc oxide (1.84) (GÜMÜŞ, 2006), and EVA (1.48) (Brandrup, 2006). A refractive index of **1.53** can be used for all these glazing materials and would keep the change in P_{mp} RMSE below 0.05%.

3.4.4.5 Material Band Gap Energy

The range of the material band gap energy ($E_{g,ref}$) that results in less than a 1% change in P_{mp} RMSE includes values characteristic of multiple cell technologies. The range for $E_{g,ref}$, [0.88, 1.52] eV includes the values for silicon (1.1 eV), CIS (1.02 eV), as well as CIGS (1.15 eV), cadmium telluride (1.49 eV), gallium arsenide (1.43 eV) and many others (Luque, 2003). The average of this band gap range, **1.2 eV**, could be used for all of these cell technologies and would keep the change in P_{mp} RMSE below 0.9%. This average value would be especially useful for multi-junction cells that include materials of different band gap energies.

3.4.5 Model Simplification

Using the above characteristic values for α_{Isc}, $E_{g,ref}$, $K{\cdot}L$, n_{glaz}, and ρ_g and also setting C, the temperature dependence of the material band gap, to zero, the change in modeling errors for the four different panels is shown in Figure 3.13. Figure 3.14 shows results from a similar analysis but with α_{Isc} set to zero. It can be seen in the first figure that using the characteristic values and setting C to zero has very little effect on model performance- less than 0.5% change in P_{mp} RMSE for all four of the technologies. Removing the model's dependence on α_{Isc} by setting it to zero, however, has a significant effect, as seen in the second figure.

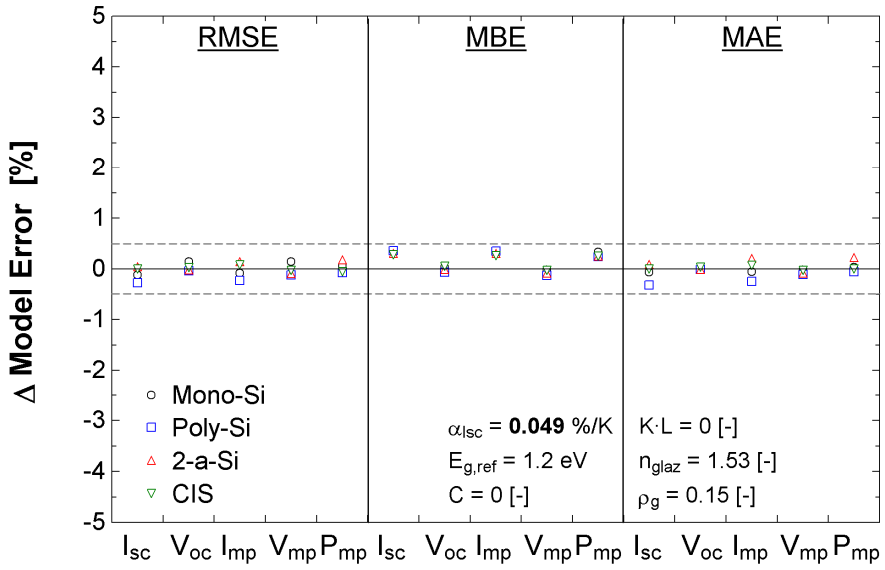

Figure 3.13: Changes in modeling error for the 'Clear Days…' dataset from using accepted values to using characteristic values of α_{Isc}, $E_{g,ref}$, $K{\cdot}L$, n_{glaz}, and ρ_g and setting C to zero

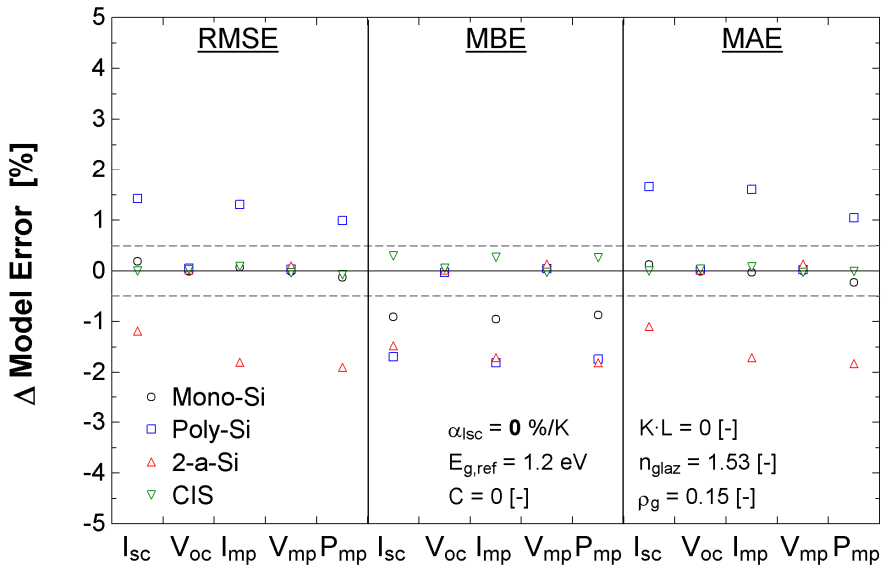

Figure 3.14: Changes in modeling error for the 'Clear Days…' dataset from using accepted values to using characteristic values of $E_{g,ref}$, $K{\cdot}L$, n_{glaz}, and ρ_g and setting C and α_{Isc} to zero

Chapter 4

Model Modifications

The five-parameter model accurately predicts the performance of monocrystalline silicon but exhibits larger modeling errors for other technologies, especially amorphous silicon. These larger errors are not just the result of uncertainties in the measured data because the model would then have a similar performance for every module and cell technology. The larger modeling errors for the amorphous silicon array indicate either inaccurate characterization data or a deficiency in the model for predicting the behavior of non-crystalline technologies; both of these possibilities are analyzed here.

4.1 Accounting for Aging of Amorphous Silicon

Five different sets of SRC data for the 2-a-Si modules installed in the *vertical curtain wall* were measured when the modules had progressively larger amounts of cumulative lifetime exposure to solar radiation. Three sets of SRC data were measured from identical control modules within one month of initial solar exposure. Two later sets of SRC data were measured from one of the installed modules approximately 20 months later. These five sets of SRC data and the corresponding exposures are given in Appendix A. The SRC data values are all lower than those in the earliest set.

The earliest 2-a-Si SRC data, measured after nine days of solar exposure, were used to calculate model parameters for the five-parameter model validation studies presented in previous sections. These parameters, calculated from higher SRC values, led the model to

over-estimate performance after the degradation period. The 2-a-Si modeling errors for the 'Clear Days…' dataset using parameters calculated from each of the four additional SRC datasets are shown in Figure 4.1, with the calculated parameters given in Appendix C. The modeling errors are lower when using parameters calculated from the higher exposure data because it is more representative of the module performance during the time period the dataset was measured, which is presumably after the degradation period. The errors given in the last plot, Figure 4.1d., are within 1% of those calculated using parameters derived from operating data at low incidence angles, as described in Section 3.2.4.2. Model validation work presented in the following sections use SRC data measured after the module has reached stable performance, in this case after 631 days of solar exposure.

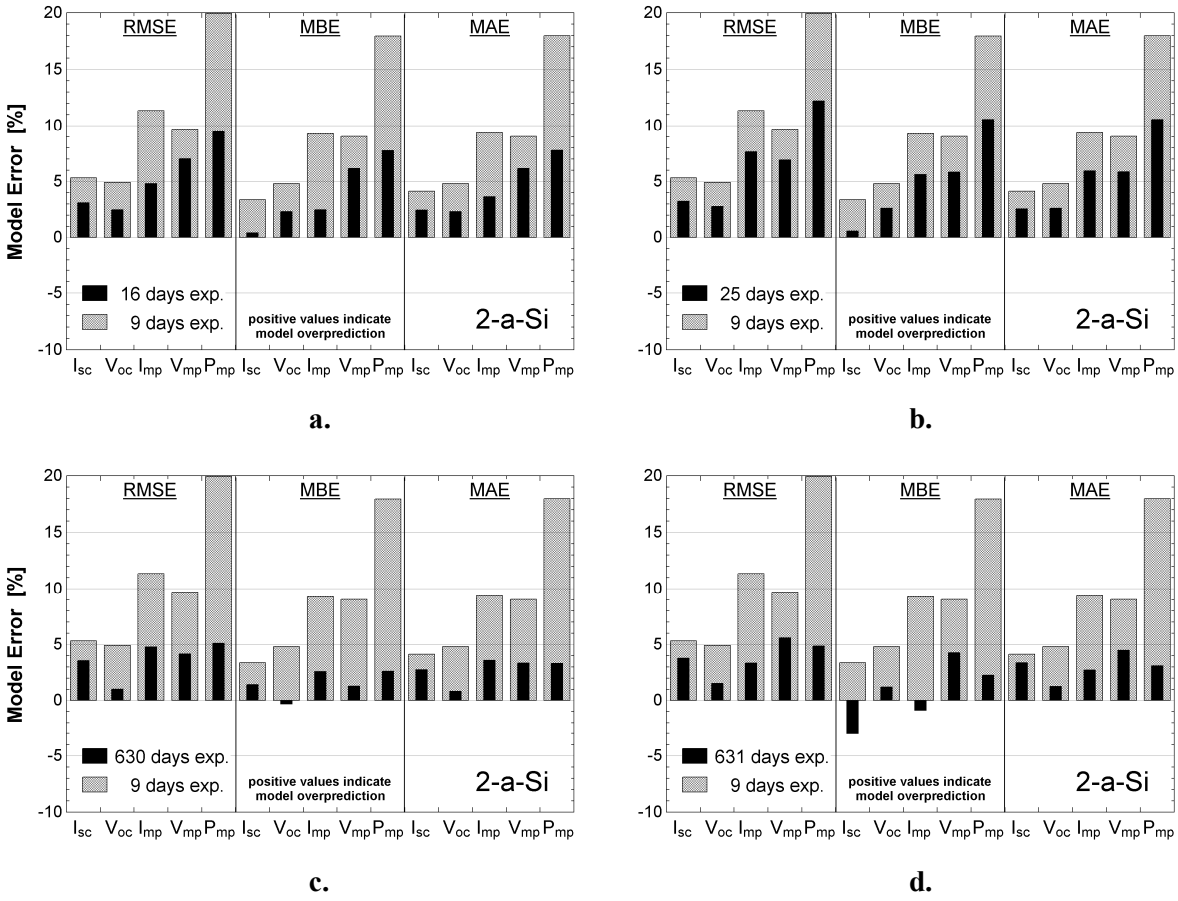

Figure 4.1: Statistical modeling errors of the five-parameter model for the 2-a-Si array on the *vertical curtain wall* test bed using the 'Clear Days…' dataset and different sets of SRC data measured at progressively larger amounts of solar exposure

4.2 Seven-Parameter Model

4.2.1 Description

The seven-parameter model is based on the one-diode equivalent circuit model of a PV cell and is similar to the five-parameter model. This model is an extension of the six-parameter model, which is currently used by the California Energy Commission (CEC) and is one of the models in the Solar Advisory Model (SAM) being developed by NREL. The seven-parameter model uses the same reference parameter values as the five-parameter model, but

adds two additional parameters that provide temperature and radiation dependence for two of the original parameters (Beckman, 2009).

4.2.2 Additional model parameters

The first new parameter is a non-linear series resistance temperature dependence, delta (δ), as given in Equation (4.1). The five-parameter model assumes a constant series resistance (R_s).

$$R_s\big|_T = R_{s,ref} e^{\delta\left(T - T_{ref}\right)} \tag{4.1}$$

The temperature coefficient of maximum power (γ) provides the additional information to solve for δ. Gamma is provided by NIST, who supplied these validation data, but is also provided by nearly all manufacturers on the module datasheets. The series resistance, R_s, was shown by De Soto (2006) to affect the area of the I-V curve nearest to the maximum power point. Both γ and δ provide temperature dependence in this operating region, and they are correlated with R_s by Equations (4.2) and (4.3) in the seven-parameter model.

$$I_{mp} V_{mp}\big|_T = P_{mp,ref}\left(1 + \gamma\left(T - T_{ref}\right)\right) \tag{4.2}$$

$$I_{mp}\big|_T = I_L - I_o\left(e^{\frac{V_{mp} + I_{mp} R_s}{a}} - 1\right) - \frac{V_{mp} + I_{mp} R_s}{R_{sh}}\Bigg|_T \tag{4.3}$$

The second new parameter is the *diode reverse saturation current radiation dependence*, $\underline{m}$, as given in Equation (4.4). The five-parameter model assumes only temperature dependence

for the diode reverse saturation current (I_o). The seven-parameter model adds radiation dependence to this parameter.

$$I_o\big|_{T,S} = I_{o,ref}\left(\frac{S_{ref}}{S}\right)^{m}\left(\frac{T}{T_{ref}}\right)^{3}\exp\left[\frac{1}{k}\left(\frac{E_g}{T}\bigg|_{T_{ref}} - \frac{E_g}{T}\right)\right] \tag{4.4}$$

The maximum power current and voltage at 200 W/m^2 and 25°C provide additional information to solve for $\underline{m}$. Although the 200 W/m^2 data will soon be provided by manufacturers as required by the California Energy Commission (CEC, 2008), it was determined in the present analysis by linear regression of approximately 20 operating points nearest to these conditions. Details on individual regressions are given in Appendix J. The parameter, $\underline{m}$, is solved by fitting the derivative (slope) of the maximum power characteristic equation to zero at 200 W/m^2 and 25°C. This fit at 200 W/m^2 is intended to provide better modeling at low radiation. Model code and solution procedure are provided in Appendix B and model parameters are given in Appendix C.

4.2.3 Model Error

Modeling errors are calculated for the seven-parameter model for the *vertical curtain wall* Mono-Si and 2-a-Si arrays which represent the best and worst modeled technologies, respectively, using the five-parameter model. The errors are given in Figure 4.2 and Figure 4.3 for the 'Clear Days…' and 'January…' data sets, respectively. Modeled versus measured values are given in Appendix D.

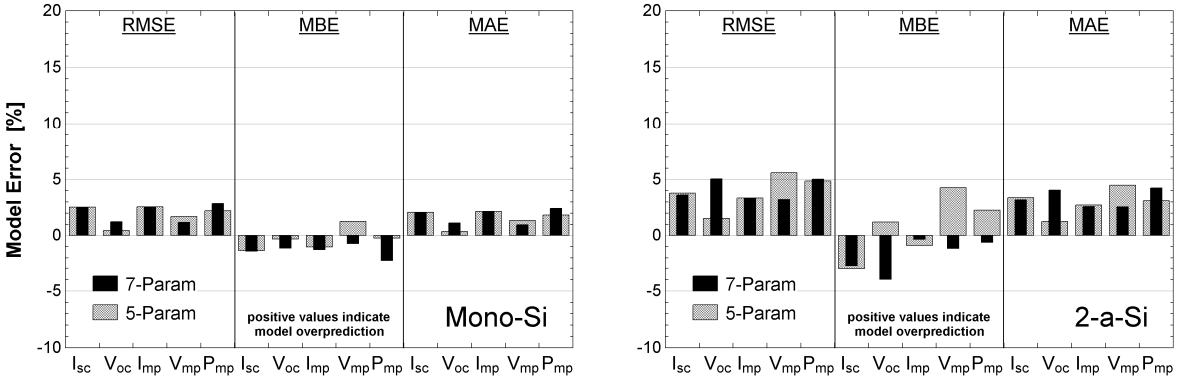

a. **b.**

Figure 4.2: Five and seven-parameter modeling errors using the 'Clear Days…' data set for (a.) Mono-Si and (b.) 2-a-Si technologies

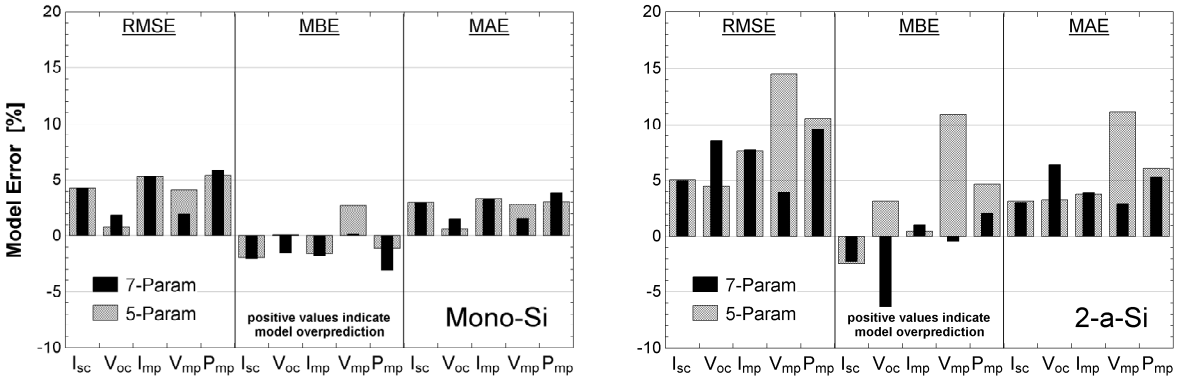

a. **b.**

Figure 4.3: Five and seven-parameter modeling errors using the 'January…' data set for (a.) Mono-Si and (b.) 2-a-Si technologies

It is shown in the above figures that the primary differences in predictions between the five and seven-parameter models are for V_{oc} and V_{mp}. The seven-parameter model exhibits *higher* V_{oc} and *lower* V_{mp} RMS modeling errors as a result of a negative shift in the predicted voltages, as shown by the bias errors and better illustrated by the absolute errors shown in Figure 4.4. The much lower V_{mp} modeling errors for the 'January…' dataset results in approximately 1% lower RMSE for P_{mp}.

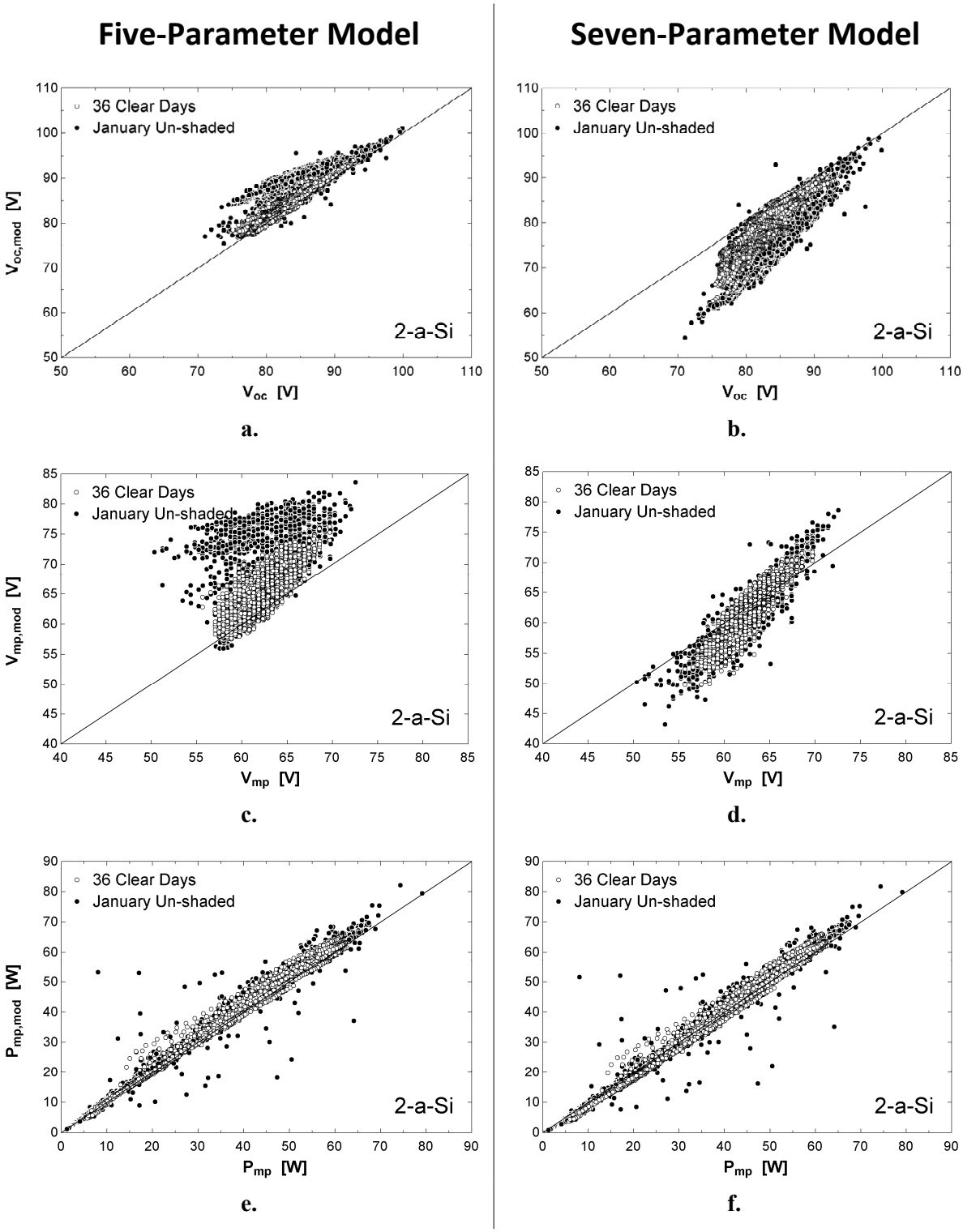

Figure 4.4: Modeled versus measured values for 2-a-Si using the 'Clear Days…' and 'January…' datasets. Modeled values using the five-parameter model are in the left column of plots and those modeled with the seven-parameter model are in the right column.

The seven-parameter model can be made a six-parameter model by setting either the δ or m parameters to zero, because the original five parameters are not dependent on the additional manufacturer data needed to solve for δ and m. The modeling errors of these two six parameter model iterations are calculated for the 2-a-Si array using the 'January…' data set, and are given in Figure 4.5. These results show that the difference in behavior between the five and seven-parameter models is caused almost entirely by the addition of the m parameter, with the δ parameter having minimal effect.

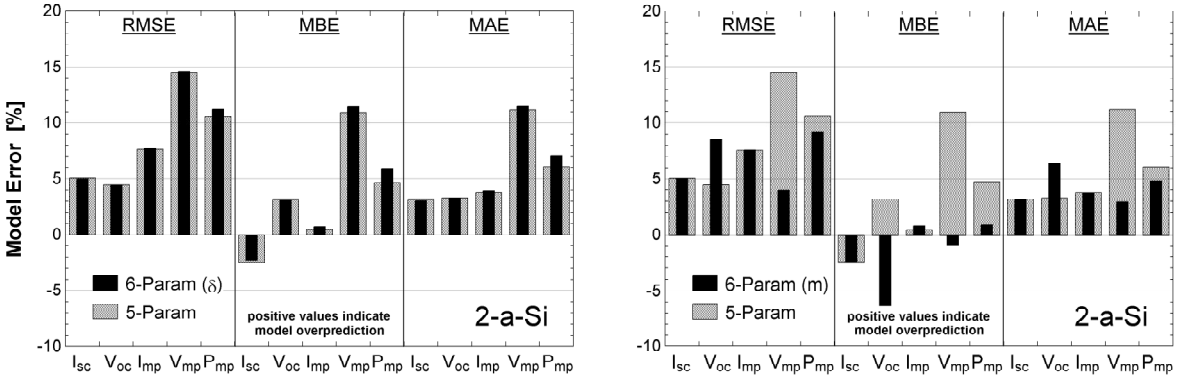

Figure 4.5: Five and six-parameter modeling errors for 2-a-Si using the 'January…' dataset. The six-parameter model errors in (a.) are when $\underline{m} = 0$, while those in (b.) are when $\delta = 0$.

An explanation of the shift in predicted voltages from the five to seven-parameter models is found by examining the effect of $\underline{m}$, as shown in Figure 4.6. (The effects of other model parameters are given in Appendix K). Constraining the model at maximum power using the 200 W/m^2 data translates V_{mp}, lowering its respective bias error, but it also translates V_{oc}, increasing its respective bias error.

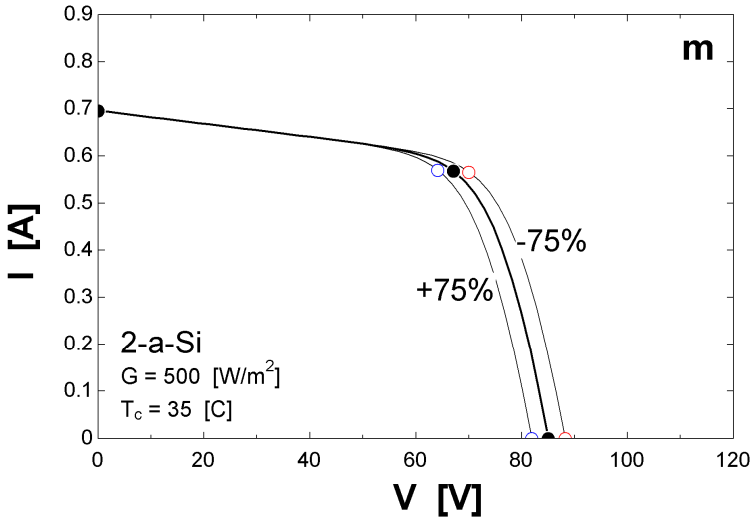

Figure 4.6: Effect of parameter *m* in the seven-parameter model on the behavior of the I-V curve

4.3 Evaluation of Parameter Temperature and Radiation Dependence

4.3.1 Test Procedure

The model parameters were back-calculated from the model characteristic equation using measured 2-a-Si data from the 'January…' dataset and the four remaining model parameters to determine if there are any additional radiation or temperature dependencies of the parameters in the five-parameter model. The four parameters used for back-calculation were transformed from the reference parameters using the current temperature and radiation relations given in Section 3.1.2. The calculated parameters for 2-a-Si are overlaid on the modeled parameters in the left plots in Figure 4.7.

4.3.2 Data Dependence

All calculated parameter values show slight disagreement with modeled values, with the modified ideality factor (a) having the largest apparent disagreement. A linear regression of the calculated values of $\underline{a}$ as a function of temperature was used in place of the current temperature relation and the model was re-run for the dataset using this regression. The calculated parameters using the regression for $\underline{a}$ are overlaid on the modeled parameters in the right plots in Figure 4.7. Better agreement between the modeled and calculated values of I_o, and R_{sh} result, with little change in I_L and R_s. The light current (I_L) is still in good agreement with the current relation, and R_s still has no discernable correlations with temperature or radiation.

Using original temperature relation for *a*

Using linear regression of calculated values for *a*

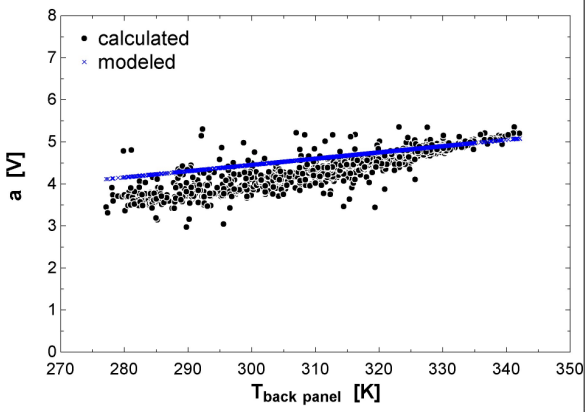

a.

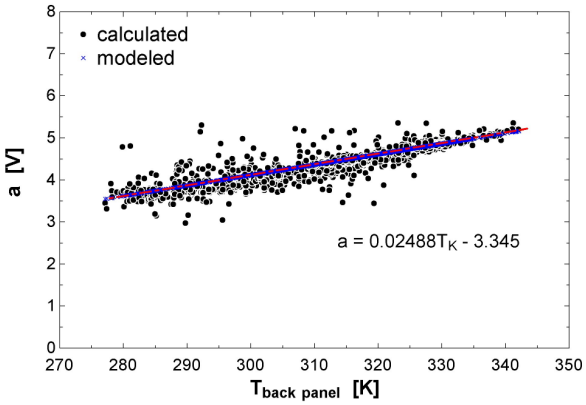

b.

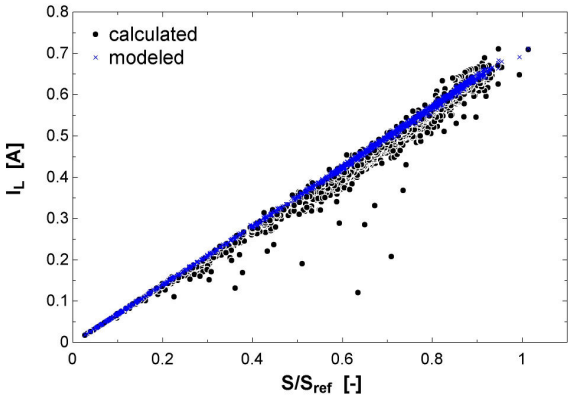

c.

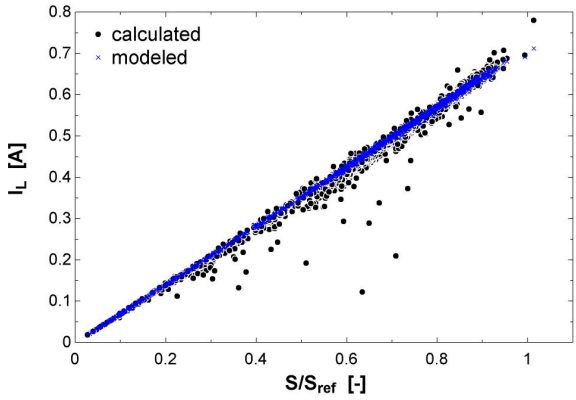

d.

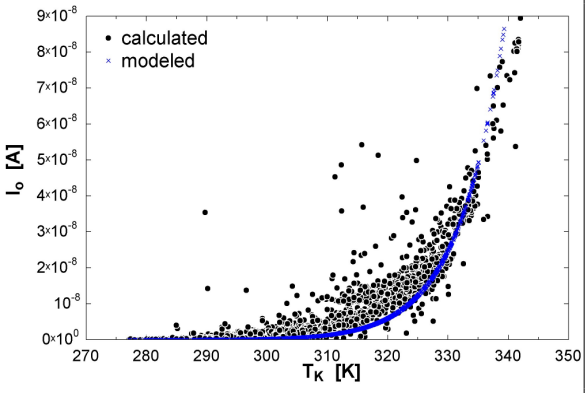

e.

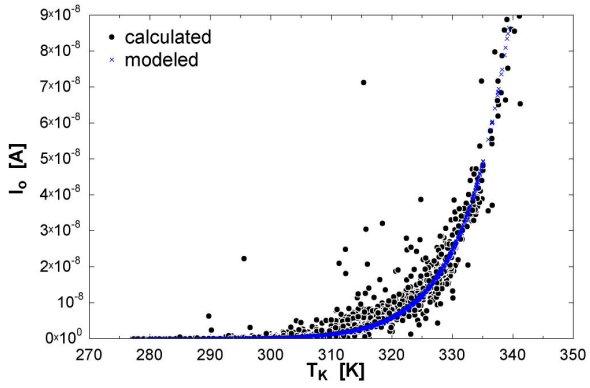

f.

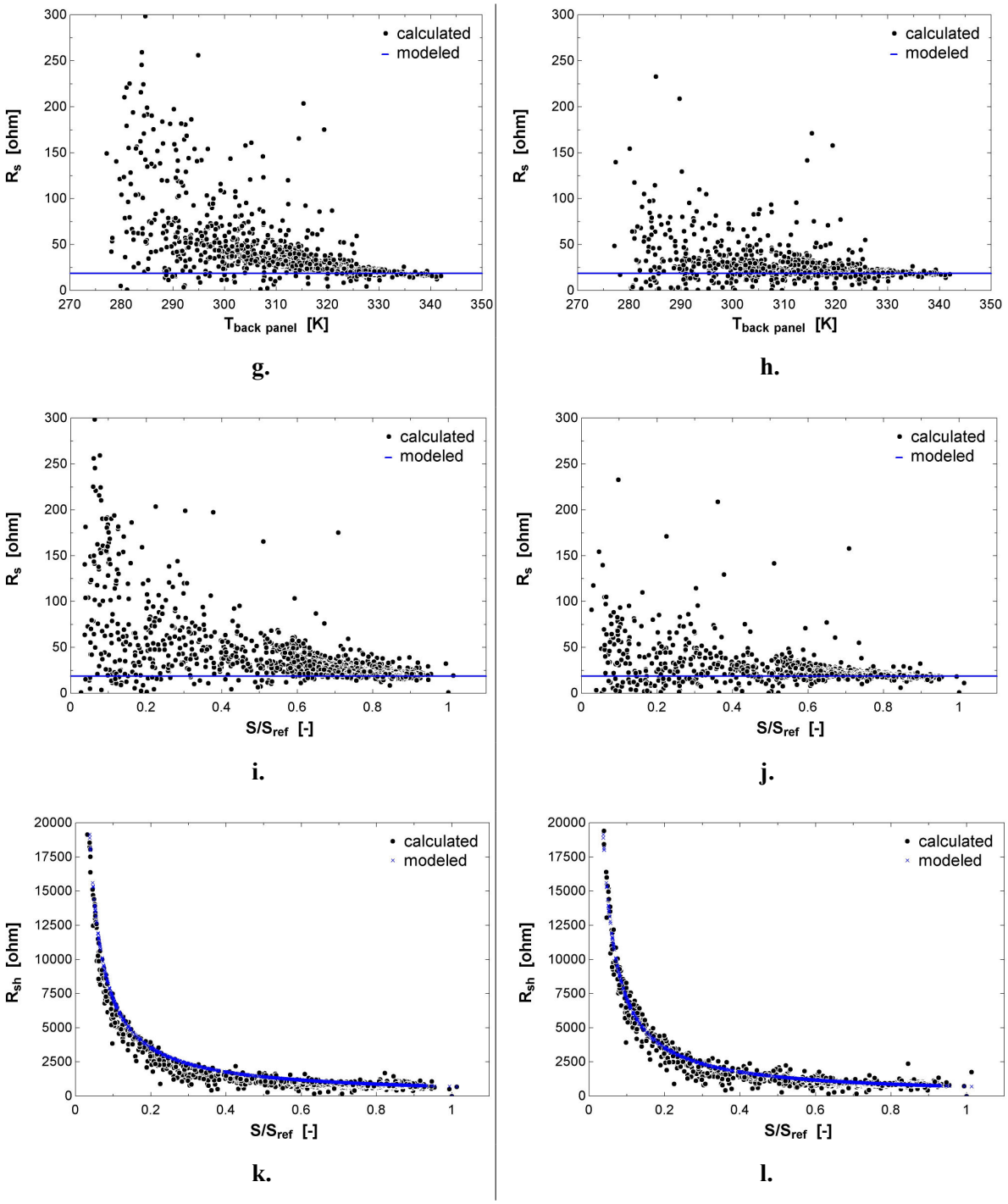

Figure 4.7: Parameters in the five-parameter model, modeled using the current temperature and radiation relations, and back calculated using the model characteristic equation and the four other modeled parameters

4.3.3 Analysis

In the above figures, all model parameters appear correctly related to temperature and radiation at maximum power when using the regression for $\underline{a}$. The large scatter in R_s (Figure 4.7g.-j.) reinforces the finding in Section 4.2.3 that δ (the new parameter in the seven-parameter model affecting R_s) has little effect on the model. The $\underline{a}$ regression resulted in a 3% drop in P_{mp} RMSE modeling errors using the 'January…' dataset, as shown in Figure 4.8a. This improvement is caused by a biasing, or shifting, of the maximum power voltage. The open-circuit voltage was also shifted by the modified $\underline{a}$, which is consistent with changes to $\underline{a}$, illustrated by Figure 4.8b. The statistical errors for the dataset, however, are still ~3% RMSE higher than those for the Mono-Si, shown in Figure 4.9. Since the model parameters appear to have the correct temperature and radiation relations after using the modified $\underline{a}$, and the modeling errors could still decrease ~3%, the model deficiency may be an incorrect equivalent circuit, rather than a parameter relation.

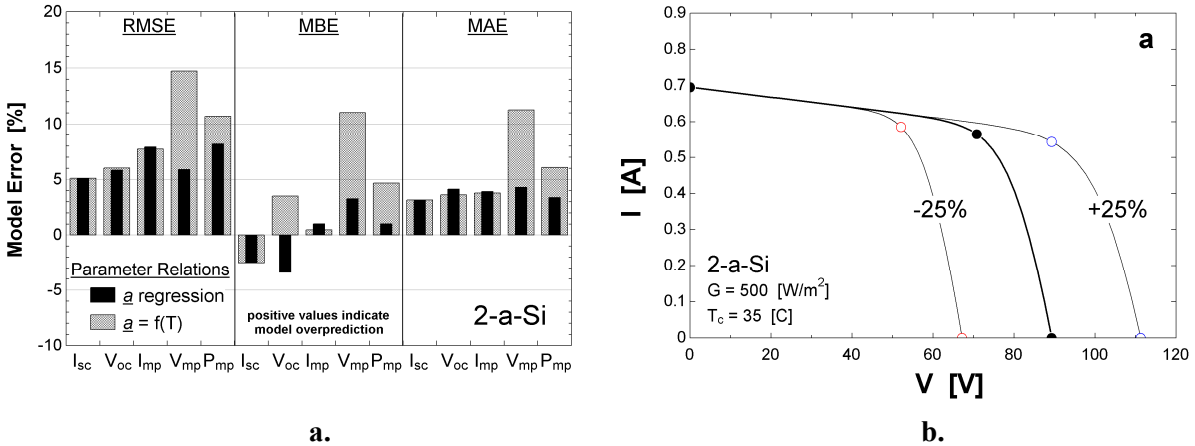

a. b.

Figure 4.8: Effect of changes in the $\underline{a}$ parameter on (a.) the modeling errors which compare the use of a best-fit linear regression for $\underline{a}$ to the current temperature relation and (b.) the individual I-V curves

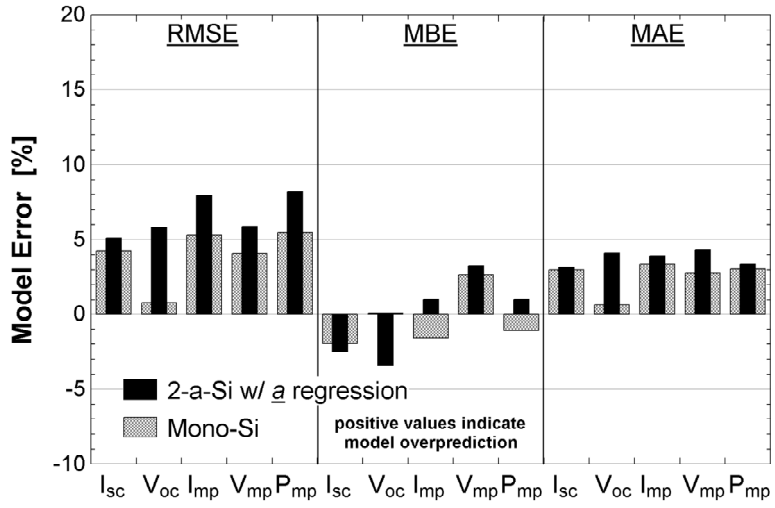

Figure 4.9: Five-parameter modeling errors using the 'January…' dataset for Mono-Si and for 2-a-Si using a linear regression of the back-calculated values for *a*

4.4 Recombination Current Differentiation

4.4.1 Model Description

Previous electrical circuit modeling efforts in this research have used the equivalent circuit shown in Figure 4.10 (minus the dotted lines). A circuit proposed by Merten (1998) that includes an additional current sink, shown by the dotted lines in Figure 4.10, seeks to differentiate the recombination currents in the middle intrinsic layer of an amorphous silicon cell from the currents in the outer semiconductor regions. This intrinsic layer is not present in crystalline silicon cells but is the site of intense recombination in amorphous cells (Merten, 1998). Recombination currents are modeled in the five-parameter model as a single lumped current through the diode (Luque, 2003), and may not accurately capture their separate behaviors.

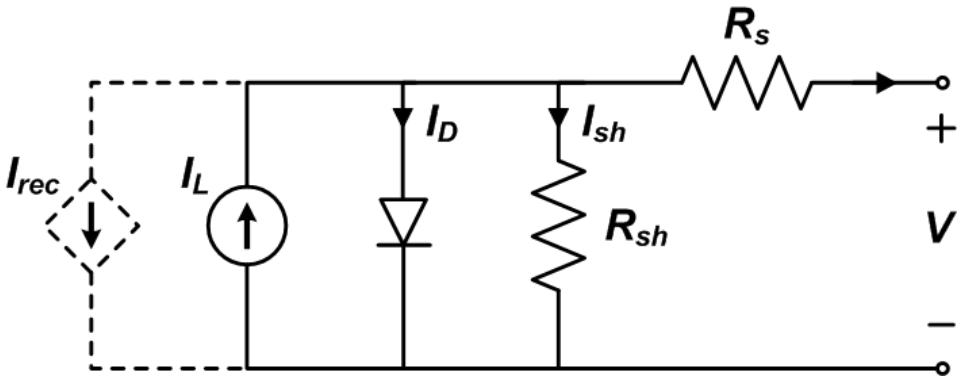

Figure 4.10: Equivalent circuit of a photovoltaic solar cell used in the five-parameter model with an added current sink shown in dotted lines

The additional current sink proposed by Merten is defined by Equation (4.5); it is dependent on the light current (I_L), the bias voltage ($V+IR_s$), the built-in voltage (V_{bi}), the thickness of the intrinsic layer (d_i), and a new parameter, the $\mu\tau_{eff}$ product. The built-in voltage (V_{bi}) for a module is calculated in this research as the product of the built-in single junction cell voltage (V_c), the number of junctions per cell (N_j), and the number of cells in series (N_s), as given by Equation (4.6). The built-in single junction cell voltage (V_c) is 0.9 V for amorphous silicon (Nonomura, 1982) and approximately 0.6 V for crystalline silicon (Luque, 2003), while N_j is provided by the manufacturer and N_s is either provided by the manufacturer or easily determined by a visual inspection of the module. The intrinsic layer thickness (d_i) terms and the $\mu\tau_{eff}$ product can be combined into a single new model parameter, designated as chi (χ) in future calculations.

$$I_{rec} = I_L \frac{d_i}{(\mu\tau)_{eff}\left[V_{bi} - (V + IR_s)\right]/d_i} \tag{4.5}$$

$$V_{bi} = V_c N_j N_s \tag{4.6}$$

4.4.2 Calculations

The new parameter χ ($d_i^2/\mu\tau_{eff}$) is simultaneously determined along with the original five parameters by constraining the characteristic equation of the new circuit with the maximum power temperature coefficient (γ) at maximum power and a non-reference temperature. The non-reference temperature used in this research is 10 K above the reference temperature, the same temperature difference used to solve for the parameters in the five-parameter model. The relations that relate γ to the model are similar to those in Equations (4.2) and (4.3) used to solve for δ in the seven-parameter model, but use a characteristic equation for the circuit that includes the current sink. This new characteristic equation is defined by Equations (4.7) – (4.9). The derivative of the characteristic equation is still needed to constrain the model, and is provided by Equation (4.10). The original constraints for the five-parameter model are used with the maximum power constraint previously described to solve for the six parameters; no temperature or radiation dependence is assumed for χ. Model code and solution procedure are provided in Appendix B and model parameters are given in Appendix C.

$$I = I_L - I_{rec} - I_D - I_{sh} \tag{4.7}$$

$$I(V) = I_L - I_L \frac{\chi}{V_{bi} - (V + IR_s)} - I_o \left(e^{\frac{V+IR_s}{a}} - 1 \right) - \frac{V + IR_s}{R_{sh}} \tag{4.8}$$

$$\chi \equiv \frac{d_i^{\,2}}{(\mu\tau)_{eff}} \tag{4.9}$$

$$\frac{dI}{dV} = \frac{\dfrac{-I_L\chi}{\left(V_{bi}-\left(V+IR_s\right)\right)^2} - \dfrac{I_o}{a}e^{\frac{V+IR_s}{a}} - \dfrac{1}{R_{sh}}}{1+\dfrac{I_L\chi R_s}{\left(V_{bi}-\left(V+IR_s\right)\right)^2} + \dfrac{I_oR_s}{a}e^{\frac{V+IR_s}{a}} + \dfrac{R_s}{R_{sh}}} \tag{4.10}$$

4.4.3 Model Error

Modeling errors are calculated for the six-parameter current sink model for the *vertical curtain wall* Mono-Si and 2-a-Si arrays, the best and worst modeled technologies using the five-parameter model, and are given in Figure 4.11 for the 'January…' data set.

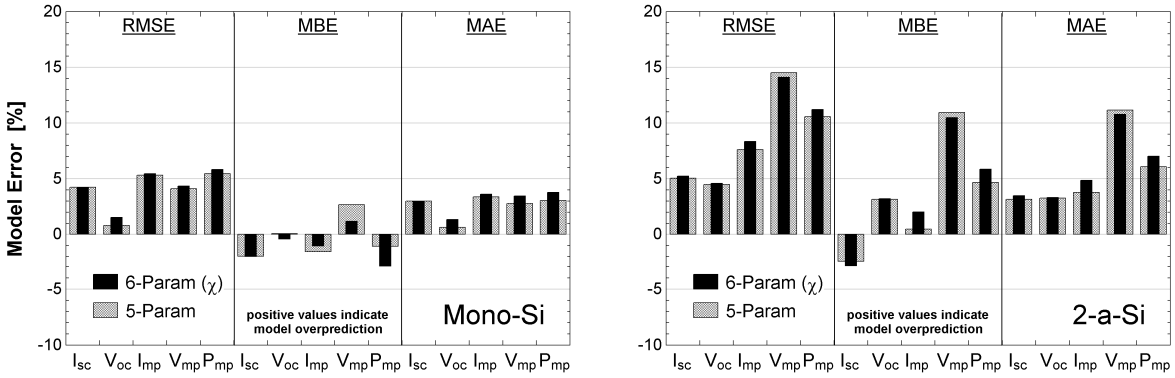

Figure 4.11: Six-parameter current sink modeling errors using the 'January…' data set for (a.) Mono-Si and (b.) 2-a-Si technologies

It is shown in the above figures that the primary difference in predictions between the five and six-parameter current sink models occurs at maximum power, with the six-parameter model resulting in 1% higher RMS P_{mp} modeling errors. This effect on the maximum power

model predictions is consistent with the effect of χ on the individual I-V curves, as shown in Figure 4.12.

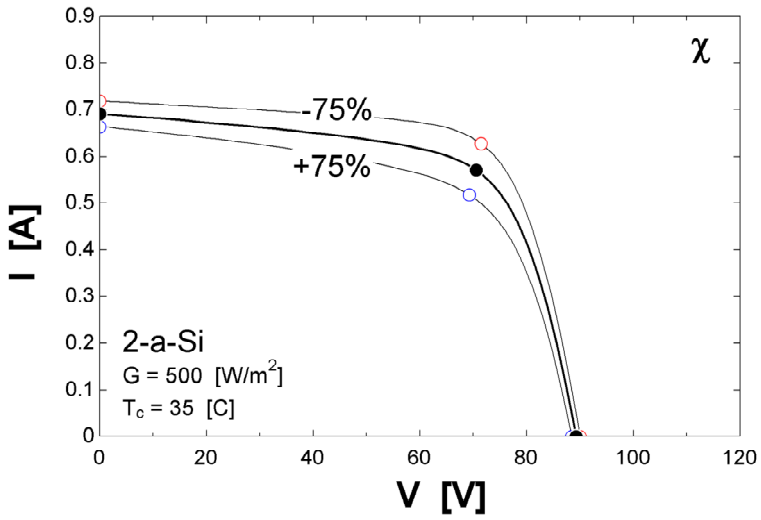

Figure 4.12: Effect of the χ parameter in the six-parameter current sink model on the behavior of the I-V curve

A sensitivity analysis of the model to V_{bi} was performed using data from the 2-a-Si array that also tested whether the calculated value of this only new model input provides the best model predictions. The modeling errors were calculated using values for V_{bi} ±15% of the baseline value; solutions to the model parameters do not converge at larger deviations. Results for the analysis are provided in Appendix L and show that the model is rather insensitive to V_{bi}, with only a 0.09% change in P_{mp} RMSE at V_{bi} + 15%, and only a 0.6% change in P_{mp} RMSE at V_{bi} - 15%. The V_{bi} parameter had less of an influence on the other operating points. The higher modeling errors for the six-parameter current sink model relative to the five-parameter model can therefore not be contributed to an uncertainty in V_{bi} and must either be caused by an uncertainty in γ or a deficiency in the model.

Chapter 5

Conclusions and Recommendations

5.1 Conclusions

The five-parameter equivalent circuit model analyzed in this research accurately predicts the performance of crystalline solar modules under varied operating conditions but it does not perform as well for amorphous and thin-film technologies. The difference between model-predicted and measured maximum power values for the monocrystalline and polycrystalline silicon modules is approximately 3% and 6% RMS for clear days and one month in January, respectively, while the differences are about twice as high for CIS (6% and 10%, respectively) and more than four times as high for tandem-junction amorphous (20% and 27%, respectively). The predictions for the amorphous technology can be improved to 5% for clear days and 11% for the one month in January if the model parameters are calculated from characterization data obtained after the module underwent an initial degradation in output due to aging, which is a characteristic behavior of amorphous silicon. Accurate model predictions were also obtained for every investigated module and array using model parameters calculated from operating data; these modeling errors are within 2% RMS of those calculated using data measured at standard rating conditions. The short-circuit temperature coefficient, a necessary datum for parameter calculation, was not accurately calculated in this research; however, a sensitivity analysis of the five-parameter model shows that a single representative value can be used for every technology. Representative values can also be used for all other inputs that are difficult to determine and not provided by manufacturer datasheets such as glazing material properties, the semiconductor band gap

energy, and the ground reflectance. The use of these values result in less than a 0.25% RMS change in modeling errors relative to using the accepted values.

Modifications to the five-parameter model that were tested during this research did not appreciably improve overall model performance. The temperature and radiation dependence of the model parameters well approximate the data behavior and additional dependence introduced by a seven-parameter model had less than a 1% RMS effect on maximum power predictions for the amorphous technology but increased the modeling errors for this array 4% RMS at open-circuit conditions. Adding a current sink to the equivalent circuit to better account for recombination currents was found to have less than a 1% RMS effect on all characteristic operating points.

5.2 Recommendations

There are a few remaining areas for continued research related to this project:

1. Multiple recombination currents can be modeled with an additional diode in place of a current sink. Multiple diode equivalent circuits have been researched for many years and the additional parameters they introduce could possibly be now solved with newly provided manufacturer data. The ratio of the two diode reverse saturation currents (I_{o2}/I_{o1}) is shown by Markvart and Castañer (2003) to affect the region of the I-V curve near maximum power, similar to the series resistance. This model addition may help to improve the prediction deficiency for V_{mp} and subsequently P_{mp}.

2. The accuracy of the absorbed radiation calculation should be investigated, especially for polymer glazings and high incidence angles. The five-parameter model is very sensitive to absorbed radiation and the error statistics presented in this research do not differentiate between uncertainties in the radiation and in the five-parameter electrical performance models. The approximate uncertainty in the absorbed radiation on a per module basis may be determined by comparing the absorbed radiation modeled by the transmittance-absorptance product (Equation (2.1), Section 2.1.2) to that modeled by the empirical incidence angle modifier function by King (2004) which directly captures the optical behavior of the glazing as a function of incidence angle.

3. The uncertainty in the radiation model can be completely removed from future model validation studies by using an effective irradiance to calculate the absorbed radiation (Marion, 2008). The effective irradiance (E_e) is equivalent to the absorbed radiation (S), and is calculated as a function of the measured module temperature (T) and short-circuit current (I_{sc}), as given in Equation (5.1), where α_{Isc} is the short-circuit current temperature coefficient.

$$E_e = \frac{I_{sc} S_{ref}}{I_{sc,ref}\left[1+\alpha_{Isc}\left(T - T_{ref}\right)\right]} \tag{5.1}$$

This relationship is useful for model validation but it cannot be used for predictive studies that rely on only typical meteorological datasets because of the need for measured module data.

4. Continued model validation studies should include a larger sample of modules and cell technologies to more thoroughly test the model. The tilted and horizontal roof datasets described in Section 2.2.1 were not used for validation because of abnormally large differences between modeled and measured short-circuit and maximum power currents. Differences in only the current predictions indicate uncertainties in the absorbed radiation, which could be removed from these two datasets if the effective irradiance is used in place of the radiation model.

References

American Concrete Pavement Association (ACPA). (2002). AIBEDO: A Measure of Pavement Surface Reflectance. Concrete Pavement Research and Technology Update, Number 3.05.

Beckman, W. (2009). *Seven-Parameter Model*. Under development at the University of Wisconsin Solar Energy Laboratory (SEL). Personal communication, September 23, 2009.

Brandrup, J. Immergut, E.H., and Grulke, E.A. (1999). *Polymer Handbook*, fourth ed. Wiley-Interscience.

California Energy Commission (CEC). (2008). Guidelines for California's Solar Electric Incentive Programs (Senate Bill 1) Second Edition. CEC-300-2008-007-CMF, State of California Energy Commission.

Cameron, C., Boyson, W., Riley, D. (2008). Comparison of PV System Performance-Model Predictions with Measured PV System Performance. *Proceedings of the 33rd IEEE PV Specialist Conference (PVSC)*, San Diego, CA.

Davis, M., Fanney, A., Dougherty, B. (2000). Prediction of Building Integrated Photovoltaic Cell Temperatures. *ASME Journal of Solar Energy Engineering*, Volume 123, Number 3, Pages 200-210.

Del Cueto, J. (2000). Model for the Thermal Characteristics of Flat-Plate Photovoltaic Modules Deployed at Fixed Tilt. *Proceedings of the 28th IEEE PV Specialist Conference (PVSC)*, Anchorage, AK.

De Soto, W., Klein, S.A., Beckman, W.A. (2006). Improvement and Validation of a Model for Photovoltaic Array Performance. *Solar Energy*, Volume 80, Issue 1, Pages 78-88.

Dougherty, B., Fanney, A., and Davis, M. (2005). Measured Performance of Building Integrated Photovoltaic Panels-Round 2. *Journal of Solar Energy Engineering*, Volume 127, Issue 3, Pages 314-324.

Duffie, J., Beckman, W. (2006). *Solar Engineering of Thermal Processes*, third ed. John Wiley & Sons Inc., New York.

DuPont. (2006). Teflon Films. Retrieved from http://www2.dupont.com/Teflon_Industrial/en_US/assets/downloads/k15778.pdf, January 8, 2009.

Eikelboom, J., Reinders A. (1997). Determination of the Irradiation Dependent Efficiency of Multicrystalline Si PV Modules on Basis of IV Curve Fitting and Its Influence on the Annual Performance. *Proceedings of the 14th European Photovoltaic Solar Energy Conference*, Barcelona, Spain.

Fanney, A., Dougherty, B., Davis, M. (2002). Evaluating Building Integrated Photovoltaic Performance Models. *Proceedings of the 29th IEEE PV Specialist Conference (PVSC)*, New Orleans, LA.

Fanney, A., King, D. (2006). Comparison of Photovoltaic Module Performance Measurements. *Transactions of the ASME*, Volume 128, Pages 152-159.

Fuentes, M. (1987). A Simplified Thermal Model for Flat-Plate Photovoltaic Arrays. SAND85-0330, Albuquerque, NM: Sandia National Laboratories.

Gümüş, C, Ozkendir, O., Kavik, H. (2006). Structural and optical properties of zinc oxide thin films prepared by spray pyrolysis method. *Journal of Optoelectronics and Advanced Materials*, Volume 8, No. 1, Pages 299-303.

Hirshman, W., Hering, G., Schmela, M. (2008). Market Survey: Cell & Module Production 2007. *Photon International*, March Issue, Pages 140-174.

Kaneka. (2009). Products (Amorphous). Retrieved from: http://www.pv.kaneka.co.jp, December 11, 2009.

Ken-ichi, K., Hiroyuki, M. (2005). New Two-Diode Model for Detailed Analysis of Multicrystalline Silicon Solar Cells. *Japanese Journal of Applied Physics*, Volume 44, No. 12, Pages 8314-8321.

King, D., Boyson, W., Kratochvill, J. (2004). Photovoltaic Array Performance Model. SAND2004-3535, Albuquerque, NM: Sandia National Laboratories.

King, D., Dudley, J., Boyson, W. (1996). PVSIM: A Simulation Program for Photovoltaic Cells, Modules, and Arrays. *Proceedings of the 25th IEEE Photovoltaic Specialists Conference (PVSC)*, Washington, DC.

King, D., Kratochvil, J., Boyson, W. (1997). Temperature Coefficients for PV Modules and Arrays: Measurement Methods, Difficulties, and Results. *Proceedings of the 26th IEEE Photovoltaic Specialists Conference (PVSC)*, Anaheim, California.

Klein, S.A. (2009). *EES – Engineering Equation Solver*, F-Chart Software. http://www.fchart.com.

Luque, A., et. al. (2003). *Handbook of Photovoltaic Science and Engineering*. John Wiley & Sons Inc., New York.

Marion, B. (2008). Comparison of Predictive Models for Photovoltaic Module Performance. *Proceedings of the 33rd IEEE PV Specialist Conference (PVSC)*, San Diego, CA.

Marion, B. et al. (2001). PVWATTS Version 2 – Enhanced Spatial Resolution for Calculating Grid-Connected PV Performance. *Proceedings of the 2001 NCPV Program Review Meeting*, Lakewood, CO.

Marion, B., del Cueto, J., Sekulic, B. (2004). Modeling Current-Voltage Curves Using Bilinear Interpolation. *Proceedings of the World Renewable Energy Congress (WREC) VIII*, Denver, CO.

Markvart, T., Castañer, L. (2003). *Practical Handbook of Photovoltaics: Fundamentals and Applications*. Elsevier Advanced Technology, Oxford, UK.

Merten, J. et al. (1998). Improved Equivalent Circuit and Analytical Model for Amorphous Silicon Solar Cells and Modules. *IEEE Transactions on Electron Devices*, Volume 45, Number 2.

Müllejans, H., et al. (2004). Reliability of Routine 2-Diode Model Fitting of PV Modules. *Proceedings of the 19th European Photovoltaic Conference*, Paris, France.

Nonomura, S., Okamoto, H., Hamakawa, Y. (1982). Determination of the Built-in Potential in a-Si Solar Cells by Means of Electroabsorption Method. *Japanese Journal of Applied Physics*, Volume 21, Number 8, Pages L464-L466.

Nozik, A. (2005). Efficiency of Converting Solar Irradiance into Electrical or Chemical Free Energy. Presentation, Golden CO: National Renewable Energy Laboratory. Retrieved from: http://www.lbl.gov/solar/pwfiles/plenary/Nozik.Berkeley.Mar05.ppt

Reda, I. (1999). Improving the accuracy of using pyranometers to measure the clear sky global solar irradiance. *Ninth ARM Science Team Meeting Proceedings*, San Antonio, Texas.

Skoplaki, E., Boudouvis, A., Palyvos, J. (2008). A Simple Correlation for the Operating Temperature of Photovoltaic Modules of Arbitrary Mounting. *Solar Energy Materials & Solar Cells*, Volume 92, Pages 1392-1402.

Solarbuzz. (2009). http://www.solarbuzz.com

Solon. (2009). Black 230/02. Module Datasheet, Retrieved from: http://www.solon.com, December, 11, 2009.

Stutenbaeumer, U., Mesfin, B. (1999). Equivalent Model of Monocrystalline, Polycrystalline and Amorphous Silicon Solar Cells. *Renewable Energy*, Volume 18, Issue 4, Pages 501-512.

Van Zeghbroeck, B. (2007). *Principles of Semiconductor Devices*. Retrieved from: http://ecee.colorado.edu/~bart/book/book/chapter2/ch2_3.htm, October 12, 2009.

Wu, C.F., Hamada, M., (2000). *Experiments: Planning, Analysis, and Parameter Design Optimization*, first ed. John Wiley & Sons Inc., New York.

Xinchang. (2009). Products - Cell. Retrieved from: http://www.e-polysilicon.cn, December 11, 2009.

Appendix A

Module SRC and Characteristic Data

A.1 Vertical Curtain Wall Modules

Table A.1: SRC and characteristic data for the monocrystalline silicon module measured by the manufacturer and NIST

Mono-Si		Manufacturer	NIST
I_{sc}	A	5.25	4.37
V_{oc}	V	42.40	42.93
I_{mp}	A	4.54	3.96
V_{mp}	V	33.68	33.68
P_{mp}	W	153.0	133.4
α_{Isc}	A/°C	0.005	0.00175
β_{Voc}	V/°C	-0.081	-0.152
γ_{Pmp}	%/°C	-	-0.495
α_{Imp}	%/°C	-	-0.0390
β_{Vmp}	%/°C	-	-0.456
$I_{mp,200}$ [2]	A	-	0.86
$V_{mp,200}$ [2]	V	-	33.3
NOCT	°C	-	43.7
total cell area	m^2	-	1.020
coverage area	m^2	-	1.160
glazing material	-	-	glass
glazing thickness	mm	-	6
cells in series	-	72	-
parallel series strings	-	1	-
modules in series	-	-	1
modules in parallel	-	-	1

Table A.2: SRC and characteristic data for the polycrystalline silicon module with the glass glazing measured by the manufacturer and NIST

Poly-Si (glass)		Manufacturer	NIST
I_{sc}	A	4.68	4.81
V_{oc}	V	42.95	42.73
I_{mp}	A	4.22	4.28
V_{mp}	V	34.85	34.17
P_{mp}	W	147.0	146.4
α_{Isc}	A/°C	-	0.00384
β_{Voc}	V/°C	-	-0.137
γ_{Pmp}	%/°C	-	-0.396
α_{Imp}	%/°C	-	0.0246
β_{Vmp}	%/°C	-	-0.420
NOCT	°C	-	46.0
total cell area	m^2	-	1.134
coverage area	m^2	-	1.167
glazing material	-	-	glass
glazing thickness	mm	-	6
cells in series	-	72	-
parallel series strings	-	1	-
modules in series	-	-	1
modules in parallel	-	-	1

Table A.3: SRC and characteristic data for the polycrystalline silicon module with the ETFE glazing measured by the manufacturer and NIST

Poly-Si (ETFE)		Manufacturer	NIST
I_{sc}	A	4.97	5.05
V_{oc}	V	43.22	42.77
I_{mp}	A	4.43	4.61
V_{mp}	V	34.77	33.45
P_{mp}	W	153.9	154.2
α_{Isc}	A/°C	-	0.00360
β_{Voc}	V/°C	-	-0.131
γ_{Pmp}	%/°C	-	-0.398
α_{Imp}	%/°C	-	0.0185
β_{Vmp}	%/°C	-	-0.416
NOCT	°C	-	39.5
total cell area	m^2	-	1.134
coverage area	m^2	-	1.168
glazing material	-	-	ETFE
glazing thickness	mm	-	0.05
cells in series	-	72	-
parallel series strings	-	1	-
modules in series	-	-	1
modules in parallel	-	-	1

Table A.4: SRC and characteristic data for the polycrystalline silicon module with the PVDF glazing measured by the manufacturer and NIST

Poly-Si (PVDF)		Manufacturer	NIST
I_{sc}	A	4.92	5.00
V_{oc}	V	43.29	42.91
I_{mp}	A	4.38	4.48
V_{mp}	V	35.12	34.32
P_{mp}	W	153.7	153.7
α_{Isc}	A/°C	-	0.00339
β_{Voc}	V/°C	-	-0.132
γ_{Pmp}	%/°C	-	-0.390
α_{Imp}	%/°C	-	0.0256
β_{Vmp}	%/°C	-	-0.415
NOCT	°C	-	39.9
total cell area	m^2	-	1.134
coverage area	m^2	-	1.168
glazing material	-	-	PVDF
glazing thickness	mm	-	0.05
cells in series	-	72	-
parallel series strings	-	1	-
modules in series	-	-	1
modules in parallel	-	-	1

Table A.5: SRC and characteristic data for the tandem-junction amorphous silicon module measured by the manufacturer and NIST

2-a-Si		Manufacturer[1]	NIST
I_{sc}	A	0.84	0.729
V_{oc}	V	98.00	99.56
I_{mp}	A	0.61	0.612
V_{mp}	V	70.50	76.51
P_{mp}	W	43.01	46.82
α_{Isc}	A/°C	0.0006	0.00060
β_{Voc}	V/°C	-0.41	-0.412
γ_{Pmp}	%/°C	-0.35	-0.355
α_{Imp}	%/°C	0.08	0.0997
β_{Vmp}	%/°C	-0.43	-0.455
NOCT	°C	-	40.7
total cell area	m^2	-	1.487
coverage area	m^2	-	1.487
glazing material	-	-	glass
glazing thickness	mm	-	3
cells in series	-	68	-
parallel series strings	-	1	-
modules in series	-	-	1
modules in parallel	-	-	2

[1] Measured from a standard-length module 120 cm. long. The module used by NIST was shortened to 116 cm by the manufacturer, but contains the same number of cells.

Table A.6: SRC and characteristic data for the copper indium selenide (CIS) module measured by the manufacturer and NIST

CIS		Manufacturer	NIST
I_{sc}	A	2.68	2.76
V_{oc}	V	23.3	23.66
I_{mp}	A	2.41	2.39
V_{mp}	V	16.6	16.18
P_{mp}	W	40.0	38.67
α_{Isc}	A/°C	0.00035	-0.00001
β_{Voc}	V/°C	-0.100	-0.0916
γ_{Pmp}	%/°C	-0.6	-0.422
α_{Imp}	%/°C	0	-0.0533
β_{Vmp}	%/°C	-0.6	-0.369
NOCT	°C	47	41.8
total cell area	m^2	-	1.451
coverage area	m^2	-	1.451
glazing material	-	-	glass
glazing thickness	mm	-	3
cells in series	-	42	-
parallel series strings	-	1	-
modules in series	-	-	1
modules in parallel	-	-	4

A.2 2-a-Si Modules After Aging

Table A.7: SRC data measured from the 2-a-Si technology when the modules had progressively larger amounts of cumulative lifetime exposure to solar radiation, measured in days

Aged 2-a-Si		9 days[1]	16 days[1]	25 days[1]	630 days	631 days
I_{sc}	A	0.729	0.706	0.708	0.711	0.681
V_{oc}	V	99.56	97.45	97.70	95.27	96.53
I_{mp}	A	0.612	0.568	0.590	0.567	0.549
V_{mp}	V	76.51	74.95	74.22	71.04	73.47
P_{mp}	W	46.82	42.57	43.82	40.31	40.35
$I_{mp,200}$ [2]	A	-	-	-	-	0.115
$V_{mp,200}$ [2]	V	-	-	-	-	65.5

[1] measured from an identical control module

[2] reference data at 200 W/m^2 and 25°C calculated from the regressions described in Appendix J

Appendix B

EES Program Code and Solution Procedure

B.1 Radiation Model

The following EES (Klein, 2009) code calculates the module absorbed radiation; equation numbers are referenced from Duffie and Beckman (2006).

```
function  tau·alpha( n_air, n_glaz, K, L, theta` )                    "transmittance-absorptance product"
          theta := MAX( 1e-9 [°], theta` )
          theta_r  :=  arcSin( n_air / n_glaz * sin( theta ))         "Eqn. (5.1.4) - Snell's Law"
          tau·alpha  :=  exp( (-K*L) / cos( theta_r )) * ( 1  -  1/2 * ( (sin(theta_r - theta))^2 /  &
                         (sin(theta_r+theta))^2  +  (tan(theta_r-theta))^2 / &
                         (tan(theta_r+theta))^2 ))                    “Eqn. (5.12.4)”
end


"GEOMETRY INPUTS "
lat  =              39.17          [°]                                "latitude °N of Gaithersburg, VA"
long  =             77.17          [°]                                "longitude °W of Gaithersburg, VA"
L_st  =             75             [°]                                "standard meridian"
gamma  =            0              [°]                                "azimuth - due south"
"ENVIRONMENT INPUTS"
n_air  =            1              [-]                                "air refraction index"
rho_g  =            0.1            [-]                                "ground reflectance"
V  =                Lookup( lktPathIn$, rowTable, 'V' )               "free stream wind speed"
V_T  =              Lookup( lktPathIn$, rowTable, 'V_T' )             "POA wind speed"
"TIME INPUTS"
year  =             Lookup( lktPathIn$, rowTable, 'Year' )            "year"
month  =            Lookup( lktPathIn$, rowTable, 'Month' )           "month"
day  =              Lookup( lktPathIn$, rowTable, 'Day' )             "day"
hour_EST  =         Lookup( lktPathIn$, rowTable, 'Hour' )            "hour"
minute_EST  =       Lookup( lktPathIn$, rowTable, 'Minute' )          "minute"
time_EST  =         hour_EST + minute_EST/60 [min/hr]                 "Eastern Standard Time, no DST"
"MODULE INPUTS"
A  =                Lookup( refTable$, rowModule, 'Area' )            "area of single module (coverage)"
beta  =             Lookup( refTable$, rowModule, 'Slope' )           "slope of modules"
K  =                Lookup( refTable$, rowModule, 'K' )               "glazing extinction coefficient"
L  =                Lookup( refTable$, rowModule, 'L' )               "glazing thickness"
n_glaz  =           Lookup( refTable$, rowModule, 'n_glaz' )          "glazing refractive index"
"RADIATION INPUTS"
G_ref  =            1000           [W/m^2]                            "reference radiation for SRC"
G  =                Lookup( lktPathIn$, rowTable, 'G' )               "total irradiance on a horz. surface"
G_bn  =             Lookup( lktPathIn$, rowTable, 'G_bn' )            "beam normal irradiance"
G_d  =              Lookup( lktPathIn$, rowTable, 'G_d' )             "diffuse irradiance on a horiz. surface"
```

```
G_T  =                Lookup( lktPathIn$, rowTable, concat$('GTIV_', letterModule$) )        "POA
irradiance at time of IV trace"


"GEOMETRY AND TIME"
n  =  nDay_( month, day )                                    "day number of year"
          E  =  EqnTime_( n )                                "equation of time - minute correction"
TST  =  time_EST  +  ( 4 [min/°] * ( L_st  -  long )  +  E ) / 60 [min/hr]  "Eqn. (1.5.2) - true solar time"
omega  =  15 [°/hr] * ( TST - 12.00 [hr] )                   "hour angle"
R_b  =  R_Beam_( lat, n, omega, beta, gamma )                "ratio of rad. on tilted to horizontal surface"
theta_z  =  arcCos( CosZenAng_( lat, n, omega ) )            "zenith angle"
theta_b  =  arcCos( CosIncAng_( lat, n, omega, beta, gamma ))  "beam incidence angle"
theta_d  =  59.7 [°]  -  0.1388 * beta  +  0.001497 [1/°] * beta^2    "Eqn. (5.4.2) - eff. diffuse inc. angle"
theta_g  =  90 [°]  -  0.5788 * beta  +  0.002693 [1/°] * beta^2"Eqn. (5.4.1) - eff. grnd reflect. inc. angle"

"COVER PROPERTIES"
tau·alpha_n  =  tau·alpha( n_air, n_glaz, K, L, 0 [°] )      "trans-absorb product at normal inc."
tau·alpha_b  =  tau·alpha( n_air, n_glaz, K, L, theta_b )    "trans-absorb product at beam inc."
tau·alpha_d  =  tau·alpha( n_air, n_glaz, K, L, theta_d )    "trans-absorb product at diffuse inc."
tau·alpha_g  =  tau·alpha( n_air, n_glaz, K, L, theta_g )    "trans-absorb product at ground refl. inc."
K_tau·alpha_b  =  tau·alpha_b / tau·alpha_n                  "inc. angle modifier for beam component"
K_tau·alpha_d  =  tau·alpha_d / tau·alpha_n                  "inc. angle modifier for diffuse component"
K_tau·alpha_g  =  tau·alpha_g / tau·alpha_n                  "inc. angle mod. for ground ref. component"

"SOME RADIATION EQUATIONS"
G_b  =  G_bn * cos( theta_z )                                "beam radiation on horizontal"
G_bd  =  G_b + G_d                                           "total radiation on a horizontal surface"
G_on  =  1367 [W/m^2] * ( 1 + 0.033 * cos( 360 [°] * n / 365 ))      "Eqn. (1.4.1a) extraterr. rad. on a
normal surf."
G_o  =  G_on * cos( theta_z )                                "extraterrestrial radiation on a horiz. surf."
k_T  =  G_bd / G_o                                           "instantaneous clearness index"
k_D  =  G_d / MAX(G_bd,G_d+0.01 [W/m^2])                     "instantaneous diffuse fraction"
S_ref  =  G_ref * tau·alpha_n                                "absorbed rad. on a normal surf at SRC"

"HDKR MODEL"
A_i  =  G_bn / G_on                                          “Eqn. (2.16.3)”
f_HDKR  =  sqrt( G_b / MAX(G_bd,G_b+0.01 [W/m^2]) ) “Eqn. (2.16.6)”
G_T_HDKR  =  ( G_b + G_d * A_i ) * R_b  +  G_d * ( 1 - A_i ) * ( (1+cos(beta)) / 2 ) * &
          ( 1 + f_HDKR * ( sin( beta/2 ) )^3 )  +  G_bd * rho_g * ( (1-cos(beta)) / 2 ) “Eqn. 2.16.7”
“Eqn. 5.9.2”
S_b_HDKR  =  tau·alpha_n * ( G_b + G_d * A_i ) * R_b * K_tau·alpha_b
S_d_HDKR  =  tau·alpha_n * G_d * ( 1 - A_i ) * ( (1+cos(beta)) / 2 ) * &
          ( 1 + f_HDKR * ( sin( beta/2 ) )^3 )  &* K_tau·alpha_d
S_gr_HDKR  =  tau·alpha_n * G_bd * rho_g * ( (1-cos(beta)) / 2 ) * K_tau·alpha_g
S_HDKR  =  S_b_HDKR  +  S_d_HDKR  +  S_gr_HDKR
S_HDKR\S_ref  =  S_HDKR / S_ref

G_T_HDKR_min  = MAX( 1 [W/m^2], G_T_HDKR )
R_HDKR  =  G_T / G_T_HDKR_min                                "R factor using instantaneous G_T (POA)"
S_HDKR_c  =  S_HDKR * R_HDKR                                 "absorbed rad. corrected with G_T (POA)"
S_HDKR_c\S_ref  =  S_HDKR_c / S_ref
```

B.2 Five-Parameter Model

The following EES (Klein, 2009) code calculates the five-parameter model (De Soto, 2006) given the reference parameters calculated using the code in Appendix B.4.

```
"MODEL PARAMETERS"
E_g_ref =          1.121          [eV]     "matl. band gap energy for Si at ref. (Luque, 2003)"
C =                -0.0002677     [1/K]    "matl. band gap temp. depen. (Si) (Van Zeghbroeck, 2007)"
N_s =              Lookup( refTable$, rowModule, 'N_s' )          "number of modules in series"
N_p =              Lookup( refTable$, rowModule, 'N_p' )          "number of modules in parallel"
alpha_I_sc =       Lookup( refTable$, rowModule, 'alpha_I_sc' ) "short circuit temp. dependence"
T_K_ref =          Lookup( refTable$, rowModule, 'T_c_ref' ) + 273.15 [C]        "ref. temperature"
a_ref =            Lookup( refTable$, rowModule, 'a_ref' )        "ideality factor at SRC"
I_L_ref =          Lookup( refTable$, rowModule, 'I_L_ref' )      "light current at SRC"
I_o_ref =          Lookup( refTable$, rowModule, 'I_o_ref' )      "reverse-saturation current at SRC"
R_s_ref =          Lookup( refTable$, rowModule, 'R_s_ref' )      "series resistance at SRC"
R_sh_ref =         Lookup( refTable$, rowModule, 'R_sh_ref' )     "shunt resistance at SRC"

"OPERATING INPUTS"
T_K =              Lookup( lktPathIn$, rowTable, concat$('T_bar_', letterModule$) ) + 273.15 [C]
"five-min avg. module temp"
S\S_ref =          Lookup( lktPathOut$, rowTable, 'S_HDKR_c\S_ref' )  "S with POA correction"
E_g =              E_g_ref * ( 1 - C * ( T_K - T_K_ref ) )        "temp. depen. of matl band gap"

"SOLVING FOR FIVE OPERATING PARAMETERS"
a = a_ref * T_K/T_K_ref                                           "temperature dependence of a"
I_L = S\S_ref * ( I_L_ref + alpha_I_sc * ( T_K - T_K_ref ) )      "temp. & rad. depen of light current"
I_o = I_o_ref * ( T_K / T_K_ref )^3 * exp( E_g_ref*Convert(eV,J) / (k#*T_K_ref) - &
                   E_g*Convert(eV,J) / (k#*T_K) )                 "temp. depen. of rev. sat. current"
R_s = R_s_ref                                                     "no temp. depen. assumed for R_s"
S\S_ref_min = MAX( 0.01 [-], S\S_ref )
R_sh = R_sh_ref / S\S_ref_min                                     "radiation dependence for R_sh"

"SOLVING FOR MAX POWER"
"Characteristic equation for current evaluated for max power"
I_mp_mod1 = ( I_L - I_o * ( exp( (V_mp_mod1+I_mp_mod1*R_s)/a ) - 1 ) - ( V_mp_mod1 +
I_mp_mod1 * R_s ) / R_sh )
"Derivative of characteristic equation for power (I*V) set to 0 and evaluated for max power"
dI\dV_mp_mod = ( -I_o / a * P_3 - 1 / R_sh ) / ( 1 + (I_o * R_s) / a * P_3 + R_s / R_sh )
P_3 = exp( (V_mp_mod1 + I_mp_mod1 * R_s) / a )
0 = I_mp_mod1 + V_mp_mod1 * dI\dV_mp_mod
"Maximum power point of array"
I_mp_mod = I_mp_mod1 * N_p
V_mp_mod = V_mp_mod1 * N_s
P_mp_mod = I_mp_mod * V_mp_mod

"SOLVING FOR SHORT CIRCUIT CURRENT"
I_sc_mod1 = ( I_L - I_o * ( exp( I_sc_mod1*R_s/a ) - 1 ) - I_sc_mod1 * R_s / R_sh )
I_sc_mod = I_sc_mod1 * N_p
```

"SOLVING FOR OPEN CIRCUIT VOLTAGE"
0 = I_L - I_o * (exp(V_oc_mod1 / a) - 1) - V_oc_mod1 / R_sh
V_oc_mod = V_oc_mod1 * N_s

B.3 Solution Procedure to Solve for Model Parameters

The highly non-linear, coupled equations in the equivalent circuit models examined in this research are solved using the simultaneous equation solver software, EES (Klein, 2009). The equations to solve for the parameters of these models, given in Appendix B.4 - 0, often fail to converge even with good initial guess values. A methodology that can be used in EES to solve for equations that do not initially converge is as follows:

1. Set appropriate variable guess values in the “Variable Information” window. The button to open this window is circled in Figure B.1.

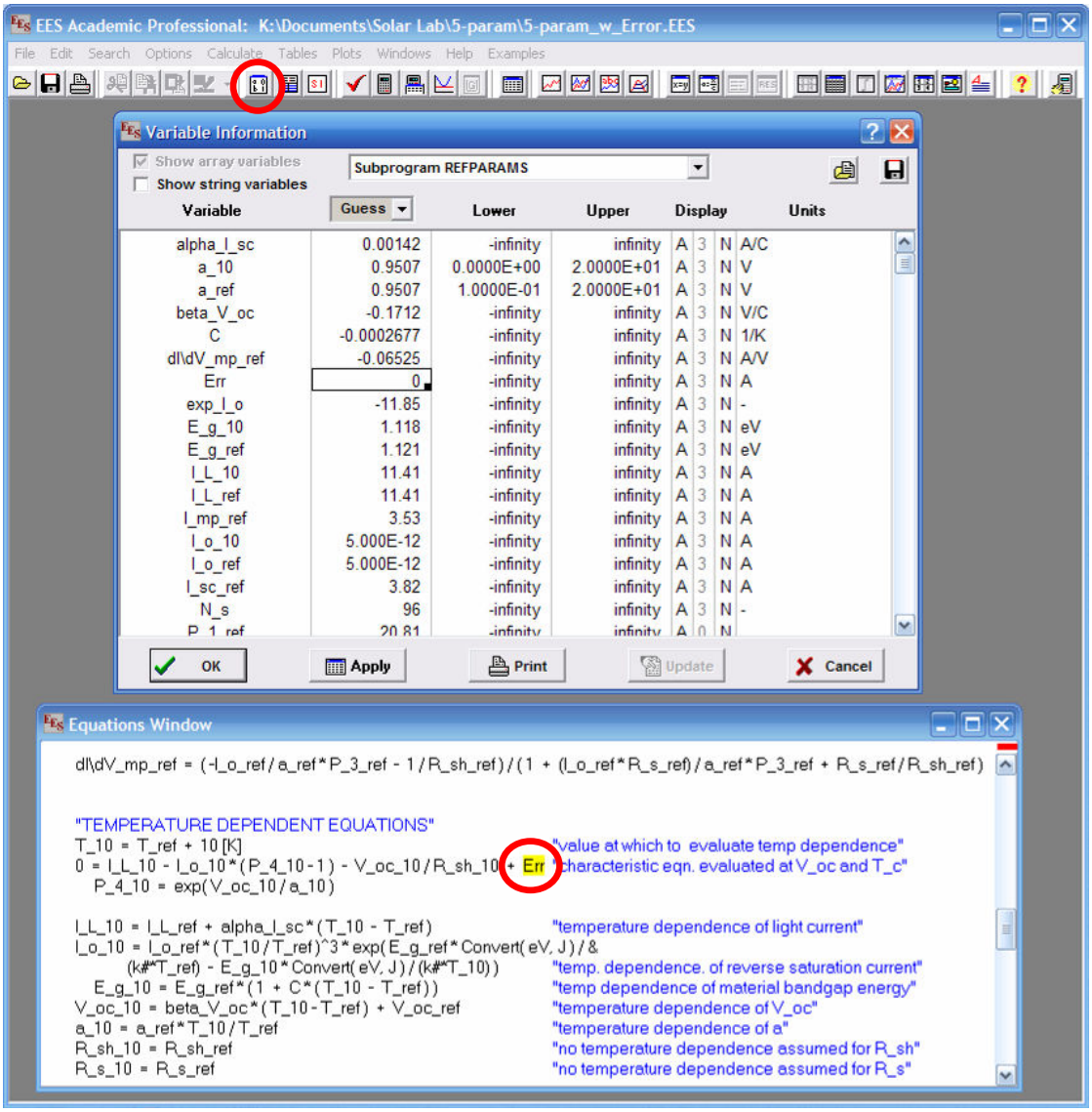

Figure B.1: A screenshot of the software program EES that identifies the button to open the “Variable Information” window that is used to set variable guess values. Also identified is the location in the model equations to insert an error term that helps solve for the model parameters.

2. Insert an error term (circled) into the equation shown in Figure B.1.

3. Create a variable that specifies the power of the I_o parameter and incorporate it into the model equations (example: I_o_ref = 1 [A] * 10^exp_I_o).

4. Create a parametric table that includes the I_o power, the new error term, and the model parameters. Set the I_o power to a range of values that includes all possible values, or between about -20 and -5. Solve this parametric table, as shown in Figure B.2, with the options "Update guess values" and "Stop if error occurs" unselected.

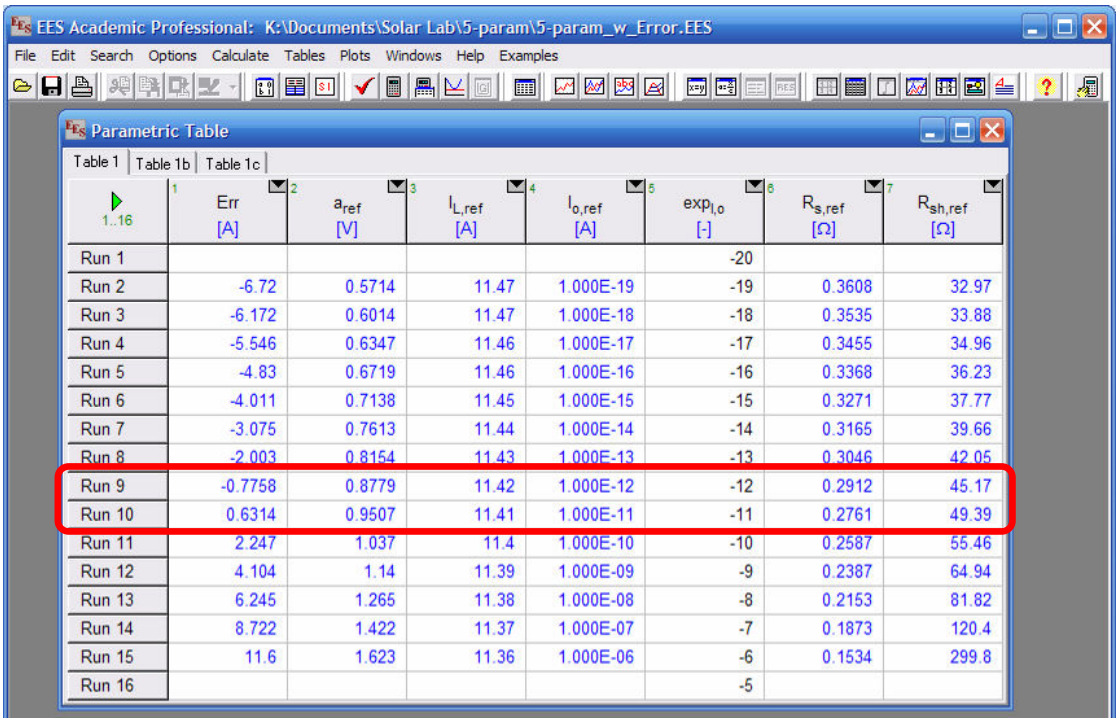

1..16	Err [A]	a_{ref} [V]	$I_{L,ref}$ [A]	$I_{o,ref}$ [A]	$exp_{I,o}$ [-]	$R_{s,ref}$ [Ω]	$R_{sh,ref}$ [Ω]
Run 1					-20		
Run 2	-6.72	0.5714	11.47	1.000E-19	-19	0.3608	32.97
Run 3	-6.172	0.6014	11.47	1.000E-18	-18	0.3535	33.88
Run 4	-5.546	0.6347	11.46	1.000E-17	-17	0.3455	34.96
Run 5	-4.83	0.6719	11.46	1.000E-16	-16	0.3368	36.23
Run 6	-4.011	0.7138	11.45	1.000E-15	-15	0.3271	37.77
Run 7	-3.075	0.7613	11.44	1.000E-14	-14	0.3165	39.66
Run 8	-2.003	0.8154	11.43	1.000E-13	-13	0.3046	42.05
Run 9	-0.7758	0.8779	11.42	1.000E-12	-12	0.2912	45.17
Run 10	0.6314	0.9507	11.41	1.000E-11	-11	0.2761	49.39
Run 11	2.247	1.037	11.4	1.000E-10	-10	0.2587	55.46
Run 12	4.104	1.14	11.39	1.000E-09	-9	0.2387	64.94
Run 13	6.245	1.265	11.38	1.000E-08	-8	0.2153	81.82
Run 14	8.722	1.422	11.37	1.000E-07	-7	0.1873	120.4
Run 15	11.6	1.623	11.36	1.000E-06	-6	0.1534	299.8
Run 16					-5		

Figure B.2: A screenshot of the software program EES that shows the parametric table used to minimize the error term and the table runs where the error term is nearest to zero.

5. Find the runs that surround the correct values, which are indicated by the sign change in the error term, as shown in Figure B.2.

6. Change the values of the I_o power to a range of values between the two that surround the correct values that were determined in step 5. Solve the table.
7. Find the first run that the error term changes signs. Solve the table again only up to this run, with the option "Update guess values" selected.
8. Clear all values from the table and set the error term to zero in the first run. Solve only the first run. The parameter values given in this row are the correct model parameters.

B.4 Solution for Five Parameters

The following EES (Klein, 2009) code calculates the parameters of the five-parameter model (De Soto, 2006).

```
"TRYING DIFFERENT I_O EXPONENTS FOR CALCULATING ERRORS IN I_L_10"
I_o_ref =           1 [A] * 10^exp_I_o

"CONSTANTS"
E_g_ref =           1.121       [eV]    "matl. band gap energy for Si at ref. (Luque, 2003)"
C =                 -0.0002677  [1/K]   "matl. band gap temp. depen. (Si) (Van Zeghbroeck, 2007)"

"SHORT-CIRCUIT, OPEN-CIRCUIT, AND MAX POWER EQUATIONS"
"Characteristic equation for current evaluated for short circuit"
P_1_ref = exp( ( I_sc_ref * R_s_ref ) / a_ref )
I_sc_ref = I_L_ref - I_o_ref * ( P_1_ref - 1 ) - ( I_sc_ref * R_s_ref ) / R_sh_ref

"Characteristic equation for current evaluated for open circuit"
P_2_ref = exp( V_oc_ref / a_ref )
0 = I_L_ref - I_o_ref * ( P_2_ref - 1 ) - V_oc_ref / R_sh_ref

"Characteristic equation for current evaluated for max power"
P_3_ref = exp( ( V_mp_ref + I_mp_ref * R_s_ref ) / a_ref )
I_mp_ref = I_L_ref - I_o_ref * ( P_3_ref - 1 ) - ( V_mp_ref + I_mp_ref * R_s_ref ) / R_sh_ref

"Derivative of characteristic equation for power (I*V) set to 0 and evaluated for max power"
0 = I_mp_ref + V_mp_ref * dI\dV_mp_ref
dI\dV_mp_ref = ( -I_o_ref / a_ref * P_3_ref - 1 / R_sh_ref ) / ( 1 + (I_o_ref * R_s_ref) / &
a_ref * P_3_ref + R_s_ref / R_sh_ref )


"TEMPERATURE DEPENDENT EQUATIONS"
T_10 = T_ref + 10 [K]                       "value at which to evaluate temp dependence"
0 = I_L_10 - I_o_10 * ( P_4_10 - 1 ) - V_oc_10 / R_sh_10 + Err      "char eqn. evaluated at
V_oc and T_c"
P_4_10 = exp( V_oc_10 / a_10 )

I_L_10 = I_L_ref + alpha_I_sc * ( T_10 - T_ref )        "temperature dependence of light current"
I_o_10 = I_o_ref * ( T_10 / T_ref )^3 * exp( E_g_ref * Convert( eV, J ) / &
            (k#*T_ref) - E_g_10 * Convert( eV, J ) / (k#*T_10) )  "temp. depen. of rev. sat. current"
   E_g_10 = E_g_ref * ( 1 + C * ( T_10 - T_ref ) )      "temp. depen. of mat. band gap energy"
V_oc_10 = beta_V_oc * ( T_10 - T_ref ) + V_oc_ref       "temp. depen. of V_oc"
a_10 = a_ref * T_10 / T_ref                             "temperature dependence of a"
R_sh_10 = R_sh_ref                                      "no temp. dependence assumed for R_sh"
R_s_10 = R_s_ref                                        "no temp. dependence assumed for R_s"
```

B.5 Solution for Seven Parameters

The following EES (Klein, 2009) code calculates the parameters of the seven-parameter model.

```
"TRYING DIFFERENT I_O EXPONENTS FOR CALCULATING ERRORS IN I_L_10"
I_o_ref =          1 [A] * 10^exp_I_o

"CONSTANTS"
E_g_ref =          1.121        [eV]    "matl. band gap energy for Si at ref. (Luque, 2003)"
C =                -0.0002677   [1/K]   "matl. band gap temp. depen. (Si) (Van Zeghbroeck, 2007)"

"SHORT-CIRCUIT, OPEN-CIRCUIT, AND MAX POWER EQUATIONS"
"Characteristic equation for current evaluated for short circuit"
P_1_ref = exp( ( I_sc_ref * R_s_ref ) / a_ref )
I_sc_ref = I_L_ref - I_o_ref * ( P_1_ref - 1 ) - ( I_sc_ref * R_s_ref ) / R_sh_ref

"Characteristic equation for current evaluated for open circuit"
P_2_ref = exp( V_oc_ref / a_ref )
0 = I_L_ref - I_o_ref * ( P_2_ref - 1 ) - V_oc_ref / R_sh_ref

"Characteristic equation for current evaluated for max power"
P_3_ref = exp( ( V_mp_ref + I_mp_ref * R_s_ref ) / a_ref )
I_mp_ref = I_L_ref - I_o_ref * ( P_3_ref - 1 ) - ( V_mp_ref + I_mp_ref * R_s_ref ) / R_sh_ref

"Derivative of characteristic equation for power (I*V) set to 0 and evaluated for max power"
0 = I_mp_ref + V_mp_ref * dI\dV_mp_ref
dI\dV_mp_ref = ( -I_o_ref / a_ref * P_3_ref - 1 / R_sh_ref ) / ( 1 + (I_o_ref * R_s_ref) / &
a_ref * P_3_ref + R_s_ref / R_sh_ref )


"TEMPERATURE DEPENDENT EQUATIONS"
T_10 = T_ref + 10 [K]                          "value at which to evaluate temp dependence"
0 = I_L_10 - I_o_10 * ( P_4_10 - 1 ) - V_oc_10 / R_sh_10 + Err      "char eqn. evaluated at
V_oc and T_c"
P_4_10 = exp( V_oc_10 / a_10 )

I_L_10 = I_L_ref + alpha_I_sc * ( T_10 - T_ref )      "temperature dependence of light current"
I_o_10 = I_o_ref * ( T_10 / T_ref )^3 * exp( E_g_ref * Convert( eV, J ) / &
          (k#*T_ref) - E_g_10 * Convert( eV, J ) / (k#*T_10) )  "temp. depen. of rev. sat. current"
   E_g_10 = E_g_ref * ( 1 + C * ( T_10 - T_ref ) )    "temp. depen. of mat. band gap energy"
V_oc_10 = beta_V_oc * ( T_10 - T_ref ) + V_oc_ref     "temp. depen. of V_oc"
a_10 = a_ref * T_10 / T_ref                           "temperature dependence of a"
R_sh_10 = R_sh_ref                                    "no temp. dependence assumed for R_sh"
R_s_10 = R_s_ref                                      "no temp. dependence assumed for R_s"
"<A_REF, I_L_REF, I_O_REF, R_S_REF, AND R_SH_REF ARE NOW FOUND>"
```

```
"CONSTRAINING max power slope at 200 W/m^2 and T_ref using derivative of characteristic
equation for power (I*V) set to 0"
G =              200      [W/m^2]
G_ref =          1000     [W/m^2]
0 = I_mp_200 + V_mp_200 * dI\dV_mp_200
P_5_200 = exp( ( V_mp_200 + I_mp_200 * R_s_ref ) / a_ref )
dI\dV_mp_200 = ( -I_o_ref*(G_ref/G)^m / a_ref * P_5_200 - 1 / (R_sh_ref*G_ref/G) ) / &
        ( 1 + (I_o_ref * (G_ref/G)^m * R_s_ref) / a_ref * P_5_200 + R_s_ref / (R_sh_ref * G_ref/G) )
"<M IS NOW FOUND>"


"Finding maximum power at G_ref and T_ref - 5 K"
"Characteristic equation for current evaluated for max power"
P_3_n5 = exp( ( V_mp_n5 + I_mp_n5 * R_s_n5 ) / a_n5 )
I_mp_n5 = I_L_n5 - I_o_n5 * ( P_3_n5 - 1 ) - ( V_mp_n5 + I_mp_n5 * R_s_n5 ) / R_sh_ref
"Derivative of characteristic equation for power (I*V) set to 0 and evaluated for max power"
0 = I_mp_n5 + V_mp_n5 * dI\dV_mp_n5
dI\dV_mp_n5 = ( -I_o_n5 / a_n5 * P_3_n5 - 1 / R_sh_ref ) / ( 1 + (I_o_n5 * R_s_n5) / a_n5 *
P_3_n5 + R_s_n5 / R_sh_ref )
"Maximum power"
P_mp_n5 = I_mp_n5 * V_mp_n5
"========"
T_n5 = T_ref - 5 [K]
I_L_n5 = I_L_ref*exp(alpha_I_sc * ( T_n5 - T_ref ) / I_L_ref)    "temp. depen. of light current
I_o_n5 = I_o_ref * ( T_n5 / T_ref )^3 * exp( E_g_ref * Convert( eV, J ) / &
        (k#*T_ref) - E_g_n5 * Convert( eV, J ) / (k#*T_n5) )      "temp. depen. of rev sat current"
   E_g_n5 = E_g_ref * ( 1 + C * ( T_n5 - T_ref ) )      "temp depen of material band gap energy"
V_oc_n5 = V_oc_ref * exp(beta_V_oc * ( T_n5 - T_ref ) / V_oc_ref)       "temp dependence of V_oc"
a_n5 = a_ref * T_n5 / T_ref      "temp dependence of a"
"->One more unknown (R_s_n5) than equations in previous set of equations"

"Finding maximum power at G_ref and T_ref + 5 K"
"Characteristic equation for current evaluated for max power"
P_3_5 = exp( ( V_mp_5 + I_mp_5 * R_s_5 ) / a_5 )
I_mp_5 = I_L_5 - I_o_5 * ( P_3_5 - 1 ) - ( V_mp_5 + I_mp_5 * R_s_5 ) / R_sh_ref
"Derivative of characteristic equation for power (I*V) set to 0 and evaluated for max power"
0 = I_mp_5 + V_mp_5 * dI\dV_mp_5
dI\dV_mp_5 = ( -I_o_5 / a_5 * P_3_5 - 1 / R_sh_ref ) / ( 1 + (I_o_5 * R_s_5) / a_5 * P_3_5 +
R_s_5 / R_sh_ref )
"Maximum power"
P_mp_5 = I_mp_5 * V_mp_5
"========"
T_5 = T_ref + 5 [K]
I_L_5 = I_L_ref*exp(alpha_I_sc * ( T_5 - T_ref ) / I_L_ref)       "temp depen of light current"
I_o_5 = I_o_ref * ( T_5 / T_ref )^3 * exp( E_g_ref * Convert( eV, J ) / &
        (k#*T_ref) - E_g_5 * Convert( eV, J ) / (k#*T_5) )        "temp. depen. of rev sat current"
   E_g_5 = E_g_ref * ( 1 + C * ( T_5 - T_ref ) )       "temp depend of material band gap energy"
V_oc_5 = V_oc_ref * exp(beta_V_oc * ( T_5 - T_ref ) / V_oc_ref)          "temp dependence of V_oc"
a_5 = a_ref * T_5 / T_ref        "temp dependence of a"
"->One more unknown (R_s_5) than equations in previous set of equations"

"Getting two more knowns than equations to solve for this and previous two sets of equations"
P_mp_ref = I_mp_ref * V_mp_ref
gamma_P_mp * P_mp_ref = (P_mp_5 - P_mp_n5) / ( T_5 - T_n5 )
```

R_s_n5 = R_s_ref * exp(delta * (T_n5 - T_ref))
R_s_5 = R_s_ref * exp(delta * (T_5 - T_ref))
"->Only new unknown is delta"
"<DELTA IS NOW FOUND>"

B.6 Solution for Six Parameters Including Current Sink Parameter

The following EES (Klein, 2009) code calculates the parameters of the six-parameter current sink model.

```
"TRYING DIFFERENT I_O EXPONENTS FOR CALCULATING ERRORS IN I_L_10"
I_o_ref =           1 [A] * 10^exp_I_o

"CONSTANTS"
E_g_ref =           1.121       [eV]    "matl. band gap energy for Si at ref. (Luque, 2003)"
C =                 -0.0002677  [1/K]   "matl. band gap temp. depen. (Si) (Van Zeghbroeck, 2007)"

"SHORT-CIRCUIT, OPEN-CIRCUIT, AND MAX POWER EQUATIONS"
"Characteristic equation for current evaluated for short circuit"
P_1_ref = exp( ( I_sc_ref * R_s_ref ) / a_ref )
I_sc_ref = I_L_ref - I_L_ref * chi / ( V_bi - I_sc_ref * R_s_ref ) - I_o_ref * ( P_1_ref - 1 ) - &
           ( I_sc_ref * R_s_ref ) / R_sh_ref

"Characteristic equation for current evaluated for open circuit"
P_2_ref = exp( V_oc_ref / a_ref )
0 = I_L_ref - I_L_ref * chi / ( V_bi - V_oc_ref ) - I_o_ref * ( P_2_ref - 1 ) - V_oc_ref / R_sh_ref

"Characteristic equation for current evaluated for max power"
P_3_ref = exp( ( V_mp_ref + I_mp_ref * R_s_ref ) / a_ref )
I_mp_ref = I_L_ref - I_L_ref * chi / ( V_bi - ( V_mp_ref + I_mp_ref * R_s_ref ) ) - &
           I_o_ref * ( P_3_ref - 1 ) - ( V_mp_ref + I_mp_ref * R_s_ref ) / R_sh_ref

"Derivative of characteristic equation for power (I*V) set to 0 and evaluated for max power"
0 = I_mp_ref + V_mp_ref * dI\dV_mp_ref
dI\dV_mp_ref = ( -I_L_ref * chi / ( V_bi - ( V_mp_ref + I_mp_ref * R_s_ref ) )^2 - &
               I_o_ref / a_ref * P_3_ref - 1 / R_sh_ref ) / ( 1 + I_L_ref * chi * R_s_ref / &
               ( V_bi - ( V_mp_ref + I_mp_ref * R_s_ref ) )^2 + &
               (I_o_ref * R_s_ref) / a_ref * P_3_ref + R_s_ref / R_sh_ref )
"<EFFECTIVELY FOUR EQUATIONS AND SIX UNKNOWNS>"

"CONSTRAINING open circuit voltage at T_ref + 10 K using char. Eqn. for current and beta_V_oc"
T_10 = T_ref + 10 [K]                       "value at which to evaluate temp dependence"
"characteristic eqn. evaluated at V_oc and T_10"
0 = I_L_10 - I_L_10 * chi / ( V_bi - V_oc_10 ) - I_o_10 * ( P_4_10 - 1 ) - V_oc_10 / R_sh_10 + Err
   P_4_10 = exp( V_oc_10 / a_10 )
"========"
I_L_10 = I_L_ref + alpha_I_sc * ( T_10 - T_ref )        "temperature dependence of light current"
I_o_10 = I_o_ref * ( T_10 / T_ref )^3 * exp( E_g_ref * Convert( eV, J ) / &
           (k#*T_ref) - E_g_10 * Convert( eV, J ) / (k#*T_10) )  "temp. depen. of rev. sat. current"
   E_g_10 = E_g_ref * ( 1 + C * ( T_10 - T_ref ) )      "temp. depen. of mat band gap energy"
V_oc_10 = beta_V_oc * ( T_10 - T_ref ) + V_oc_ref       "temp. depen. of V_oc"
a_10 = a_ref * T_10 / T_ref                             "temperature dependence of a"
R_sh_10 = R_sh_ref                                      "no temp. dependence assumed for R_sh"
R_s_10 = R_s_ref                                        "no temp. dependence assumed for R_s"
```

```
"<EFFECTIVELY EIGHT ADDITIONAL EQUATIONS AND SEVEN ADDITIONAL UNKNOWNS>"

"Finding maximum power at G_ref and T_ref + 10 K"
"Characteristic equation for current evaluated for max power"
P_3_10  =  exp( ( V_mp_10  +  I_mp_10 * R_s_ref ) / a_10 )
I_mp_10  =  I_L_10  -  I_L_10 * chi / ( V_bi - ( V_mp_10 + I_mp_10 * R_s_ref ) )  -  &
              I_o_10 * ( P_3_10 - 1 )  -  ( V_mp_10 + I_mp_10 * R_s_ref ) / R_sh_ref
"Derivative of characteristic equation for power (I*V) set to 0 and evaluated for max power"
0  =  I_mp_10  +  V_mp_10 * dI\dV_mp_10
dI\dV_mp_10  =  ( -I_L_10 * chi / ( V_bi - ( V_mp_10 + I_mp_10 * R_s_ref ) )^2  -  &
                  I_o_10 / a_10 * P_3_10  -  1 / R_sh_ref ) /  ( 1  +  I_L_10 * chi * R_s_ref / &
                  ( V_bi - ( V_mp_10 + I_mp_10 * R_s_ref ) )^2  +  &
                  (I_o_10 * R_s_ref) / a_10 * P_3_10  +  R_s_ref / R_sh_ref )
"Maximum power"
P_mp_10  =  I_mp_10 * V_mp_10
"========"

"->One more unknown (chi) than equations in previous set of equations"

"Getting two more knowns than equations to solve for this and previous two sets of equations"
P_mp_ref  =  I_mp_ref * V_mp_ref
gamma_P_mp * P_mp_ref  =  (P_mp_10 - P_mp_ref) / ( T_10 - T_ref )
"->No new unknowns"
"<CHI IS NOW FOUND>"
```

Appendix C

Model Parameters for Researched Modules

C.1 Five-Parameter Model

Figure C.1: Model parameters calculated from SRC data for the five-parameter model corresponding to the modules in this research

Module	a_{ref} **[V]**	$I_{L,ref}$ **[A]**	$I_{o,ref}$ **[A]**	$R_{s,ref}$ **[Ω]**	$R_{sh,ref}$ **[Ω]**
Mono-Si	1.77	4.40	1.19×10^{-9}	1.04	182
Poly-Si (glass)	1.68	4.85	4.04×10^{-11}	0.817	109
Poly-Si (ETFE)	1.64	5.08	2.30×10^{-11}	0.970	175
Poly-Si (PVDF)	1.65	5.04	2.29×10^{-11}	0.804	115
2-a-Si (9 days exposure)	4.48	0.742	1.41×10^{-10}	16.8	927
2-a-Si (16 days exposure)	4.45	0.723	1.77×10^{-10}	17.0	686
2-a-Si (25 days exposure)	4.44	0.723	1.73×10^{-10}	18.5	883
2-a-Si (630 days exposure)	4.41	0.735	2.37×10^{-10}	20.9	625
2-a-Si (631 days exposure)	4.43	0.699	1.94×10^{-10}	18.9	712
CIS	1.02	2.82	2.10×10^{-10}	2.05	93.5

C.2 Seven-Parameter Model

Figure C.2: Model parameters calculated from SRC data for the seven-parameter model corresponding to the modules in this research

Module	a_{ref} [V]	δ [%/°C]	$I_{L,ref}$ [A]	$I_{o,ref}$ [A]	m [-]	$R_{s,ref}$ [Ω]	$R_{sh,ref}$ [Ω]
Mono-Si	1.77	0.460	4.40	1.19×10^{-9}	0.278	1.04	182
2-a-Si (631 days exposure)	4.43	-0.482	0.699	1.94×10^{-10}	1.34	18.9	712

C.3 Six-Parameter Current Sink Model

Figure C.3: Model parameters calculated from SRC data for the six-parameter current sink model corresponding to the modules in this research

Module	a_{ref} [V]	χ [V]	$I_{L,ref}$ [A]	$I_{o,ref}$ [A]	$R_{s,ref}$ [Ω]	$R_{sh,ref}$ [Ω]	V_{bi} [V]
Mono-Si	1.88	0.0285	4.39	4.76×10^{-10}	1.02	214	43.2
2-a-Si (631 days exposure)	4.54	6.07	0.727	2.89×10^{-10}	16.7	1920	122.4

Appendix D

Model-Predicted Versus Measured Values

D.1 Five-Parameter Model

D.1.1 Monocrystalline Silicon

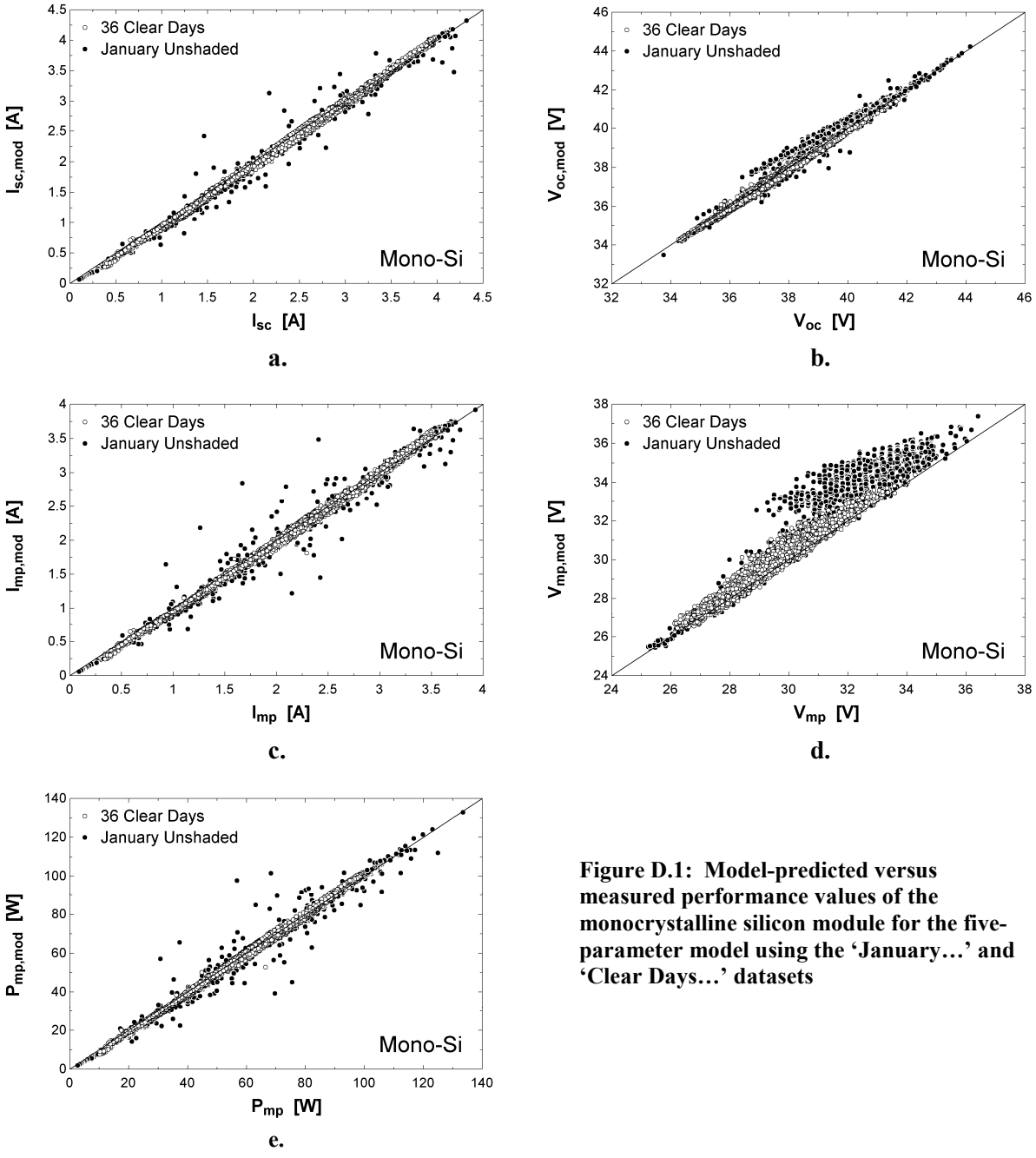

Figure D.1: Model-predicted versus measured performance values of the monocrystalline silicon module for the five-parameter model using the 'January…' and 'Clear Days…' datasets

D.1.2 Polycrystalline Silicon with Glass Glazing

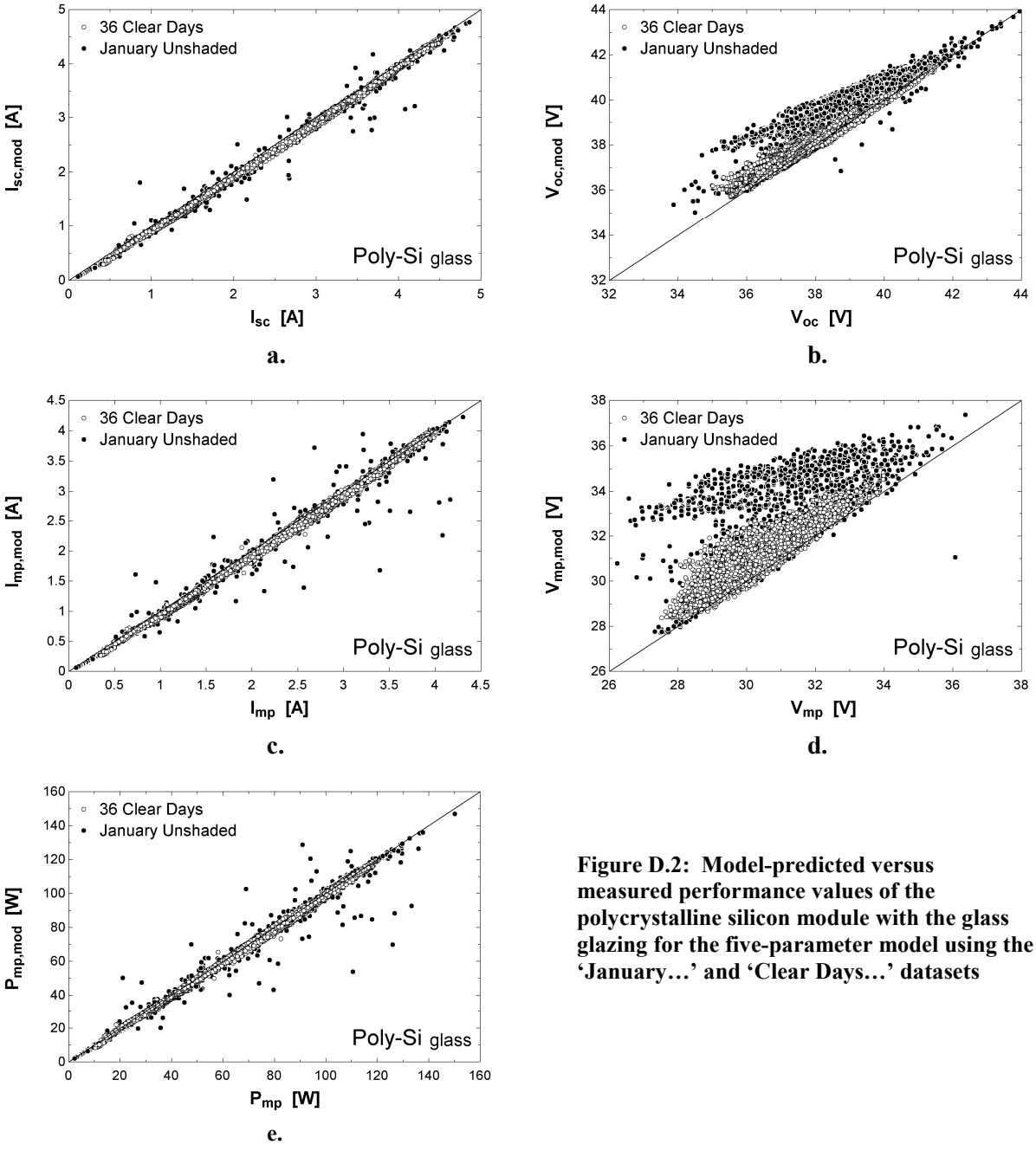

Figure D.2: Model-predicted versus measured performance values of the polycrystalline silicon module with the glass glazing for the five-parameter model using the 'January…' and 'Clear Days…' datasets

D.1.3 Polycrystalline Silicon with ETFE Glazing

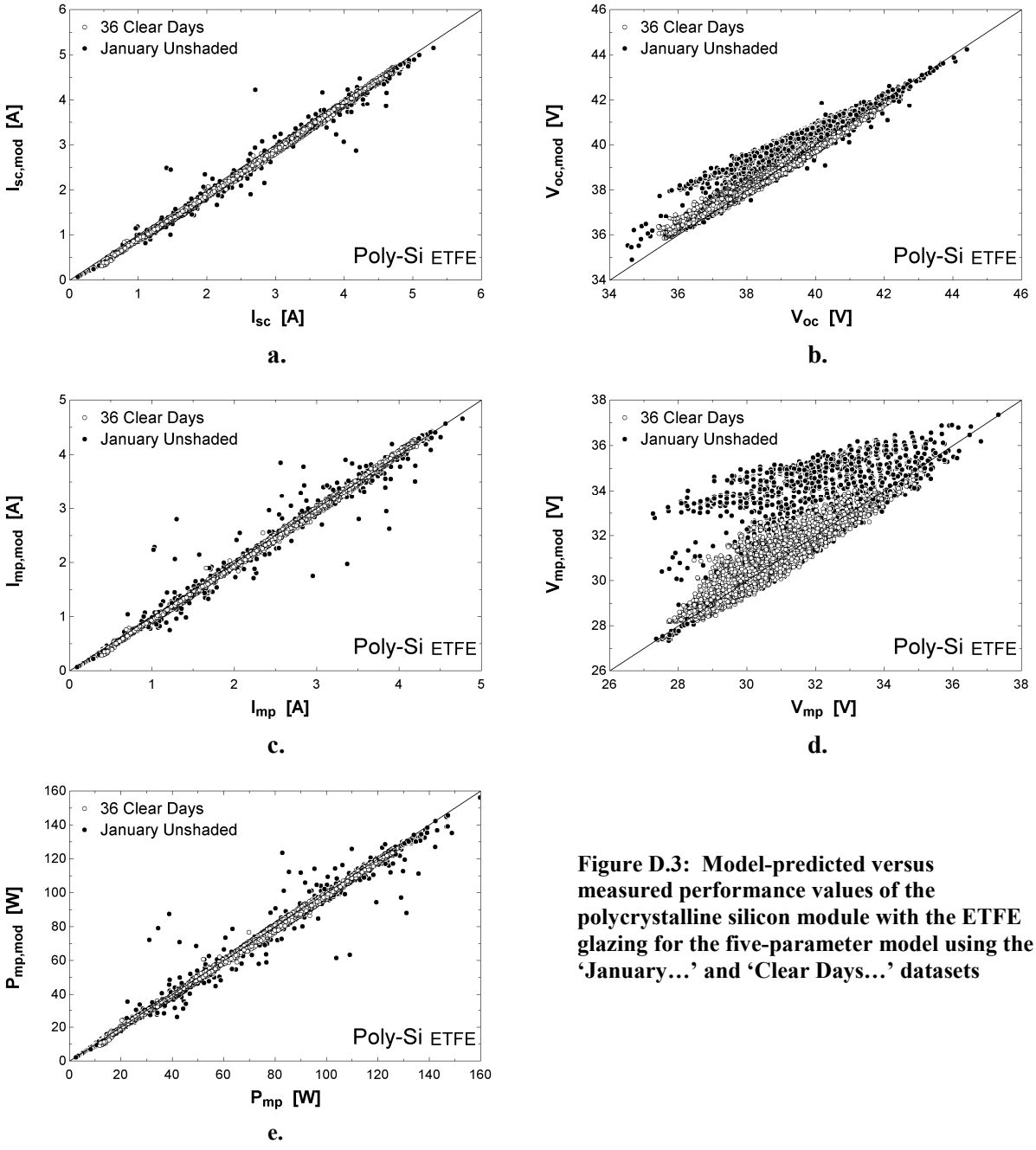

Figure D.3: Model-predicted versus measured performance values of the polycrystalline silicon module with the ETFE glazing for the five-parameter model using the 'January…' and 'Clear Days…' datasets

D.1.4 Polycrystalline Silicon with PVDF Glazing

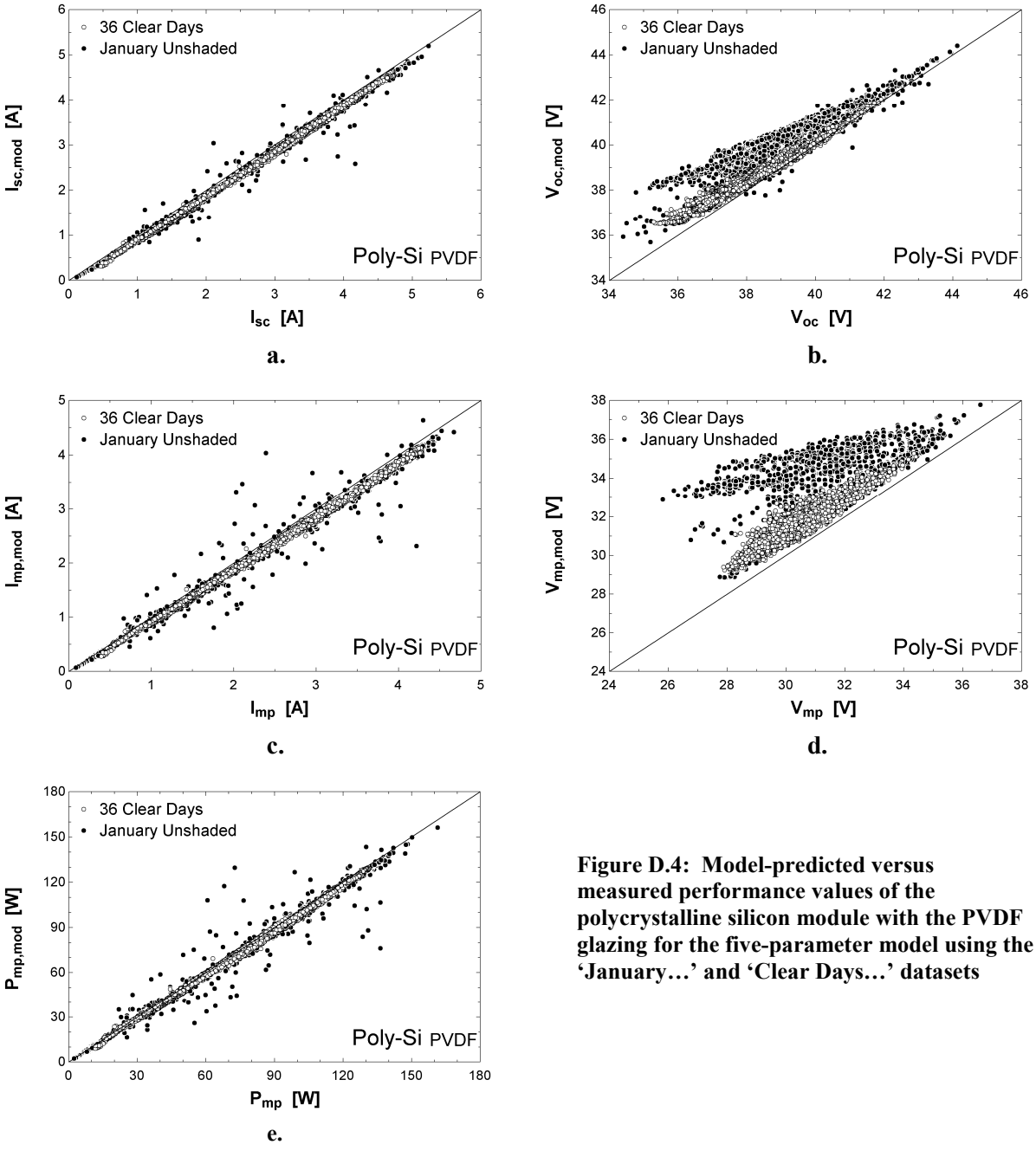

Figure D.4: Model-predicted versus measured performance values of the polycrystalline silicon module with the PVDF glazing for the five-parameter model using the 'January…' and 'Clear Days…' datasets

D.1.5 Tandem-Junction Amorphous Silicon

D.1.5.1. Aged 9 Days (Original)

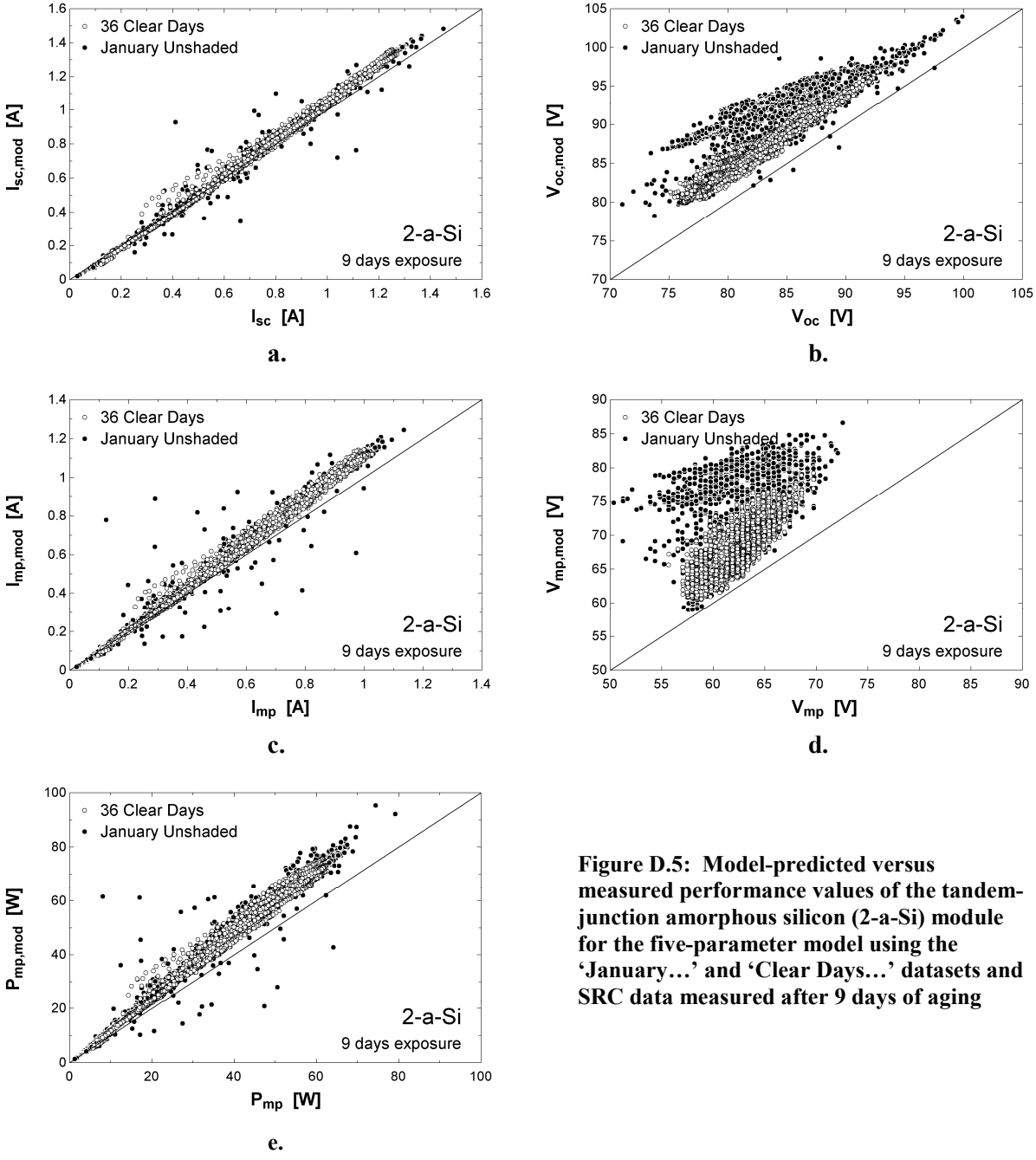

Figure D.5: Model-predicted versus measured performance values of the tandem-junction amorphous silicon (2-a-Si) module for the five-parameter model using the 'January…' and 'Clear Days…' datasets and SRC data measured after 9 days of aging

D.1.5.2. Aged 16 Days

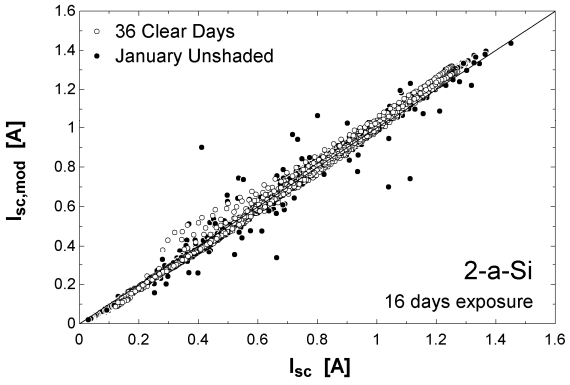

a.

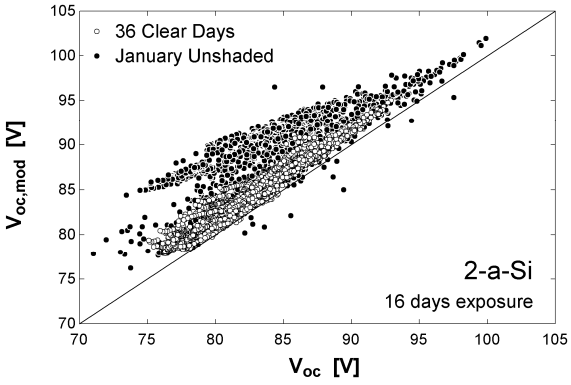

b.

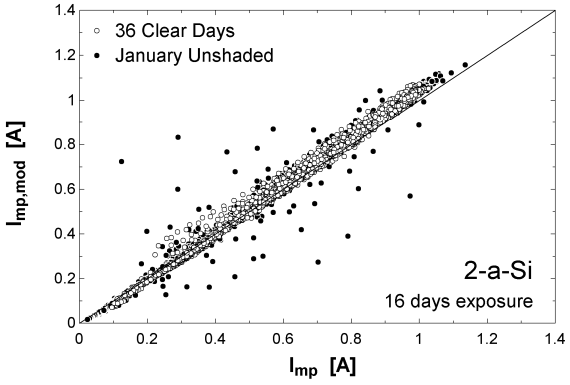

c.

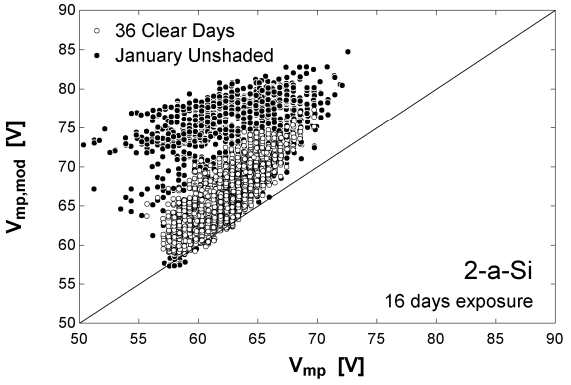

d.

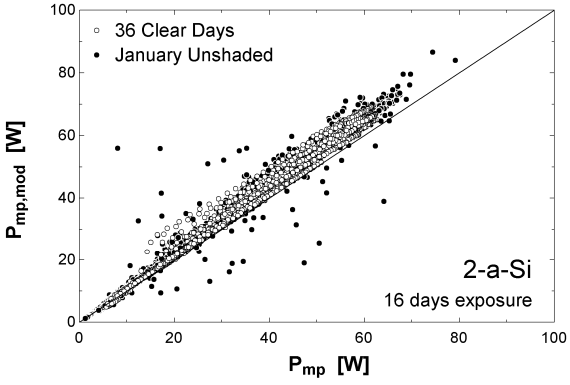

e.

Figure D.6: Model-predicted versus measured performance values of the tandem-junction amorphous silicon (2-a-Si) module for the five-parameter model using the 'January…' and 'Clear Days…' datasets and SRC data measured after 16 days of aging

D.1.5.3. Aged 25 Days

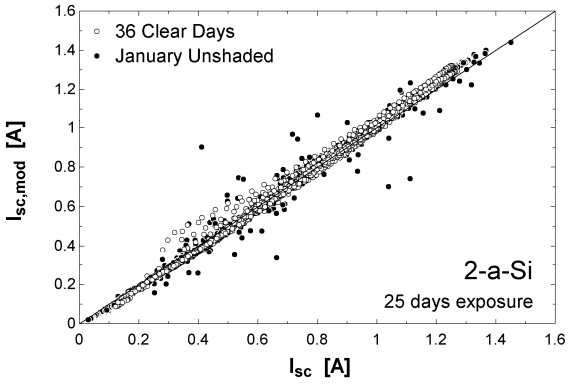

a.

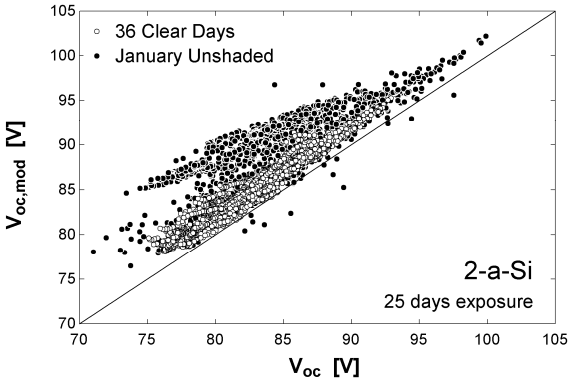

b.

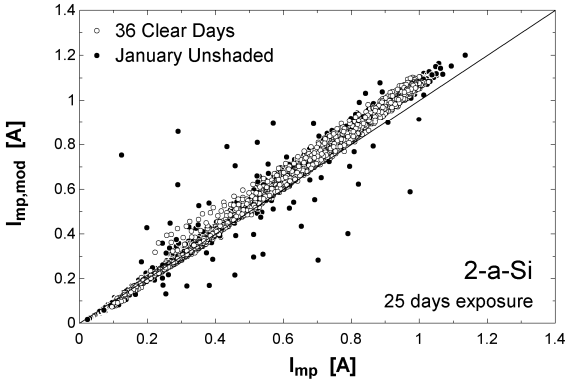

c.

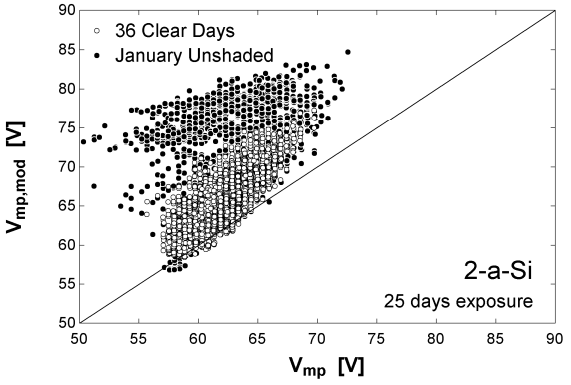

d.

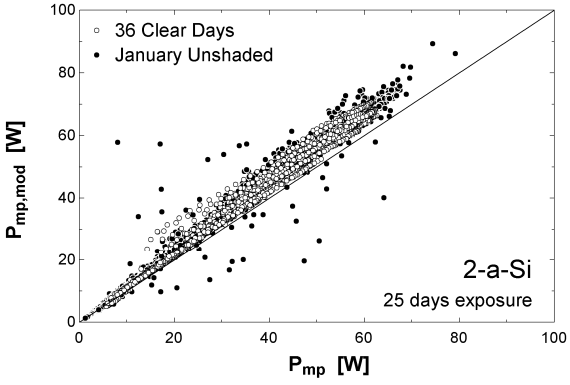

e.

Figure D.7: Model-predicted versus measured performance values of the tandem-junction amorphous silicon (2-a-Si) module for the five-parameter model using the 'January…' and 'Clear Days…' datasets and SRC data measured after 25 days of aging

D.1.5.4. Aged 630 Days

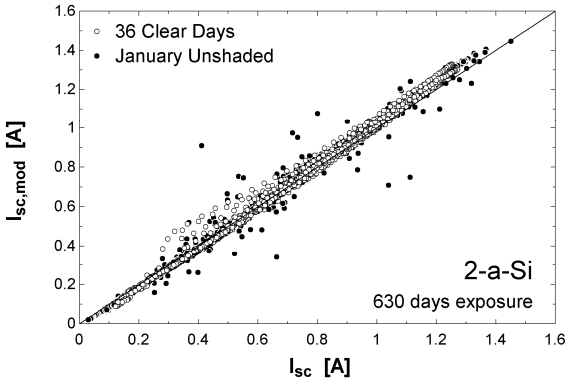

a.

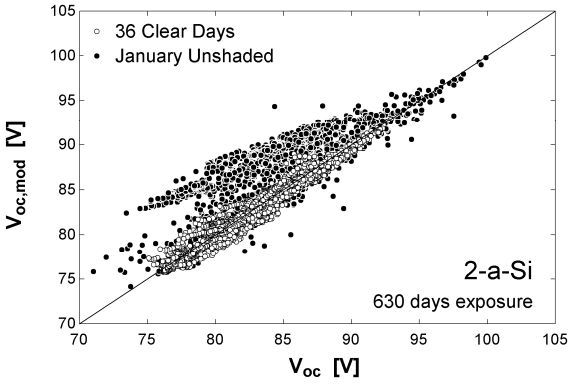

b.

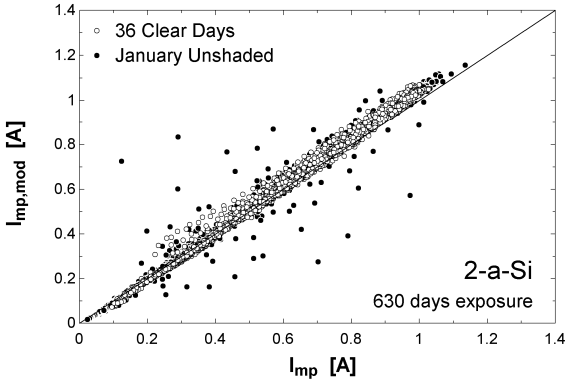

c.

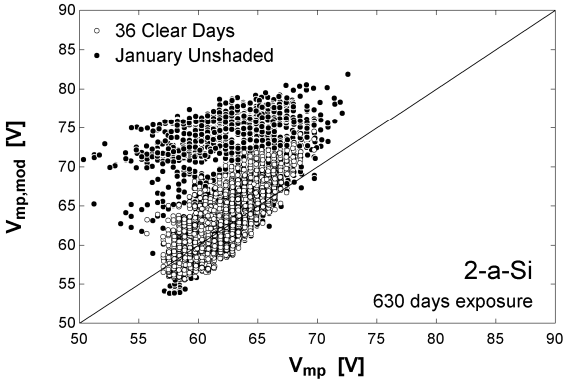

d.

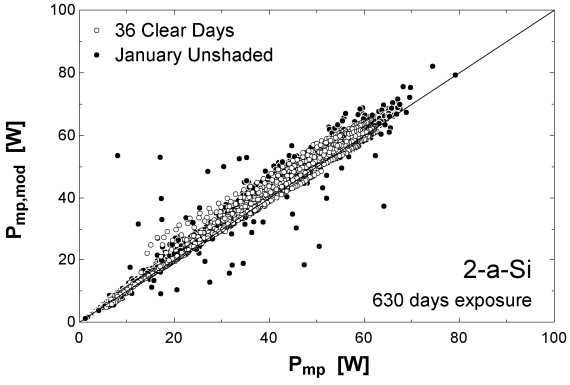

e.

Figure D.8: Model-predicted versus measured performance values of the tandem-junction amorphous silicon (2-a-Si) module for the five-parameter model using the 'January…' and 'Clear Days…' datasets and SRC data measured after 630 days of aging

D.1.5.5. Aged 631 Days

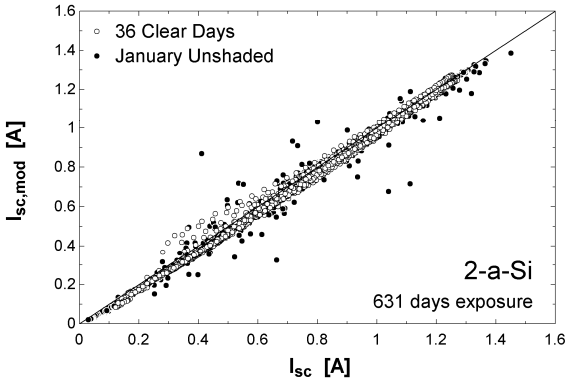

a.

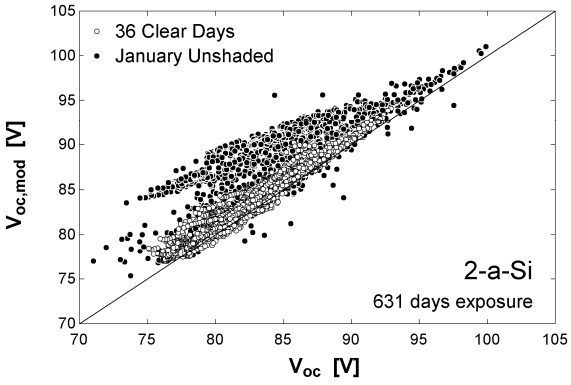

b.

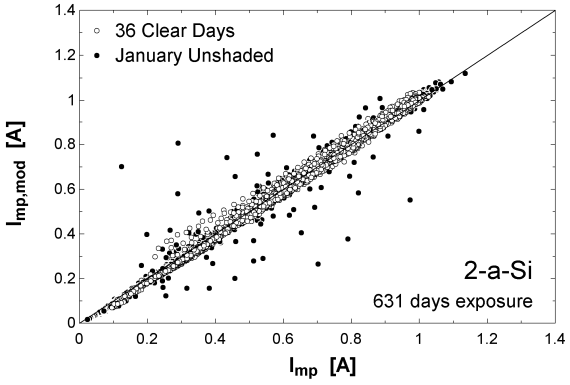

c.

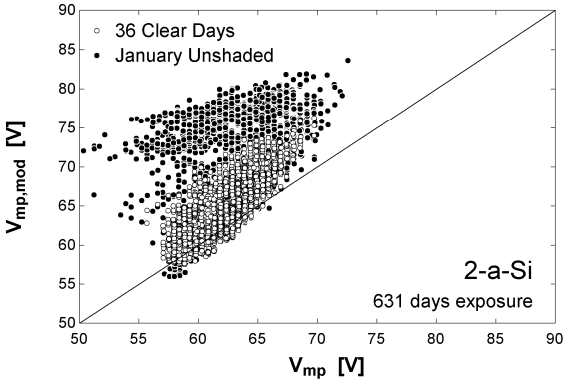

d.

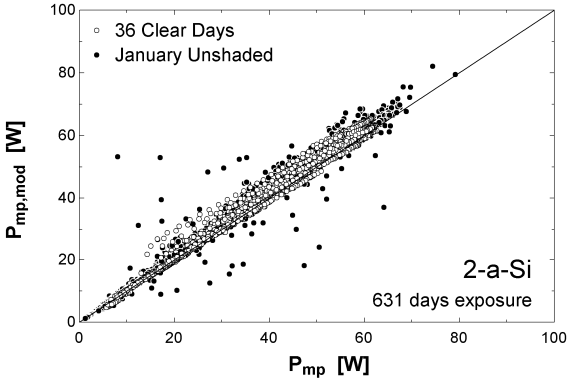

e.

Figure D.9: Model-predicted versus measured performance values of the tandem-junction amorphous silicon (2-a-Si) module for the five-parameter model using the 'January…' and 'Clear Days…' datasets and SRC data measured after 631 days of aging

D.1.6 Copper Indium Selenide (CIS)

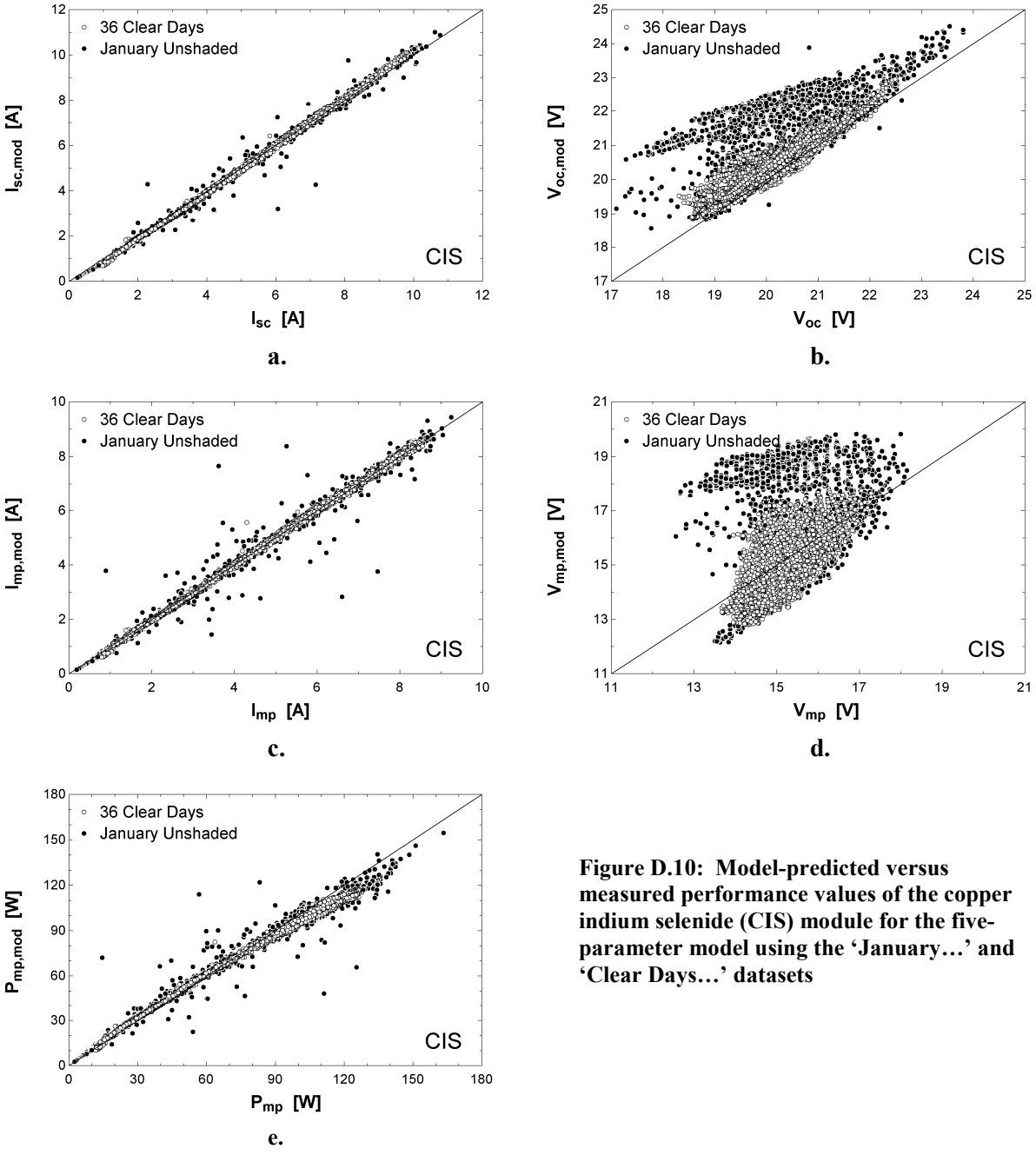

Figure D.10: Model-predicted versus measured performance values of the copper indium selenide (CIS) module for the five-parameter model using the 'January…' and 'Clear Days…' datasets

D.2 Seven-Parameter Model

D.2.1 Monocrystalline Silicon

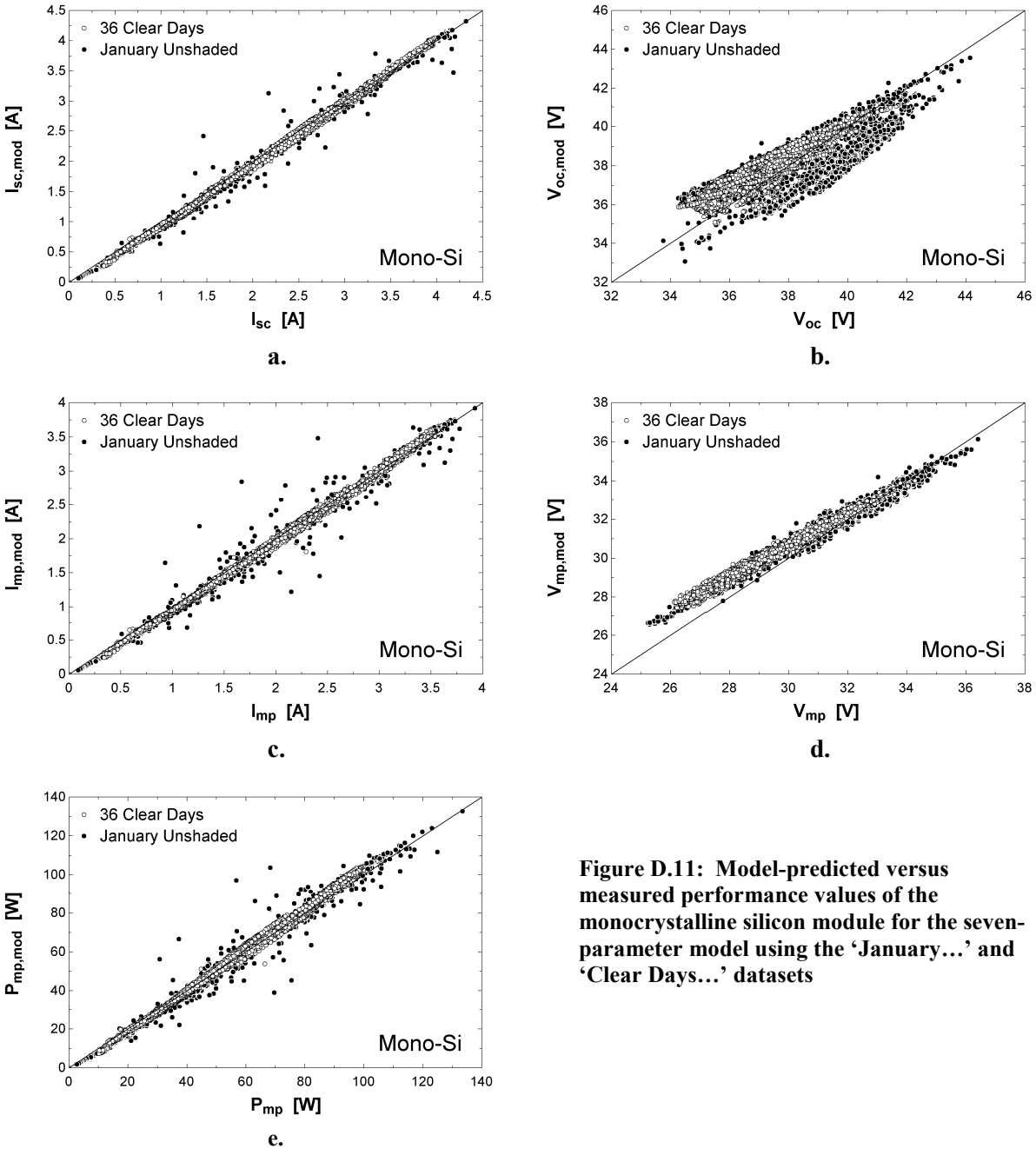

Figure D.11: Model-predicted versus measured performance values of the monocrystalline silicon module for the seven-parameter model using the 'January…' and 'Clear Days…' datasets

D.2.2 Tandem-Junction Amorphous Silicon (Aged 631 Days)

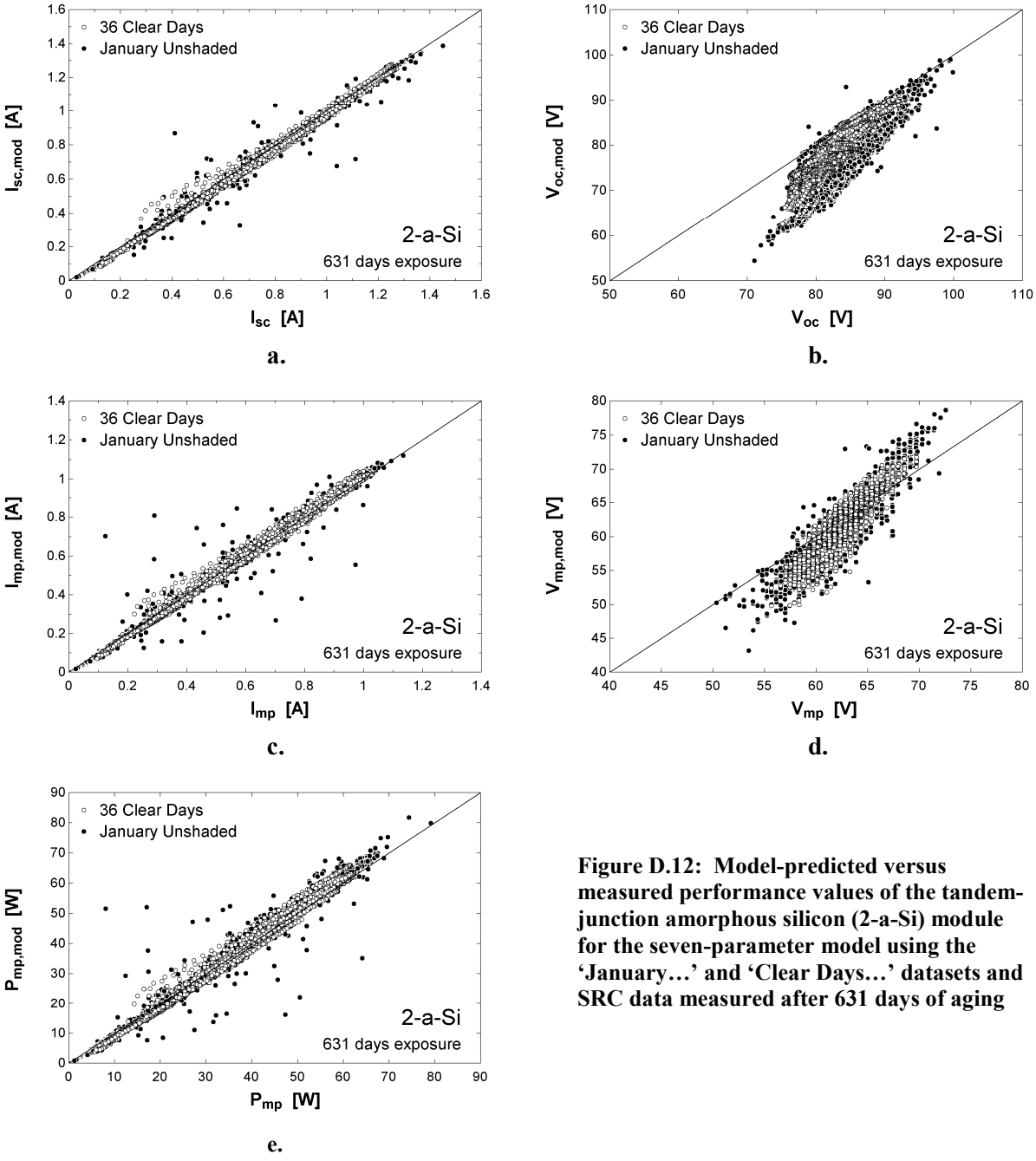

Figure D.12: Model-predicted versus measured performance values of the tandem-junction amorphous silicon (2-a-Si) module for the seven-parameter model using the 'January…' and 'Clear Days…' datasets and SRC data measured after 631 days of aging

Appendix E

Regressions for Calculation of Temperature Coefficients

E.1 Open-Circuit Voltage Versus Backside Temperature

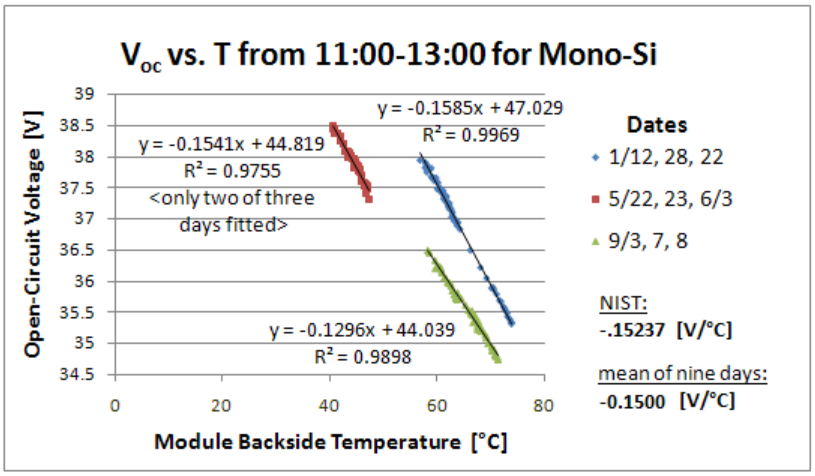

Figure E.1: Least-squares linear regression analysis of select operating data for open-circuit voltage and module temperature measured from nine clear days to determine the open-circuit voltage temperature coefficient for the Mono-Si module

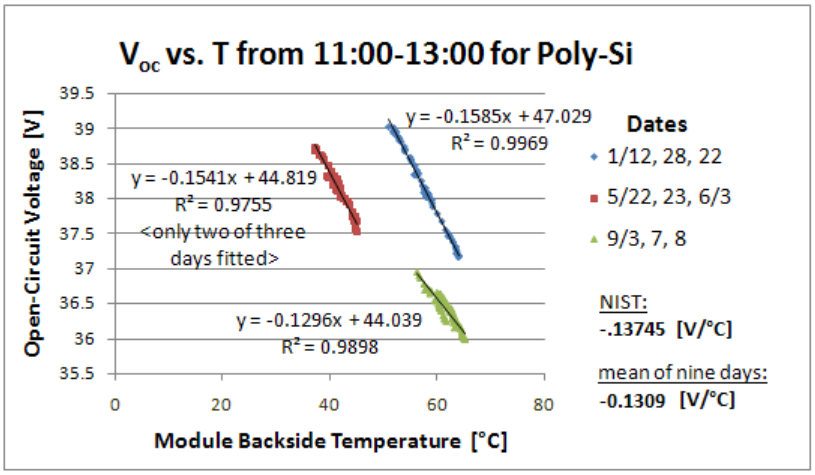

Figure E.2: Least-squares linear regression analysis of select operating data for open-circuit voltage and module temperature measured from nine clear days to determine the open-circuit voltage temperature coefficient for the Poly-Si module with the glass glazing

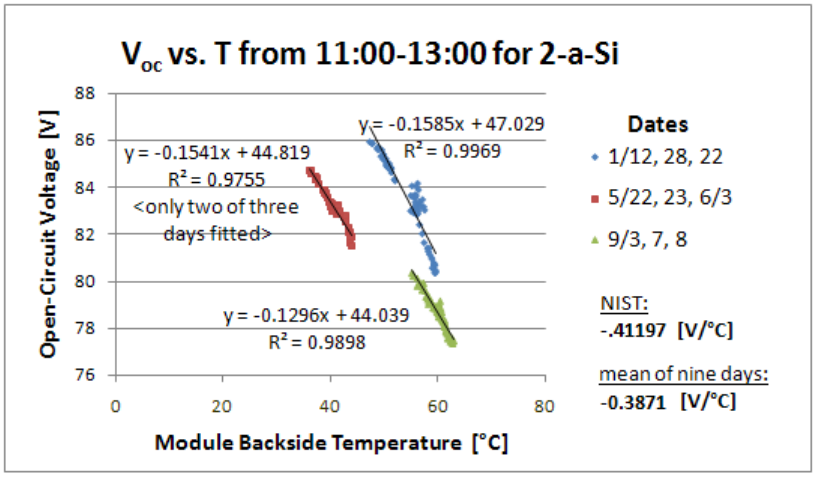

Figure E.3: **Least-squares linear regression analysis of select operating data for open-circuit voltage and module temperature measured from nine clear days to determine the open-circuit voltage temperature coefficient for the tandem-junction amorphous (2-a-Si) array**

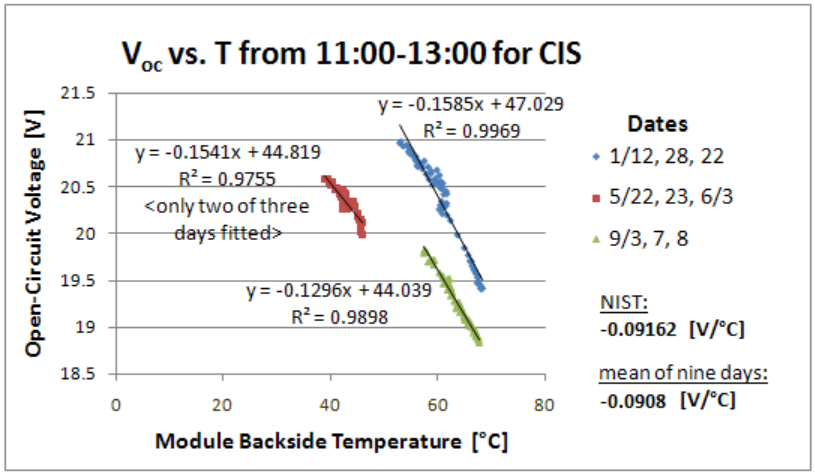

Figure E.4: **Least-squares linear regression analysis of select operating data for open-circuit voltage and module temperature measured from nine clear days to determine the open-circuit voltage temperature coefficient for the copper indium selenide (CIS) array**

E.2 Short-Circuit Current Versus Backside Temperature

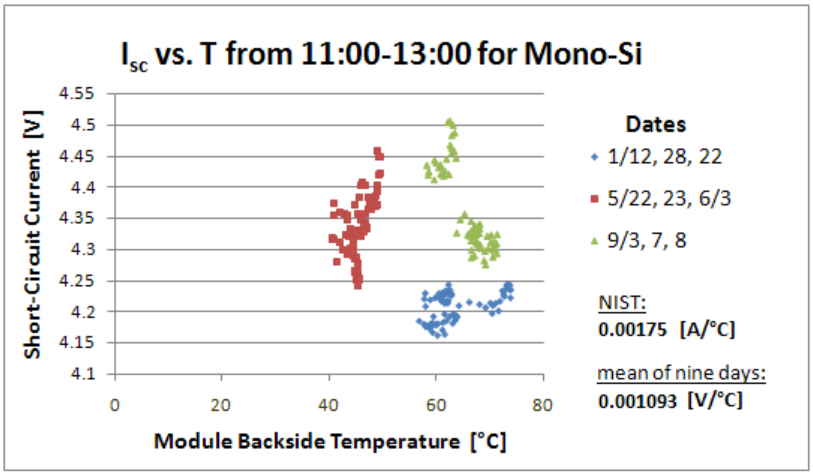

Figure E.5: **Least-squares linear regression analysis of select operating data for short-circuit current and module temperature measured from nine clear days to determine the short-circuit current temperature coefficient for the Mono-Si module**

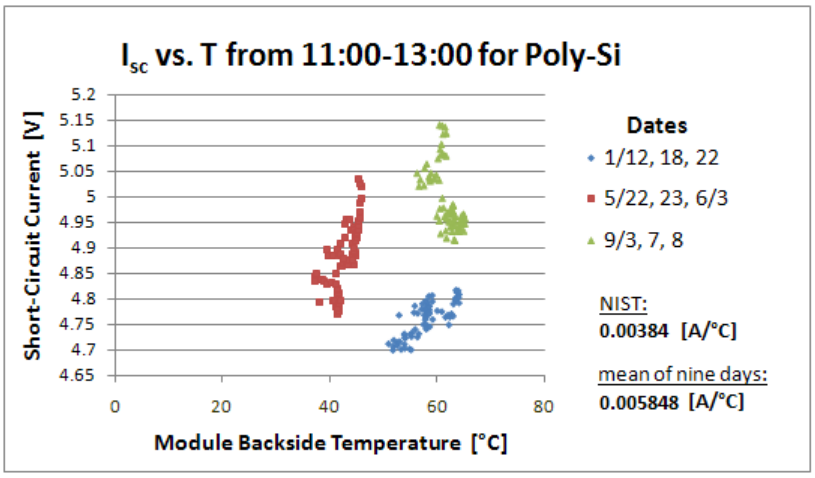

Figure E.6: **Least-squares linear regression analysis of select operating data for short-circuit current and module temperature measured from nine clear days to determine the short-circuit current temperature coefficient for the Poly-Si module with the glass glazing**

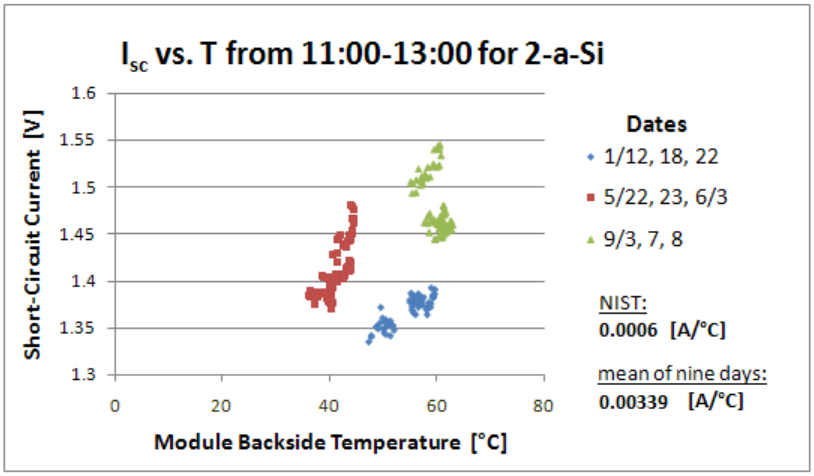

Figure E.7: **Least-squares linear regression analysis of select operating data for short-circuit current and module temperature measured from nine clear days to determine the short-circuit current temperature coefficient for the tandem-junction amorphous (2-a-Si) array**

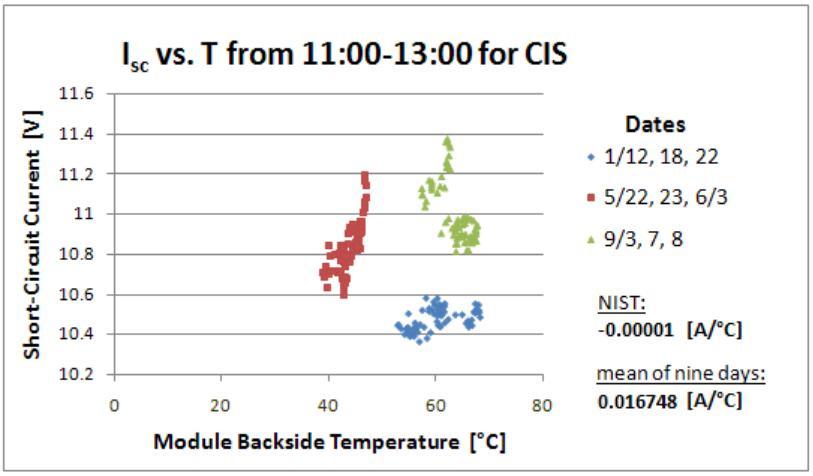

Figure E.8: **Least-squares linear regression analysis of select operating data for short-circuit current and module temperature measured from nine clear days to determine the short-circuit current temperature coefficient for the copper indium selenide (CIS) array**

Appendix F

Modeling Errors using Parameters Calculated from Operating Data

F.1 Monocrystalline Silicon

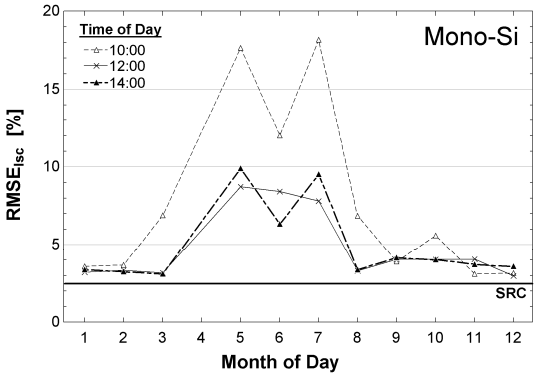

a.

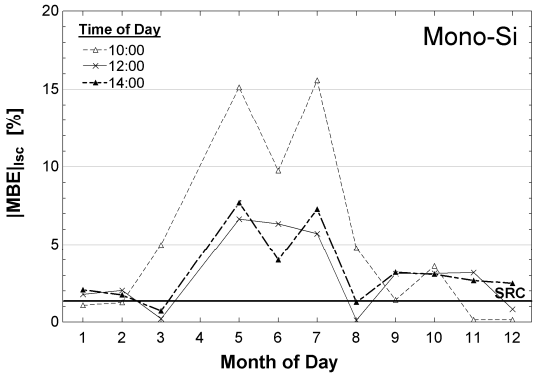

b.

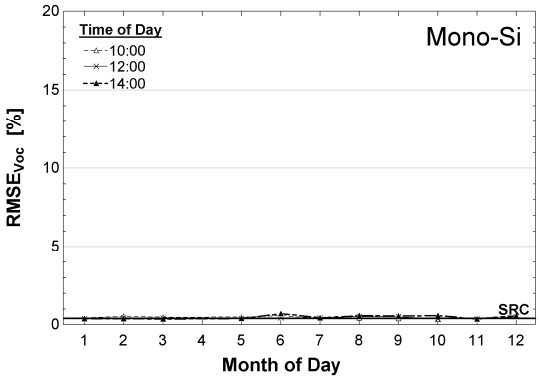

c.

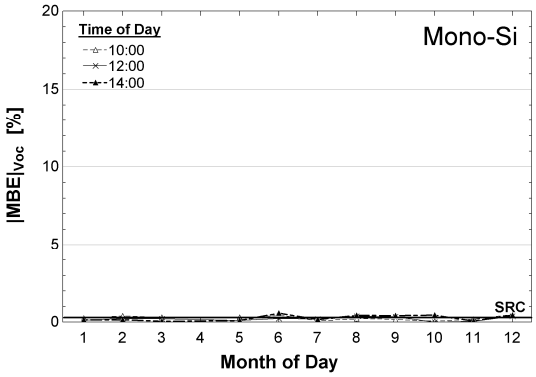

d.

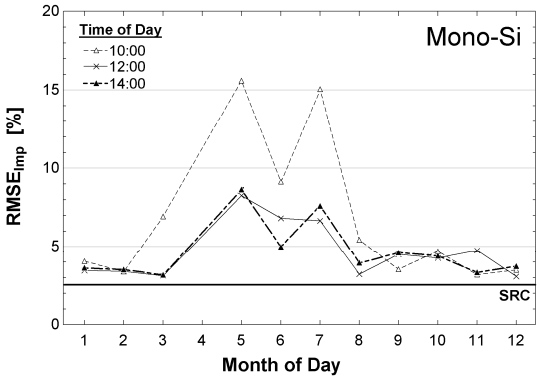

e.

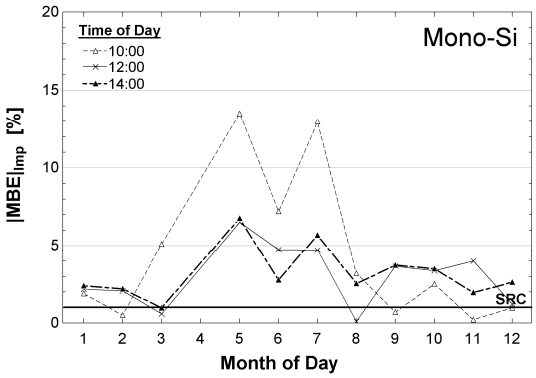

f.

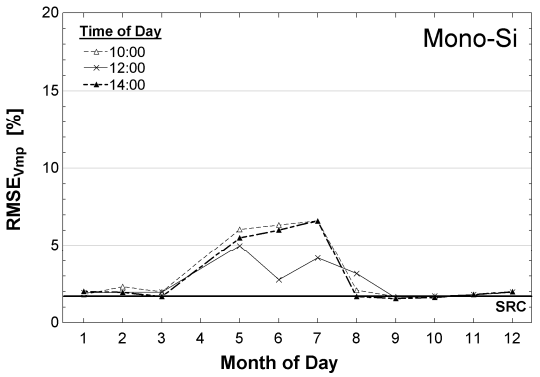

g.

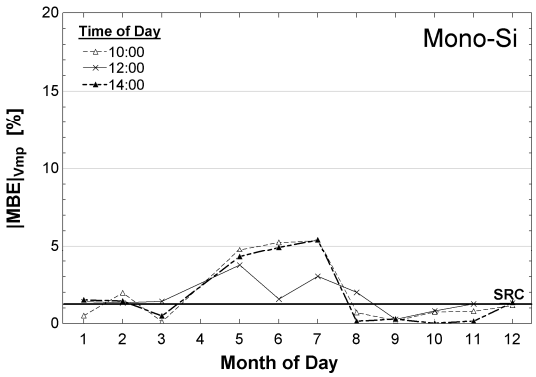

h.

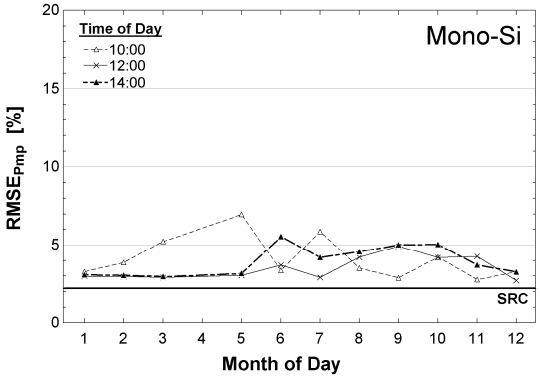

i.

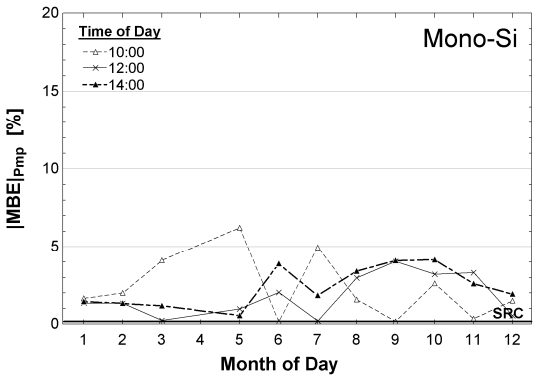

j.

Figure F.1: Modeling errors for the Mono-Si module using 33 different sets of model parameters. These parameters are calculated from operating data at 10:00, 12:00, 14:00 TST for eleven clear days nearest to middle of the indicated month. April data is excluded because there is no diffuse radiation measurement. Each data point is the modeling error for the 'Clear Days…' dataset.

F.2 Polycrystalline Silicon with Glass Glazing

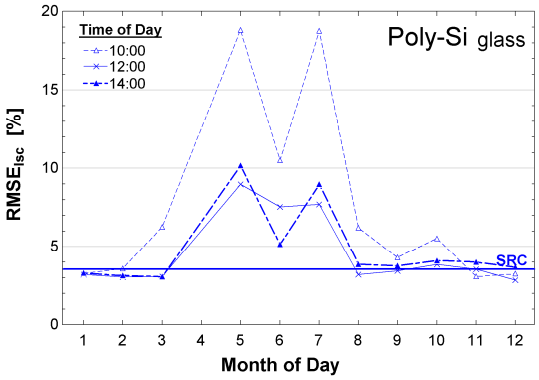

a.

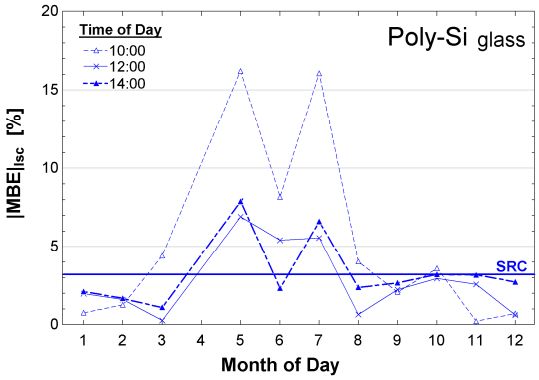

b.

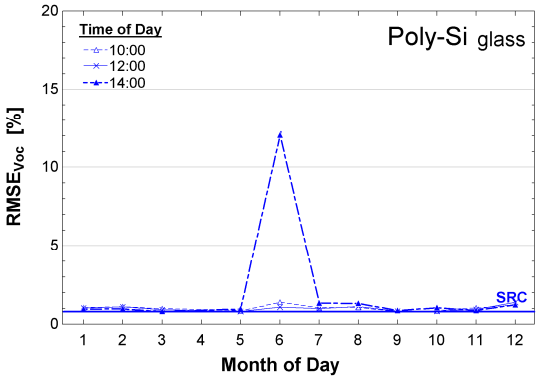

c.

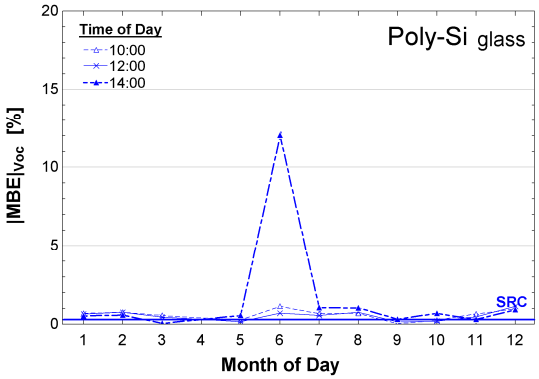

d.

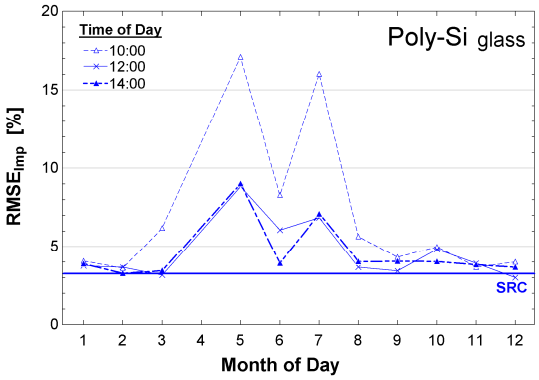

e.

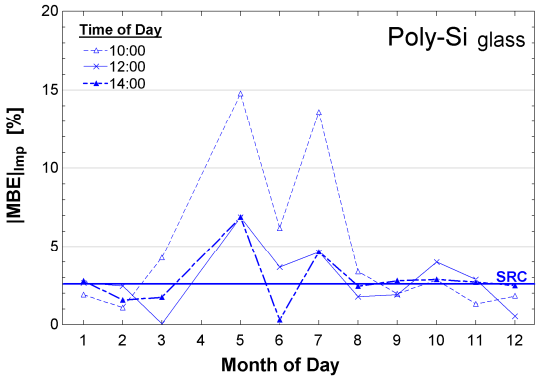

f.

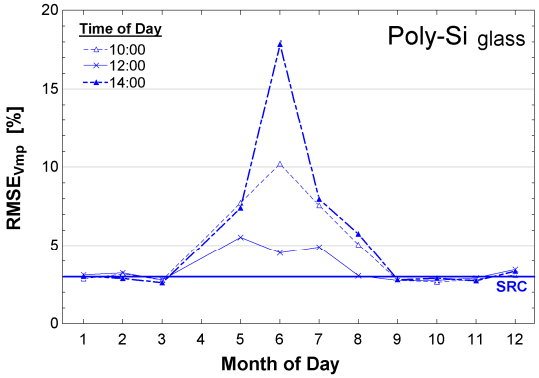

g.

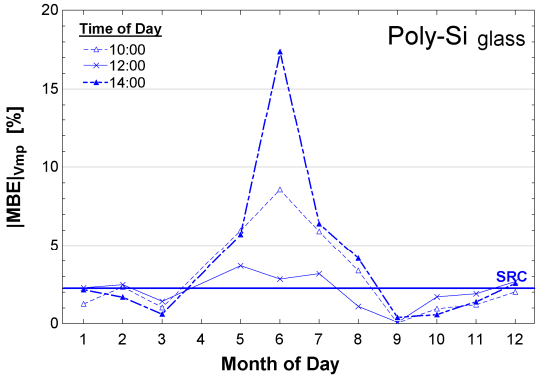

h.

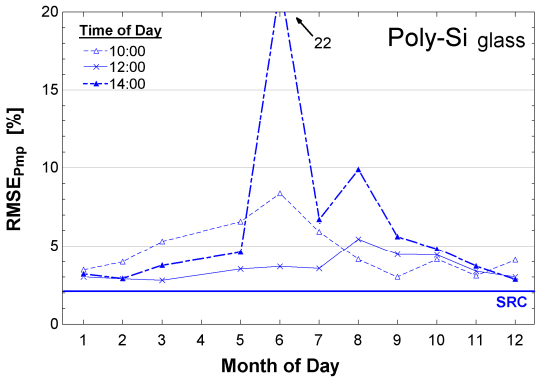

i.

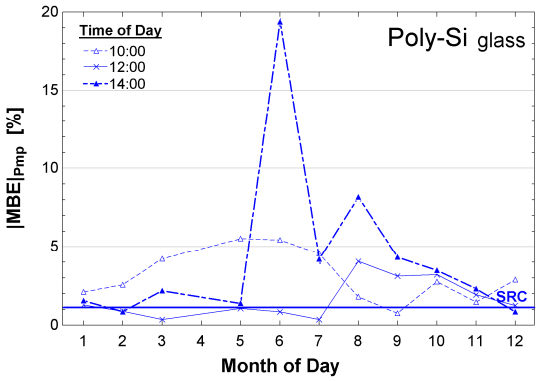

j.

Figure F.2: Modeling errors for the Poly-Si module with the glass glazing using 33 different sets of model parameters. These parameters are calculated from operating data at 10:00, 12:00, 14:00 TST for eleven clear days nearest to middle of the indicated month. April data is excluded because there is no diffuse radiation measurement. Each data point is the modeling error for the 'Clear Days…' dataset.

F.3 Tandem-Junction Amorphous Silicon

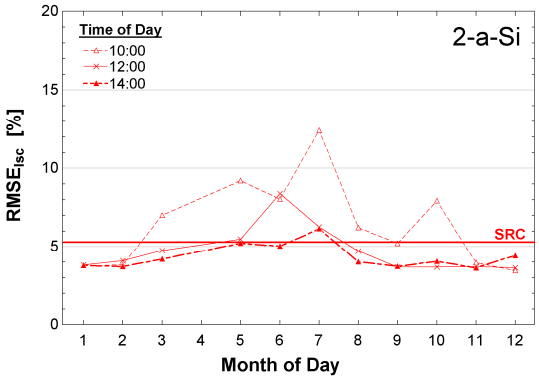

a.

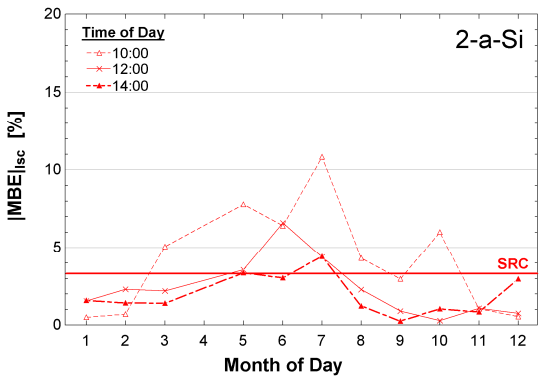

b.

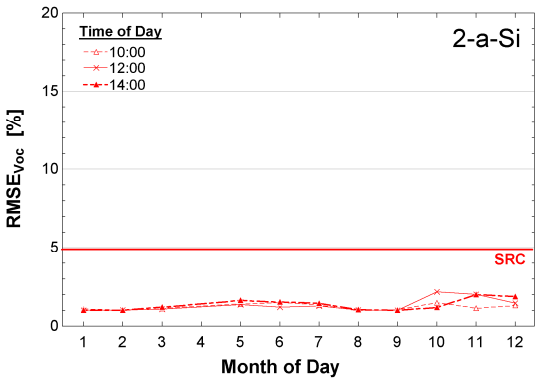

c.

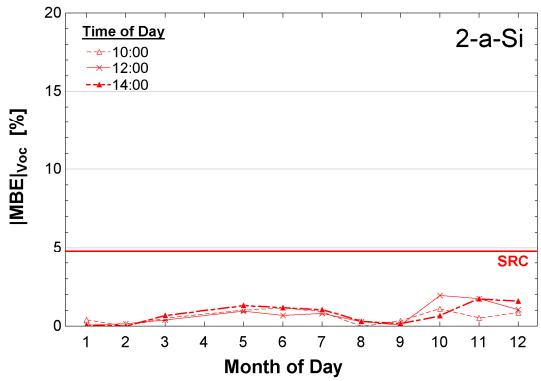

d.

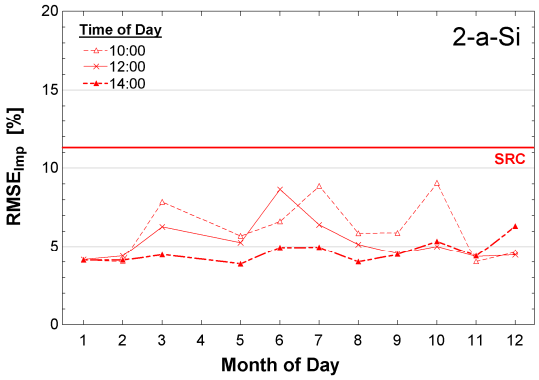

e.

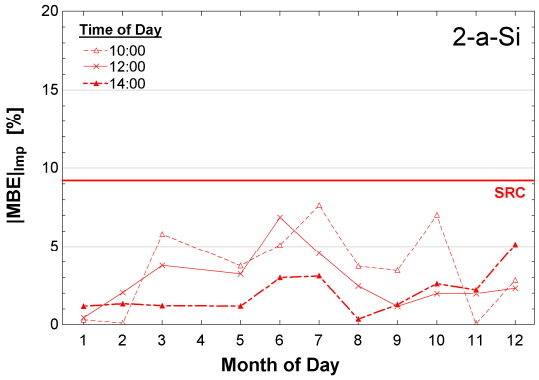

f.

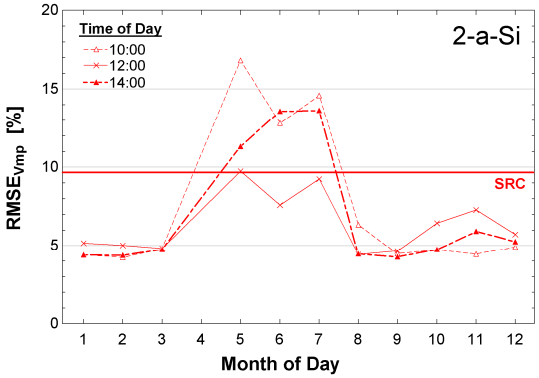

g.

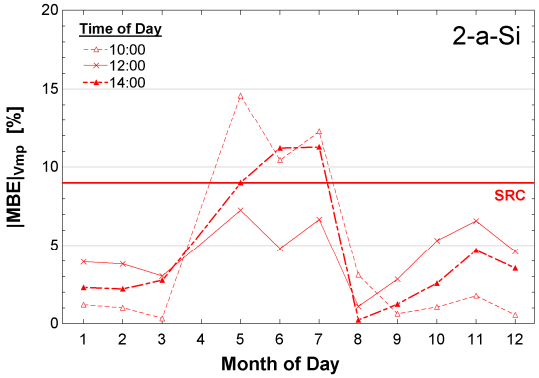

h.

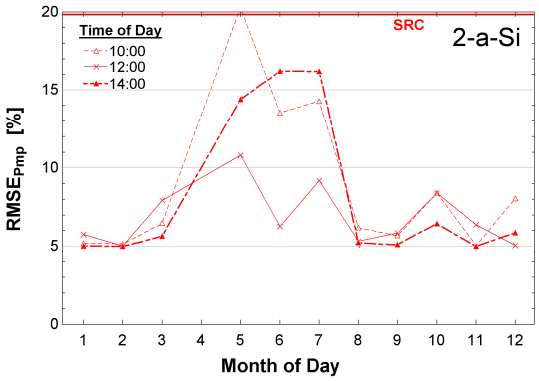

i.

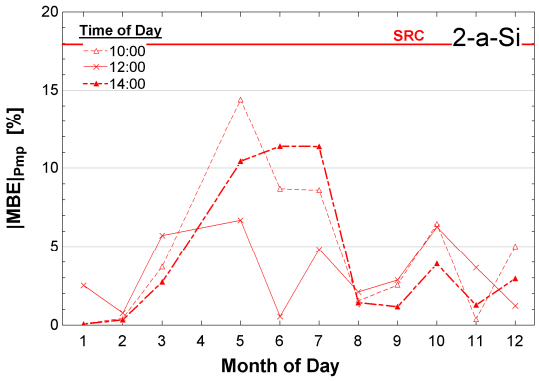

j.

Figure F.3: Modeling errors for the tandem-junction amorphous silicon (2-a-Si) array using 33 different sets of model parameters. These parameters are calculated from operating data at 10:00, 12:00, 14:00 TST for eleven clear days nearest to middle of the indicated month. April data is excluded because there is no diffuse radiation measurement. Each data point is the modeling error for the 'Clear Days…' dataset.

F.4 Copper Indium Selenide (CIS)

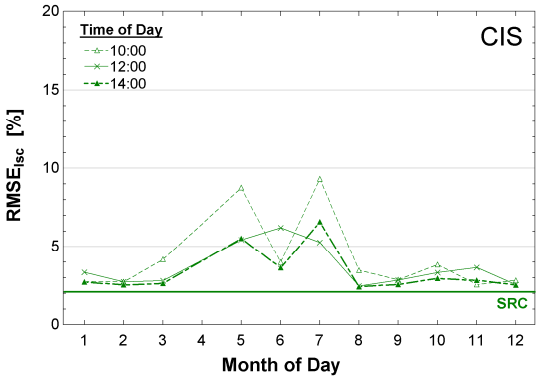

a.

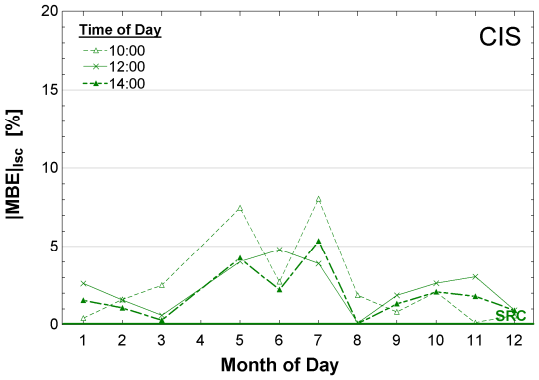

b.

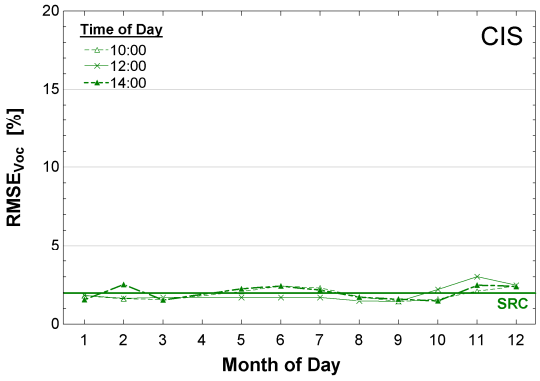

c.

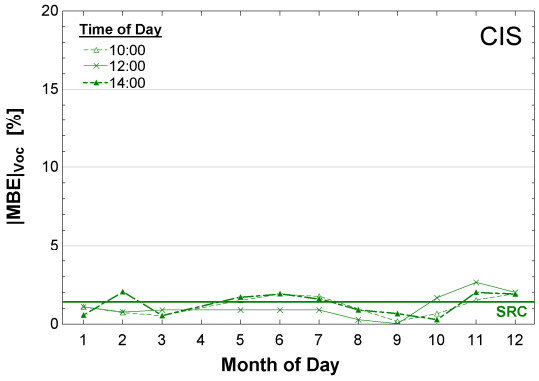

d.

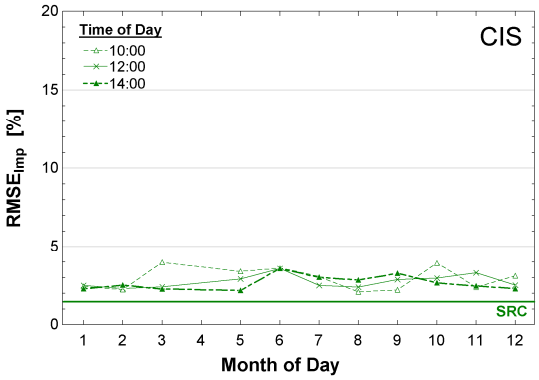

e.

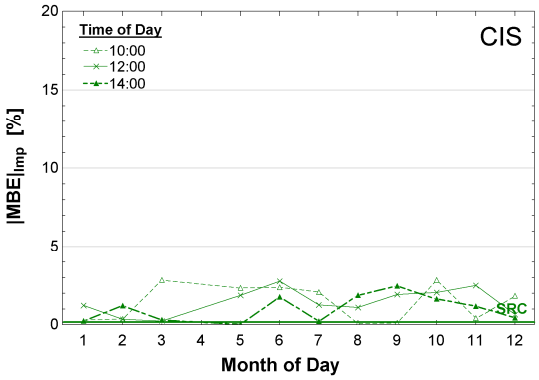

f.

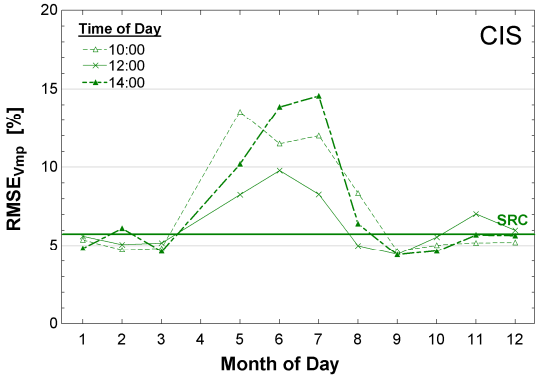

g.

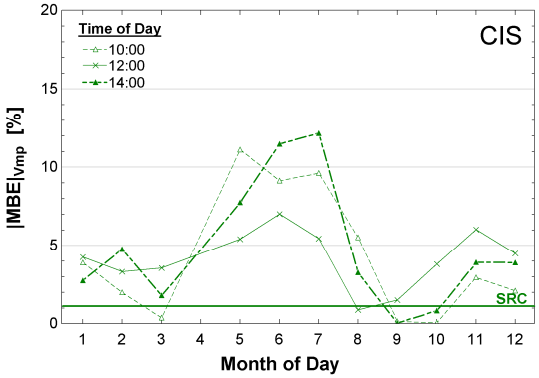

h.

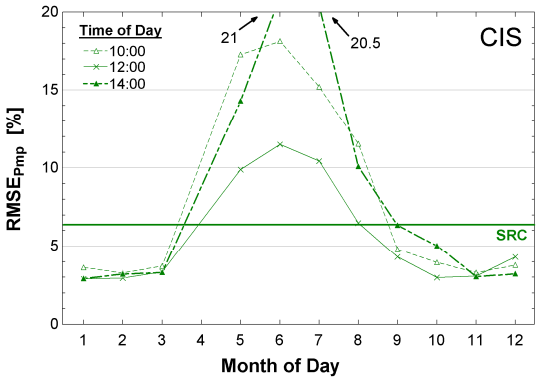

i.

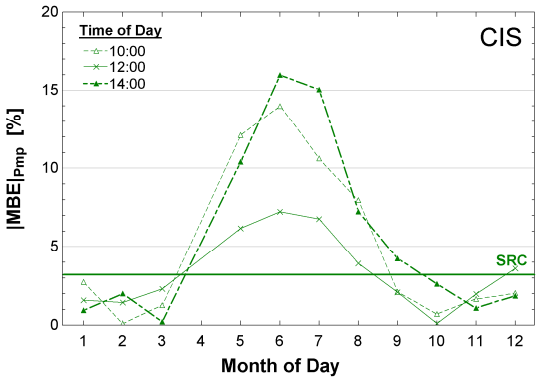

j.

Figure F.4: Modeling errors for the copper indium selenide (CIS) array using 33 different sets of model parameters. These parameters are calculated from operating data at 10:00, 12:00, 14:00 TST for eleven clear days nearest to middle of the indicated month. April data is excluded because there is no diffuse radiation measurement. Each data point is the modeling error for the 'Clear Days…' dataset.

Appendix G

Manufacturer Model Survey Including Temperature Coefficients

Table G.1: The number of models of different cell technologies and the temperature coefficients provided by manufacturers that produced more than 0.1% of the total 2007 cell market production (Hirshman, 2008). The companies are listed in descending order according to total 2007 production, measured in produced power.

		Number of Models						Temperature Coefficients				
Rank	**Company**	**Mono-Si**	**Poly-Si**	**a-Si**	**CIS**	**CdTe**		α_{Isc}	β_{Voc}	γ_{Pmp}	α_{Imp}	β_{Vmp}
1	Q-Cells	5	32	9	-	7		X	X	X	-	-
2	Sharp	1	15	-	-	-		X	X	X	-	-
3	Suntech Power	32	30	-	-	-		X	X	X	-	-
4	Kyocera	-	14	-	-	-		X	X	-	-	-
5	First Solar	-	-	-	-	9		X	X	X	-	-
6	Motech	52	148	-	-	-		X	X	X	-	-
7	SolarWorld	3	-	-	-	-		X	X	-	-	-
8	Sanyo	17	-	-	-	-		X	X	X	-	-
9	Baoding Tianwei Yingli	19	-	-	-	-		X	X	X	-	-
10	Mitsubishi	-	47	-	-	-		X	X	X	-	-
11	JA Solar	35	26	-	-	-		X	X	X	-	-
12	BP Solar	4	27	0	0	-		X	X	X	-	-
13	Ningbo Solar Electric	23	25	-	-	-		X	X	X	-	-
14	SunPower	6	0	0	0	-		X	X	X	-	-
15	Isofoton	9	-	-	-	-		X	X	X	-	-
16	Schott	1	4	-	-	-		X	X	X	-	-
17	China Sunergy	48	28	-	-	-		X	X	X	-	-
18	Evergreen	-	9	-	-	-		X	X	X	X	X
19	E-Ton Solar	38	15	-	-	-		X	X	X	-	-
20	Gintech	-	21	-	-	-		X	X	X	-	-
21	Ersol Solar	9	16	4	-	-		X	X	X	-	-
22	Delsolar	2	1	-	-	-		X	X	-	-	-
23	Shanghai Chaori	8	9	-	-	-		X	X	X	-	-
24	United Solar	-	-	3	-	-		X	X	X	X	X
25	REC Scancell	-	5	-	-	-		X	X	X	-	-
26	Kaneka	-	-	12	-	-		X	X	X	-	-
27	Canadian Solar	-	33	-	-	-		X	X	-	-	-
28	Photowatt	12	27	-	-	-		X	X	X	-	-
29	Sunways	27	35	-	-	-		X	X	X	-	-
30	Neo Solar	144	96	-	-	-		X	X	X	-	-

31	Solland	-	16	-	-	-		X	X	-	-	-
32	Jiangyin Jetion	22	18	-	-	-		X	X	X	-	-
33	Moser Baer	8	8	-	-	-		X	X	X	-	-
34	Instalaciones Pevafersa	3	13	-	-	-		X	X	X	-	-
35	Solartech Energy	21	22	-	-	-		-	-	-	-	-
36	Photovoltech NV	-	18	-	-	-		X	X	X	-	-
37	Trina	9	3	-	-	-		X	X	X	-	-
38	Chint Solar	40	40	-	-	-		X	X	X	-	-
39	Jiangsu ShunFeng	26	4	-	-	-		-	-	-	-	-
40	Kyungdong Photovoltaic	20	-	-	-	-		-	-	-	-	-
41	Shanghai Solar Energy	8	16	-	-	-		X	X	X	-	-
42	Trony Science	-	-	11	-	-		X	X	X	-	-
43	Zhejiang Shuqimeng Energy	5	-	-	-	-		X	X	X	-	-
44	Mosel Vitelic	-	33	-	-	-		X	X	X	-	-
45	Scheuten Solar	-	6	-	-	-		X	X	X	-	-
46	Ninghai Risen	17	-	-	-	-		-	-	-	-	-
47	Sinonar	-	-	92	-	-		-	-	-	-	-
48	Wurth Solar	-	-	-	8	-		X	X	X	-	-
49	Jiangsu Hauguang Solartech	37	37	-	-	-		-	-	-	-	-
50	Chinalight Solar	-	7	-	-	-		X	X	X	-	-
51	Fuji Electric	-	-	-	-	-		-	-	-	-	-
52	Suzhou Shenglong	6	-	-	-	-		X	X	X	-	-
53	Bangkok Solar	-	-	3	-	-		-	-	-	-	-
54	Changzhou EGing	1	-	-	-	-		-	-	-	-	-
55	Solar EnerTech	15	-	-	-	-		X	X	X	X	X
56	Solarwatt	52	18	-	-	-		X	X	X	-	-
57	Top Green Energy	16	32	-	-	-		-	-	-	-	-
58	Yunnan Tianda	1	-	-	-	-		X	X	X	X	X
59	Centrosolar	14	30	4	-	-		X	X	X	-	-
60	Zhejiang Sun Valley	43	-	-	-	-		-	-	-	-	-
61	Big Sun	20	11	-	-	-		X	X	X	-	-
62	EPV Solar	-	-	2	-	-		X	X	X	-	-
63	KIS	18	-	-	-	-		-	-	-	-	-
64	Solar Wind	22	-	-	-	-		X	X	X	-	-
	Total:	**919**	**995**	**140**	**8**	**16**		**52**	**52**	**17**	**8**	**8**

Appendix H

Five-Parameter and Radiation Model Inputs

(Note: '+' indicates variable is included in sensitivity analysis)

I. Variable with Uncertainty

a. Measured

i. Time Dependent

1.	G_{bn}		beam normal radiation
2.	G_d		diffuse radiation
3.	G_T		plane-of-array total radiation
4.	T_{module}		backside panel temperature

ii. Time Independent

1.	α_{Isc}	+	temperature coefficient of short-circuit current
2.	β		module slope
3.	β_{Voc}	+	temperature coefficient of open-circuit voltage
4.	C	+	material band gap temperature dependence
5.	$E_{g,ref}$	+	material band gap energy at reference temp.
6.	γ		module azimuth
7.	G_{ref}		reference irradiance
8.	$I_{mp,ref}$	+	reference maximum power current
9.	$I_{sc,ref}$	+	reference short-circuit current
10.	K	+	glazing extinction coefficient
11.	L	+	glazing thickness
12.	n_{glaz}	+	refractive index of glazing
13.	ρ_g	+	ground reflectance
14.	$T_{c,ref}$	+	reference cell temperature
15.	$V_{mp,ref}$	+	reference maximum power voltage
16.	$V_{oc,ref}$	+	reference open-circuit voltage

b. Calculated

i.	a	modified ideality factor at operating condition
ii.	a_{10}	modified ideality factor at non-reference temperature
iii.	E_g	material band gap energy at operating temperature
iv.	$E_{g,10}$	material band gap energy at non-reference temperature
v.	$G_{T,HDKR}$	radiation on tilted surface using HDKR model
vi.	I_o	diode reverse saturation current at operating condition
vii.	$I_{o,10}$	diode reverse saturation current at non-reference temperature
viii.	I_L	light current at operating condition
ix.	$I_{L,10}$	light current at non-reference temperature
x.	$\tau\alpha_b$	trans-absorb product at beam incidence angle
xi.	$\tau\alpha_d$	trans-absorb product at diffuse incidence angle
xii.	$\tau\alpha_g$	trans-absorb product at ground reflected incidence angle
xiii.	$\tau\alpha_n$	trans-absorb product at normal incidence
xiv.	R_s	series resistance at operating condition
xv.	$R_{s,10}$	series resistance at non-reference temperature
xvi.	R_{sh}	shunt resistance at operating condition

xvii.	$R_{sh,10}$		shunt resistance at non-reference temperature
xviii.	S_{HDKR}		absorbed radiation using HDKR model
xix.	S_{ref}	+	reference absorbed radiation
xx.	T_{cell}		cell temperature (assumed equal to T_{module})
xxi.	θ_d		diffuse incidence angle
xxii.	θ_g		ground reflected incidence angle
xxiii.	$V_{oc,10}$		open-circuit voltage at non-reference temperature

c. Other

i.	ΔT_{mod}	+	non-ref. temp diff. for parameter calculation (10 K)

II. Variables Assumed Accurate

a. Measured

i.	*day*	day of month
ii.	*lat*	latitude
iii.	*long*	longitude
iv.	L_{st}	standard meridian
v.	*month*	month of year
vi.	n	day of year
vii.	n_{air}	refractive index of air
viii.	N_p	number of modules in parallel
ix.	N_s	number of cells in series
x.	$time_{EST}$	eastern standard time (EST)

b. Calculated

i.	a_{ref}	modified ideality factor at reference conditions
ii.	$dI\backslash dV_{mp,mod}$	derivative of char. equation at max power
iii.	$dI\backslash dV_{mp,ref}$	derivative of char. equation at reference max power
iv.	E	equation of time – minute correction (=f(n))
v.	G_b	beam radiation (=f($G_{bn,}$ θ_b))
vi.	G_{bd}	radiation on horizontal (= G_b + G_d)
vii.	G_o	extraterrestrial rad. on horizontal surface (=f(G_{on}, θ_z))
viii.	G_{on}	extraterrestrial rad. on normal surface (=f(n))
ix.	$I_{L,ref}$	light current at reference condition
x.	$I_{o,ref}$	diode reverse saturation current at reference condition
xi.	ω	hour angle (=f(TST))
xii.	P_{mp}	maximum power (= I_{mp} * V_{mp})
xiii.	R_b	ratio of rad. on tilted to horiz. surface (= f(lat, n, ω, β, γ))
xiv.	$R_{s,ref}$	series resistance at reference condition
xv.	$R_{sh,ref}$	shunt resistance at reference condition
xvi.	θ_b	beam incidence angle
xvii.	θ_r	glazing refraction angle
xviii.	θ_z	zenith angle
xix.	TST	true solar time

III. Symbolic Variables

a.	A_i	anisotropy index (= G_{bn}/G_{on})
b.	f_{HDKR}	(= sqrt(G_b/G))
c.	$I_{mp,mod1}$	modeled I_{mp} of one module in array
d.	$I_{sc,mod1}$	modeled I_{sc} of one module in array
e.	$K_{(\tau\alpha)b}$	beam inc. angle mod. (= $\tau\alpha_b/\ \tau\alpha_n$)
f.	$K_{(\tau\alpha)d}$	diffuse inc. angle mod. (= $\tau\alpha_d/\ \tau\alpha_n$)

g. $K_{(\tau\alpha)g}$ ground refl. inc. angle mod. (= $\tau\alpha_g / \tau\alpha_n$)
h. R_{HDKR} correction factor using measured POA (= $G_T/G_{T,HDKR}$)
i. $S_{HDKR,c}$ corrected absorbed radiation (= S_{HDKR} * R_{HDKR})
j. $S_{HDKR,c} \backslash S_{ref}$ (= $S_{HDKR,c}/S_{ref}$)
k. T_{10} (= $T_{ref} + \Delta T_{mod}$)

Appendix I

Sensitivity Analysis of the Five-Parameter Model

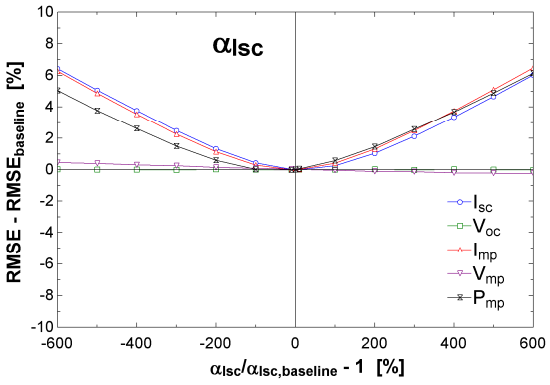

a.

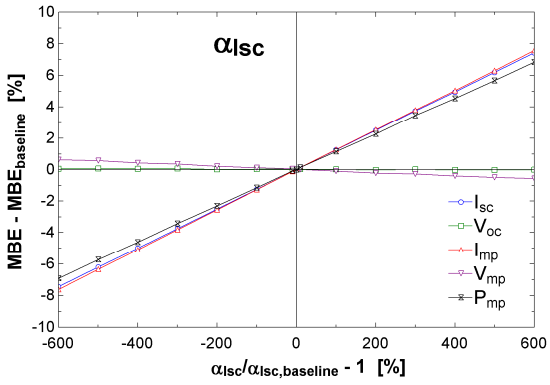

b.

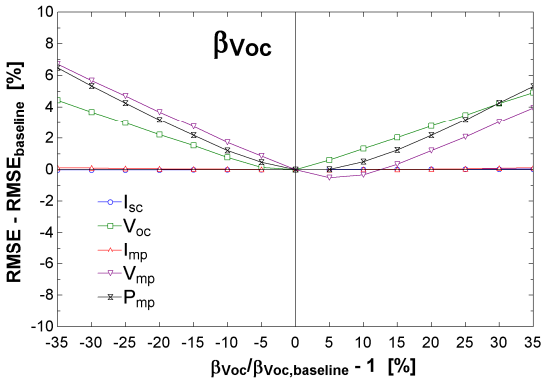

c.

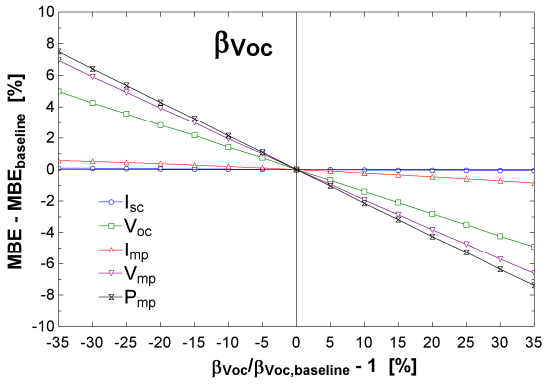

d.

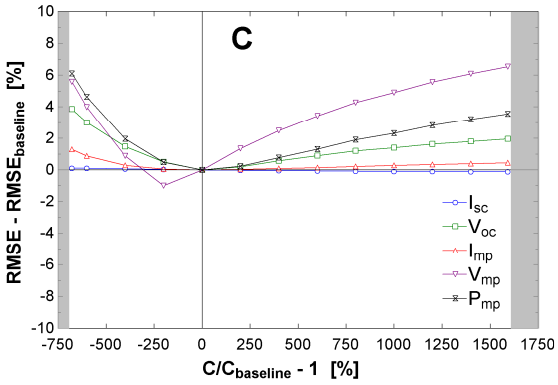

e.

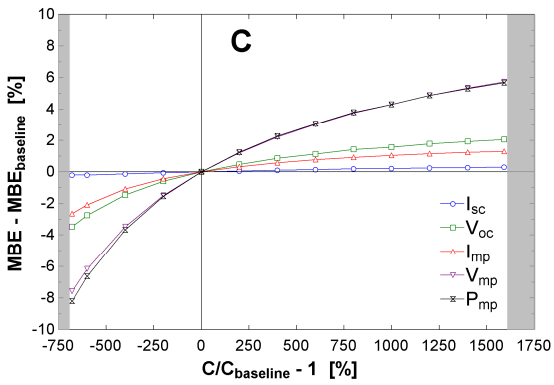

f.

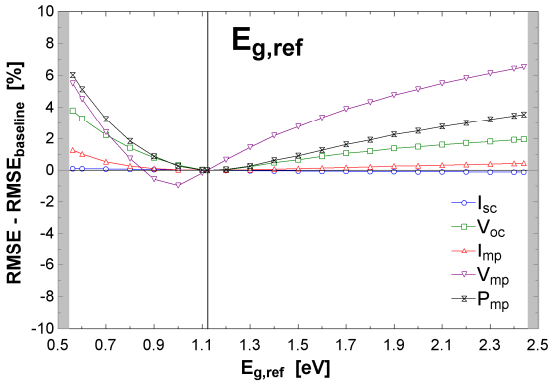
$E_{g,ref}$
RMSE - $RMSE_{baseline}$ [%]
$E_{g,ref}$ [eV]
I_{sc}
V_{oc}
I_{mp}
V_{mp}
P_{mp}

g.

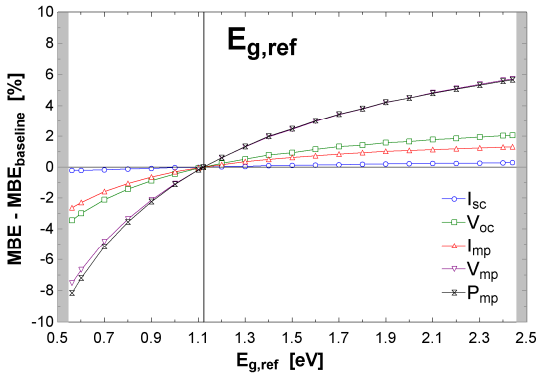
$E_{g,ref}$
MBE - $MBE_{baseline}$ [%]
$E_{g,ref}$ [eV]
I_{sc}
V_{oc}
I_{mp}
V_{mp}
P_{mp}

h.

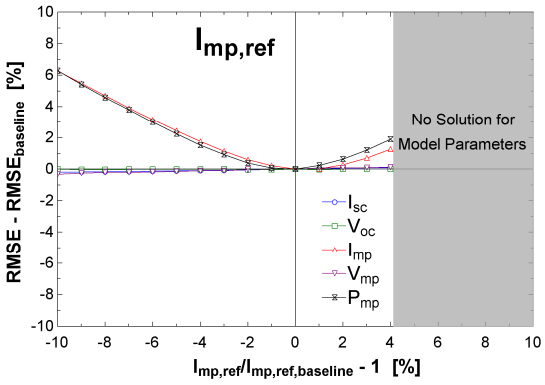
$I_{mp,ref}$
No Solution for Model Parameters
RMSE - $RMSE_{baseline}$ [%]
$I_{mp,ref}/I_{mp,ref,baseline}$ - 1 [%]
I_{sc}
V_{oc}
I_{mp}
V_{mp}
P_{mp}

i.

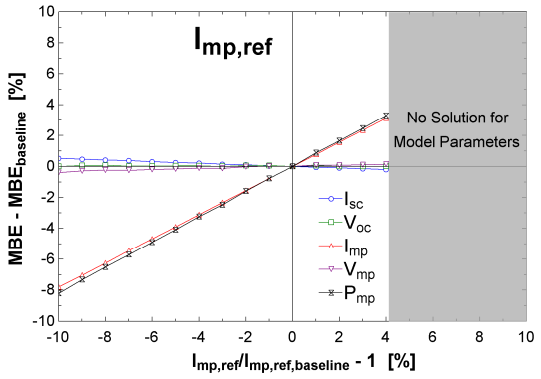
$I_{mp,ref}$
No Solution for Model Parameters
MBE - $MBE_{baseline}$ [%]
$I_{mp,ref}/I_{mp,ref,baseline}$ - 1 [%]
I_{sc}
V_{oc}
I_{mp}
V_{mp}
P_{mp}

j.

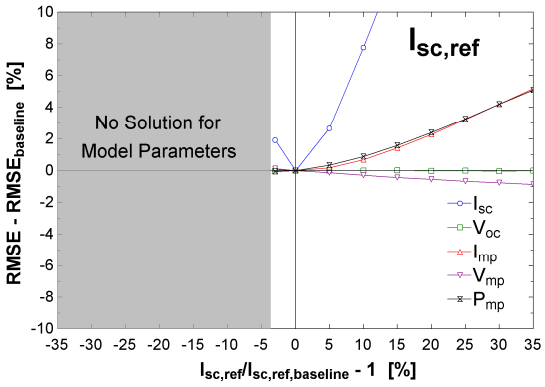
$I_{sc,ref}$
No Solution for Model Parameters
RMSE - $RMSE_{baseline}$ [%]
$I_{sc,ref}/I_{sc,ref,baseline}$ - 1 [%]
I_{sc}
V_{oc}
I_{mp}
V_{mp}
P_{mp}

k.

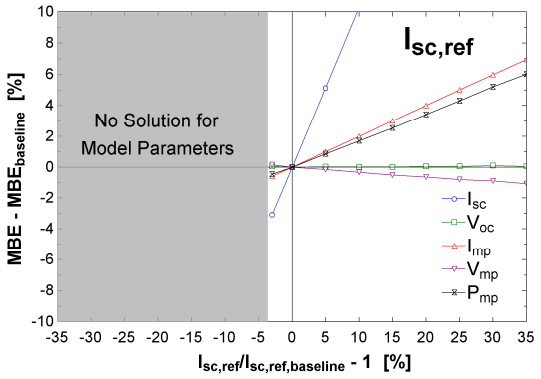
$I_{sc,ref}$
No Solution for Model Parameters
MBE - $MBE_{baseline}$ [%]
$I_{sc,ref}/I_{sc,ref,baseline}$ - 1 [%]
I_{sc}
V_{oc}
I_{mp}
V_{mp}
P_{mp}

l.

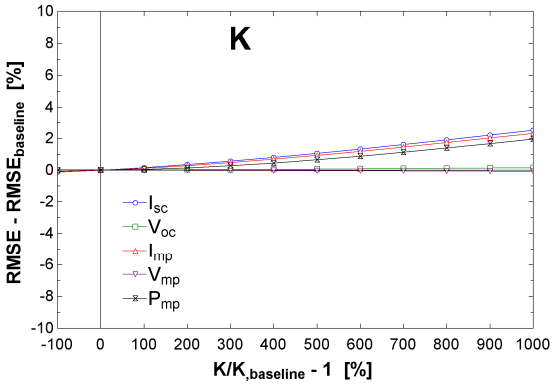
K
RMSE - RMSE$_{baseline}$ [%]
K/K$_{,baseline}$ - 1 [%]
I_{sc}
V_{oc}
I_{mp}
V_{mp}
P_{mp}

m.

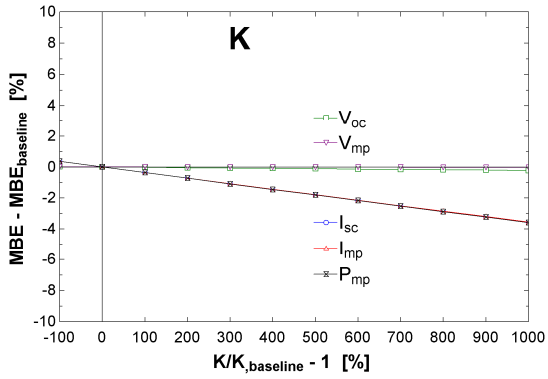
K
MBE - MBE$_{baseline}$ [%]
K/K$_{,baseline}$ - 1 [%]
V_{oc}
V_{mp}
I_{sc}
I_{mp}
P_{mp}

n.

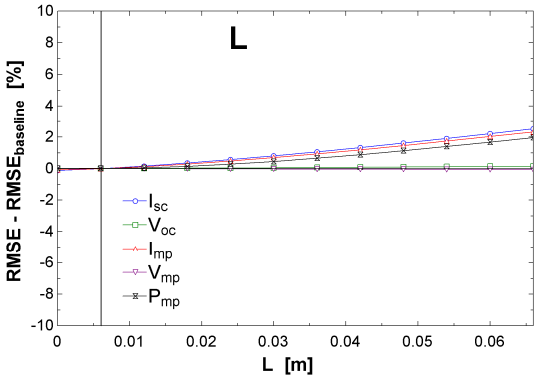
L
RMSE - RMSE$_{baseline}$ [%]
L [m]
I_{sc}
V_{oc}
I_{mp}
V_{mp}
P_{mp}

o.

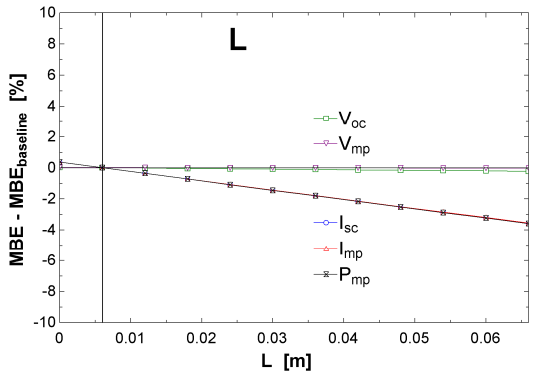
L
MBE - MBE$_{baseline}$ [%]
L [m]
V_{oc}
V_{mp}
I_{sc}
I_{mp}
P_{mp}

p.

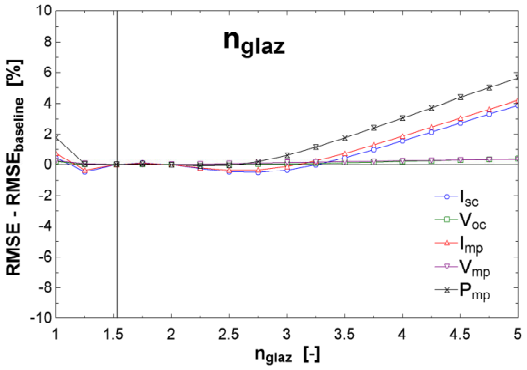
n_{glaz}
RMSE - RMSE$_{baseline}$ [%]
n_{glaz} [-]
I_{sc}
V_{oc}
I_{mp}
V_{mp}
P_{mp}

q.

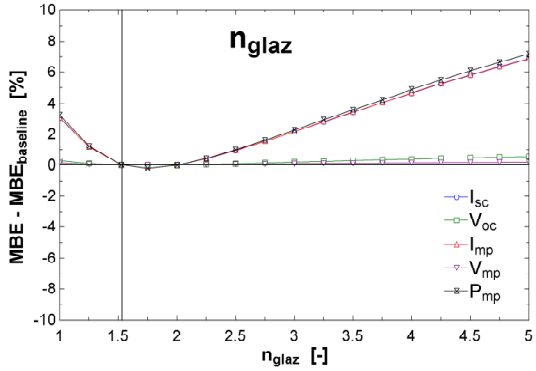
n_{glaz}
MBE - MBE$_{baseline}$ [%]
n_{glaz} [-]
I_{sc}
V_{oc}
I_{mp}
V_{mp}
P_{mp}

r.

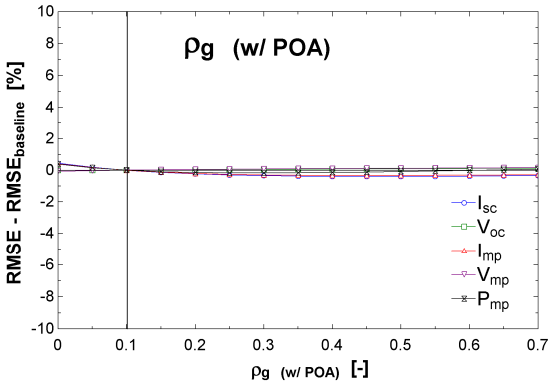
ρg (w/ POA)
RMSE - RMSEbaseline [%]
ρg (w/ POA) [-]
Isc
Voc
Imp
Vmp
Pmp

s.

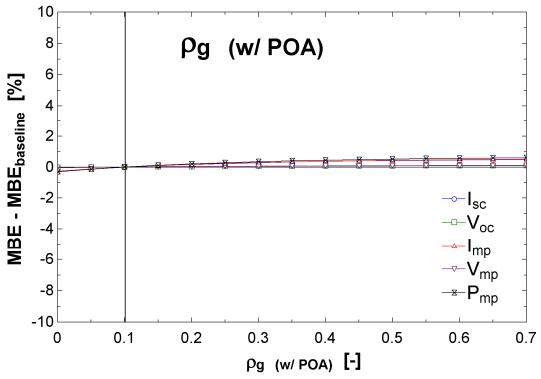
ρg (w/ POA)
MBE - MBEbaseline [%]
ρg (w/ POA) [-]
Isc
Voc
Imp
Vmp
Pmp

t.

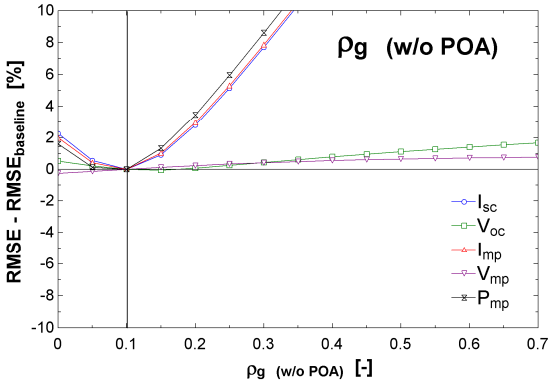
ρg (w/o POA)
RMSE - RMSEbaseline [%]
ρg (w/o POA) [-]
Isc
Voc
Imp
Vmp
Pmp

u.

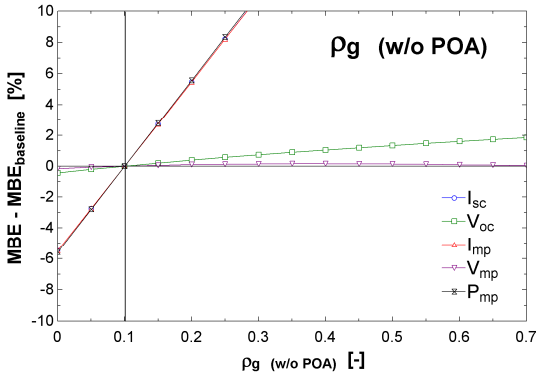
ρg (w/o POA)
MBE - MBEbaseline [%]
ρg (w/o POA) [-]
Isc
Voc
Imp
Vmp
Pmp

v.

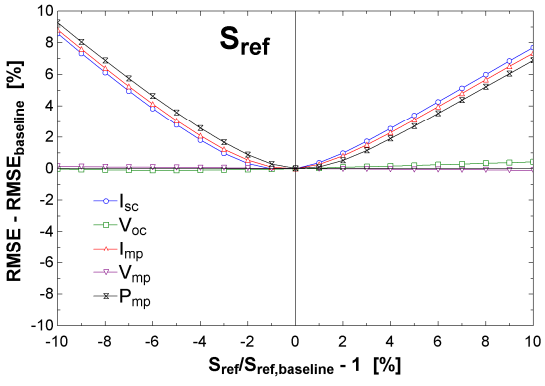
Sref
RMSE - RMSEbaseline [%]
Sref/Sref,baseline - 1 [%]
Isc
Voc
Imp
Vmp
Pmp

w.

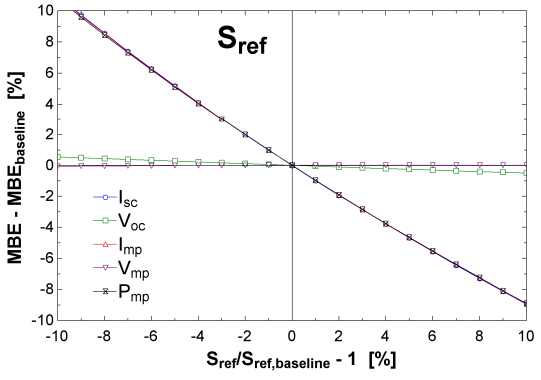
Sref
MBE - MBEbaseline [%]
Sref/Sref,baseline - 1 [%]
Isc
Voc
Imp
Vmp
Pmp

x.

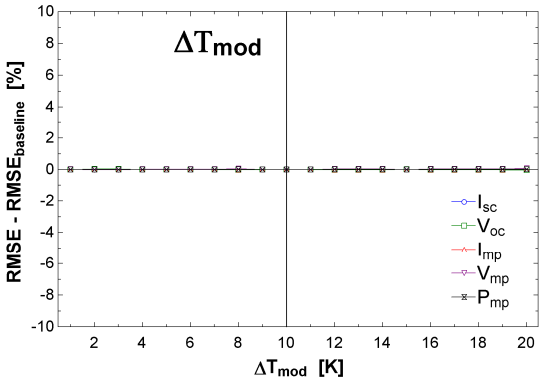
ΔTmod
RMSE - RMSEbaseline [%]
ΔTmod [K]
Isc
Voc
Imp
Vmp
Pmp

y.

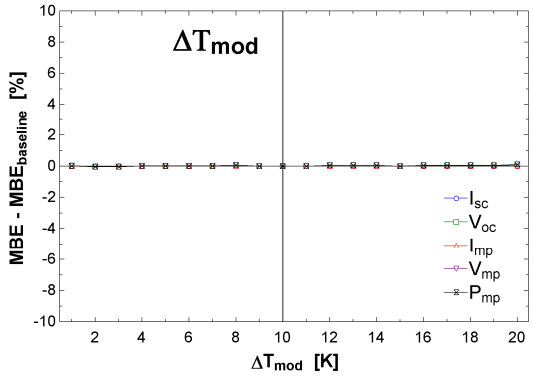
ΔTmod
MBE - MBEbaseline [%]
ΔTmod [K]
Isc
Voc
Imp
Vmp
Pmp

z.

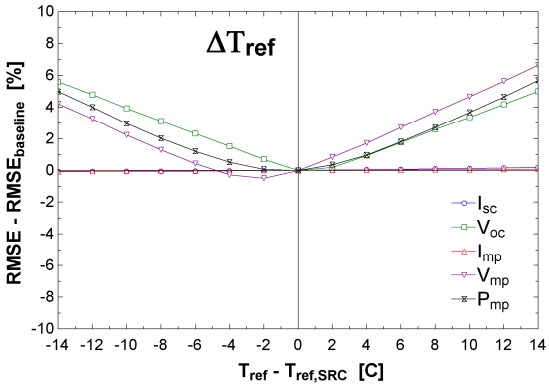
ΔTref
RMSE - RMSEbaseline [%]
Tref - Tref,SRC [C]
Isc
Voc
Imp
Vmp
Pmp

aa.

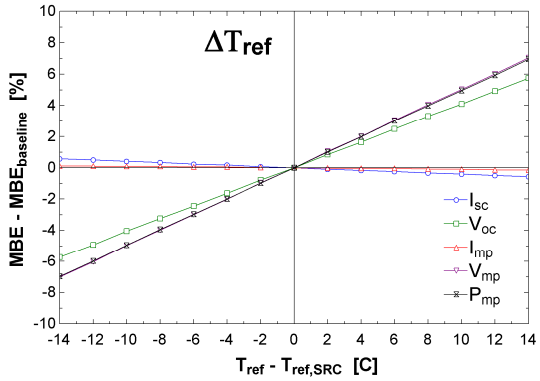
ΔTref
MBE - MBEbaseline [%]
Tref - Tref,SRC [C]
Isc
Voc
Imp
Vmp
Pmp

bb.

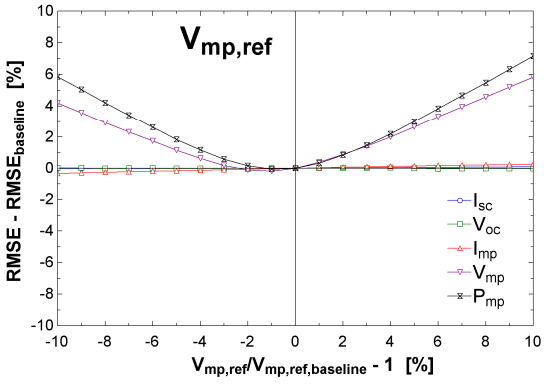
Vmp,ref
RMSE - RMSEbaseline [%]
Vmp,ref/Vmp,ref,baseline - 1 [%]
Isc
Voc
Imp
Vmp
Pmp

cc.

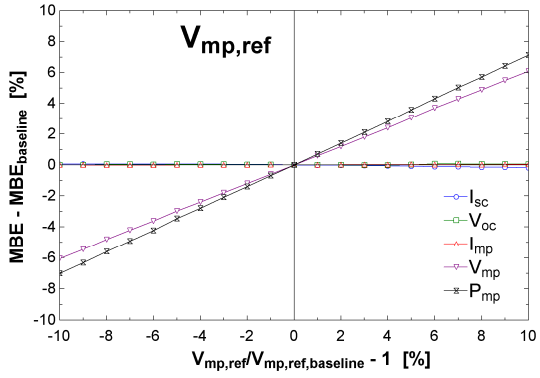
Vmp,ref
MBE - MBEbaseline [%]
Vmp,ref/Vmp,ref,baseline - 1 [%]
Isc
Voc
Imp
Vmp
Pmp

dd.

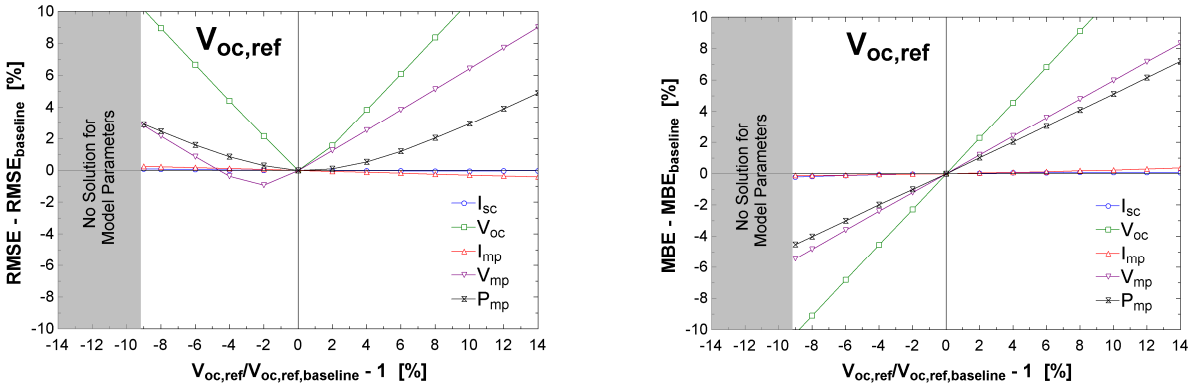

Figure I.1: Sensitivity analysis of the five-parameter model to 15 constant model inputs using data measured from the Mono-Si module

Appendix J

Regressions for Calculation of Low-Radiation SRC Data

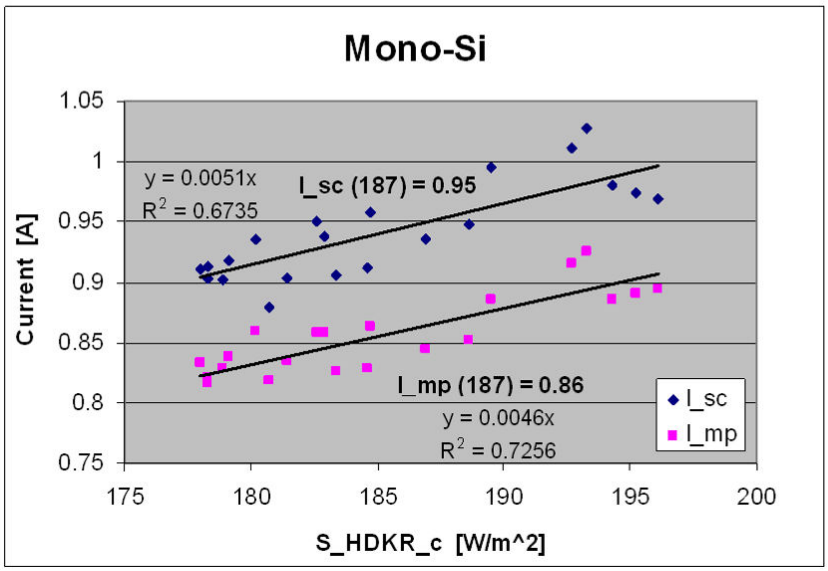

a.

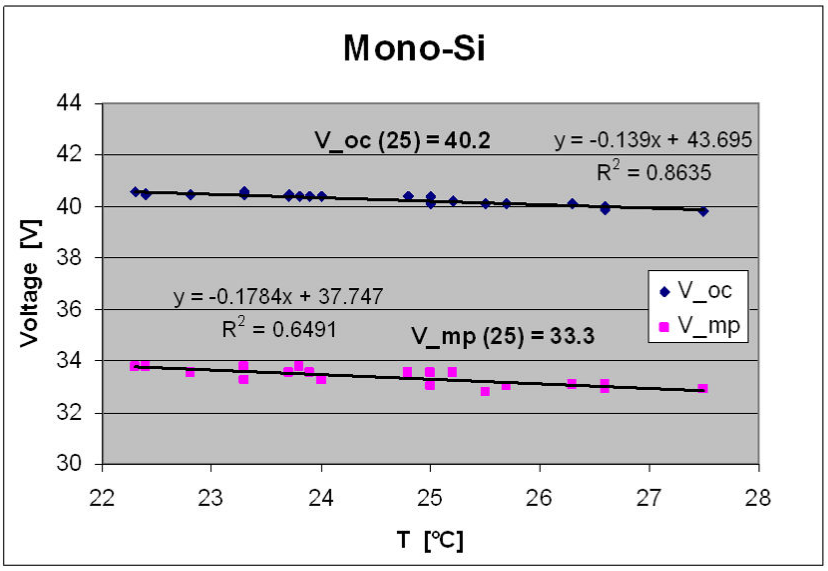

b.

Figure J.1: Linear regressions of 21 operating data points measured from the Mono-Si module that are used to calculate reference data at 200 W/m^2 (S_{200} = 187 W/m^2) and 25°C for use in the seven-parameter model

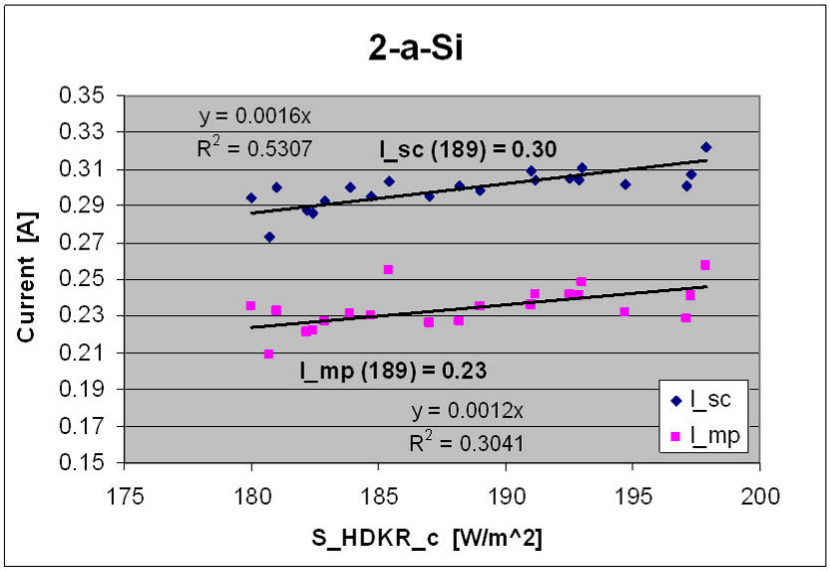

a.

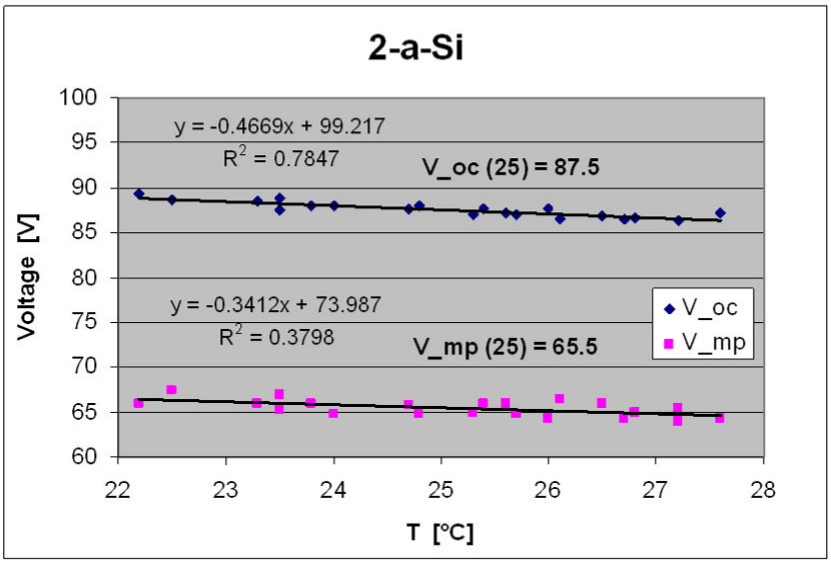

b.

Figure J.2: **Linear regressions of 21 operating data points measured from the 2-a-Si array that are used to calculate reference data at 200 W/m^2 (S_{200} = 189 W/m^2) and 25°C for use in the seven-parameter model. The value of I_{mp} (and I_{sc}) for the 2-a-Si is divided in half to get the value for one module, as the 2-a-Si data is measured from two modules wired in parallel.**

Appendix K

Effect of Seven-Parameter Model Parameters on I-V Curves

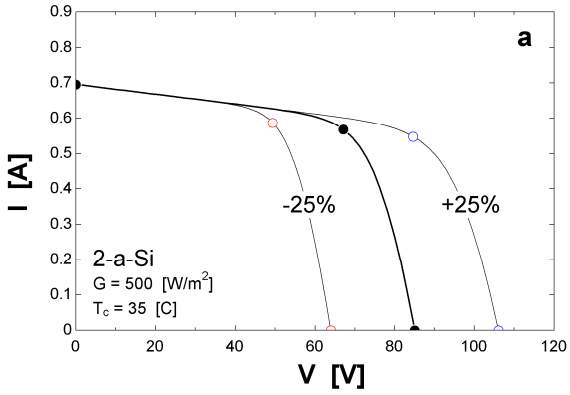

a.

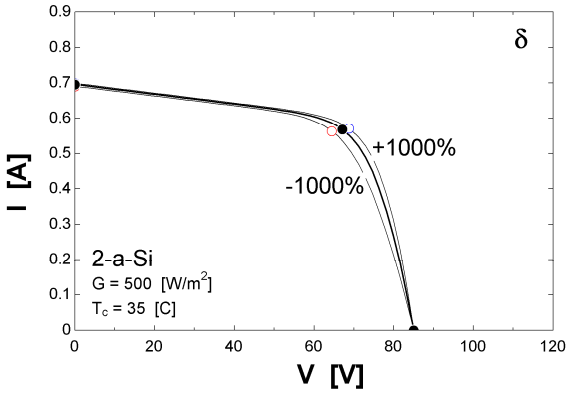

b.

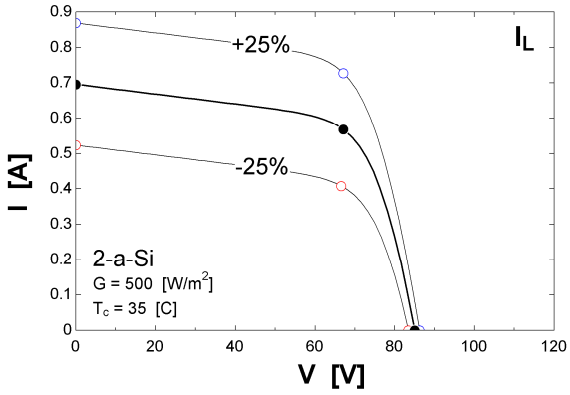

c.

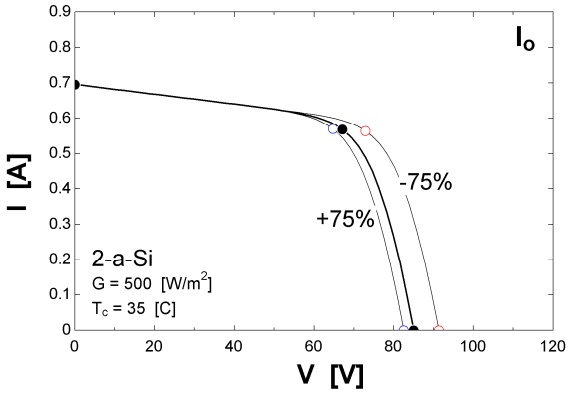

d.

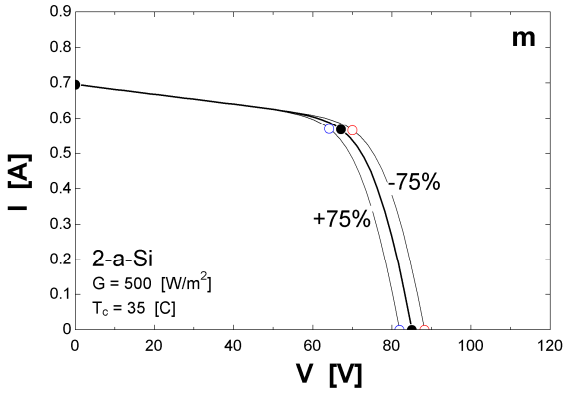

e.

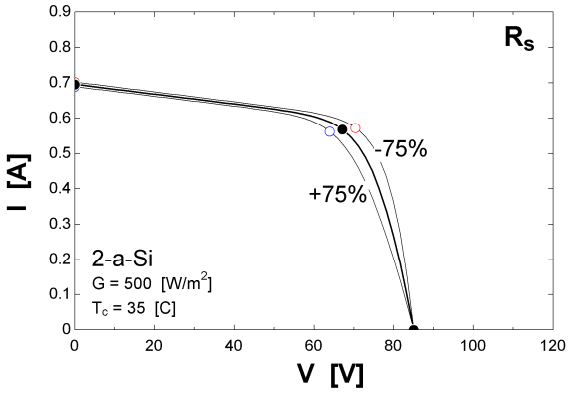

f.

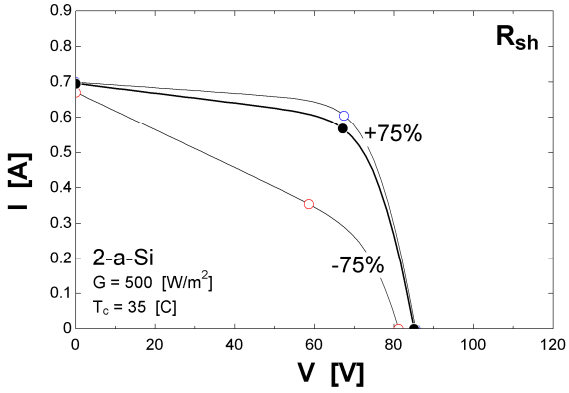

g.

Figure K.1: Effect of the seven-parameters in the seven-parameter model on the behavior of the modeled I-V curve. The parameters in both the five and seven-parameter models behave the same.

Appendix L

Sensitivity of Six-Parameter Current Sink Model to V_{bi}

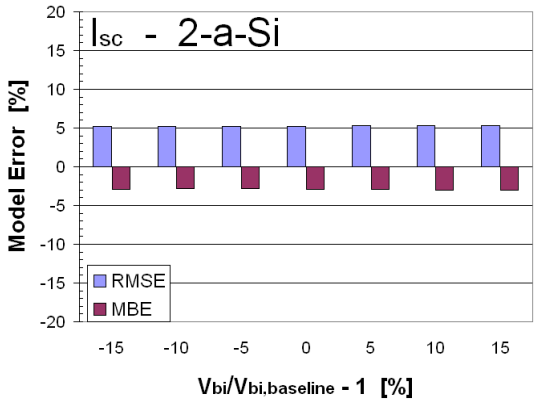

a.

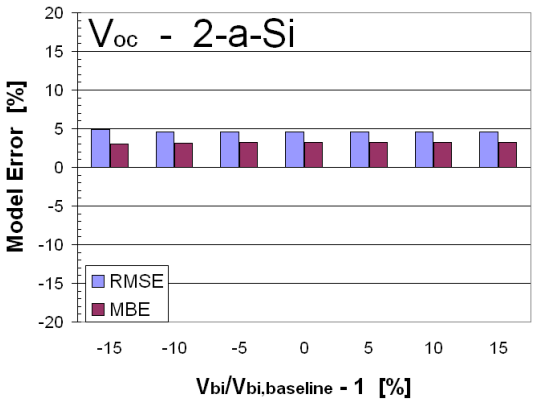

b.

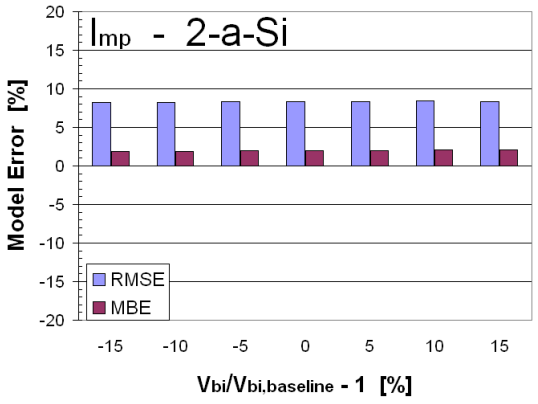

c.

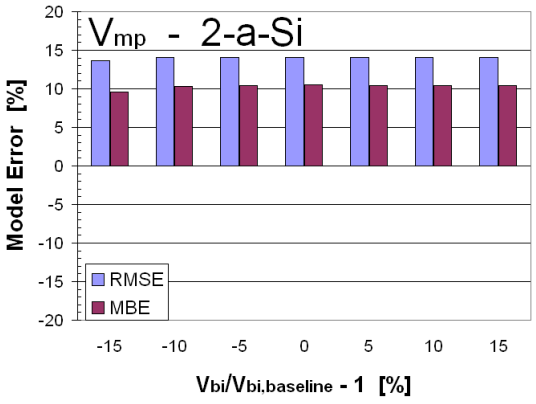

d.

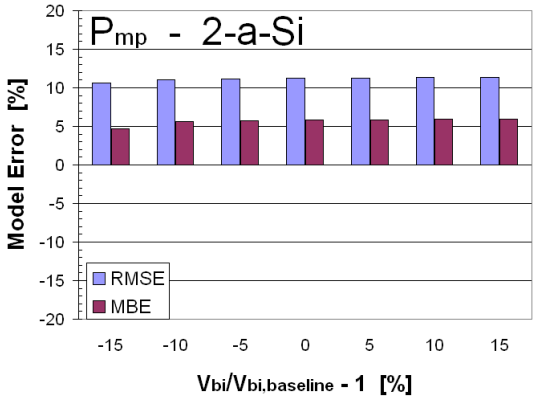

e.

Figure L.1: Sensitivity of the six-parameter current sink model to the built-in voltage (V_{bi}). Solutions to the model parameters do not converge with V_{bi} values larger than V_{bi}±15%.